Pursuant to the DOE Public Access Plan, this document represents the authors' peer-reviewed, accepted manuscript.
The published version of the article is available from the relevant publisher.

LANGMUIR

pubs.acs.org/Langmuir Review

The Overlooked Potential of Sulfated Zirconia: Reexamining Solid Superacidity Toward the Controlled Depolymerization of Polyolefins

Published as part of Langmuir virtual special issue "Highlights in Interface Science and Engineering: Polymer Upcycling and Recycling Challenges".

Scott R. Cleary, Anne K. Starace, Caleb C. Curran-Velasco, Daniel A. Ruddy, and C. Michael McGuirk*

Cite This: https://doi.org/10.1021/acs.langmuir.3c03966 Read Online

ACCESS | Metrics & More | Article Recommendations | Supporting Information

ABSTRACT: Closed-loop recycling via an efficient chemical process can help alleviate the global plastic waste crisis. However, conventional depolymerization methods for polyolefins, which compose more than 50% of plastics, demand high temperatures and pressures, employ precious noble metals, and/or yield complex mixtures of products limited to single-use fuels or oils. Superacidic forms of sulfated zirconia (SZrO) with Hammet Acidity Functions (H_0) ≤ -12 (i.e., stronger than 100% H_2SO_4) are industrially deployed heterogeneous catalysts capable of activating hydrocarbons under mild conditions and are shown to decompose polyolefins at temperatures near 200 °C and ambient pressure. Additionally, confinement of active sites in porous supports is known to radically increase selectivity, coking and sintering resistance, and acid site activity, presenting a possible approach to low-energy polyolefin depolymerization. However, a critical examination of the literature on SZrO led us to a surprising conclusion: despite 40 years of catalytic study, engineering, and industrial use, the surface chemistry of SZrO is poorly understood. Ostensibly spurred by SZrO's impressive catalytic activity, the application-driven study of SZrO has resulted in deleterious ambiguity in requisite synthetic conditions for superacidity and insufficient characterization of acidity, porosity, and active site structure. This ambiguity has produced significant knowledge gaps surrounding the synthesis, structure, and mechanisms of hydrocarbon activation for optimized SZrO, stunting the potential of this catalyst in olefin cracking and other industrially relevant reactions, such as isomerization, esterification, and alkylation. Toward mitigating these long extant issues, we herein identify and highlight these current shortcomings and knowledge gaps, propose explicit guidelines for characterization of and reporting on characterization of solid acidity, and discuss the potential of pore-confined superacids in the efficient and selective depolymerization of polyolefins.

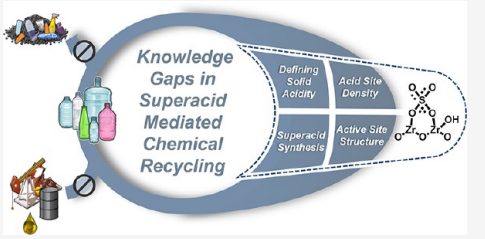

INTRODUCTION

Plastics have profoundly improved our capabilities to deliver food and water, administer healthcare, manufacture technology, and generate energy. However, the robust physical properties that proliferate their use are retained as postuse environmental pollutants.[1,2] Littering or improper disposal of 32% of plastic waste is a major contributor, but properly handled plastic waste is still environmentally harmful.[1] With only ~30% of all plastics ever made still in use today and ~9% recycled *even once*, millions of tons of plastics have been incinerated (12%) or leak as environmental pollutants through landfilling and improper disposal (60%).[3−10] This postuse pollution is compounded by the energy consumed, and thus, CO_2 generated by plastic manufacturing, emitting 4.5% of greenhouse gases in 2015 and consuming of 4−8% of the petrochemical supply (half as feedstock, half as fuel).[11−13] Additionally, the embodied energy lost in the form of landfilled plastics each year (~40%) is equal to ~12% of the energy annually used by the American industrial sector.[4,14] While incineration of plastic waste at temperatures ranging from 750 to 1000 °C recovers 60% of this stored energy as electricity and reduces environmental leaking, this process emits vast quantities of CO_2 and other toxic or carcinogenic byproducts.[1,4,14] Bans on single-use plastics in eight U.S. states and the European Union, alongside other global sustainability initiatives demonstrate mounting political action toward reducing plastic waste.[2] Despite these efforts and the ~80−120 billion U.S. dollars in value lost annually from disposal of single-use plastics, demand is only expected to grow with the modernization of developing economies and continued industrialization and consumerism of existing economic superpowers (Figure 1).[1,3,15]

Received: December 21, 2023
Revised: February 20, 2024
Accepted: February 26, 2024

Downloaded via NATL RENEWABLE ENERGY LABORATORY on March 22, 2024 at 17:35:08 (UTC).
See https://pubs.acs.org/sharingguidelines for options on how to legitimately share published articles.

Pursuant to the DOE Public Access Plan, this document represents the authors' peer-reviewed, accepted manuscript.
The published version of the article is available from the relevant publisher.

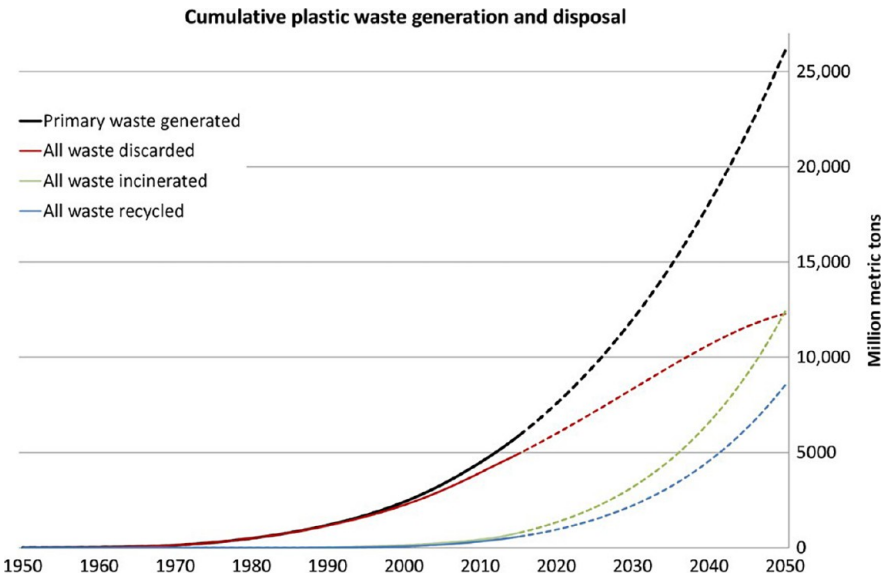

Figure 1. Cumulative plastic waste generation and handling as of 2017 and projected trends. Reprinted with permission from ref 3. Copyright 2017 Geyer et al.

Most of the small percentage of plastics that are recycled undergo mechanical recycling, which is typically limited to dense grades of polyethylene terephthalate (PET) or polyethylene (PE). Even with extensive presorting to separate plastic grade, colorants, and additives (light stabilizers, antioxidants, flame retardants, plasticizers, etc.), many plastics are not suited for mechanical recycling, such as multicomponent plastics, thin films, and food contaminated waste.[1,16,17] Dissolution can better process contaminated and complex plastics through separation based on solubility in organic solvents, reforming plastics that better retain their physical properties.[1,6,18,19] Still, lingering impurities and the friction, heating, and chemical treatments involved in mechanical and dissolution recycling invariably generate lower quality, downcycled plastics that can only be used a few times before being degraded into materials with unusable properties.[1,19] Thus, the current linear manufacturing, use, and disposal of plastics is environmentally and financially unsustainable. End-of-life plastics that can no longer be recycled by mechanical or dissolution recycling must be chemically recycled, a thermal or catalytic process that degrades plastics to lower-molecular-weight species for reuse. Thus, in addition to reducing demand for petroleum-derived plastics, cost-effective, energy-efficient, and selective chemical recycling approaches must be developed to reduce the carbon intensity of plastic waste management technologies.[10,20,21]

Chemical Recycling. Ideal chemical recycling would generate monomers that can be easily repolymerized into valuable materials that resemble the performance of virgin plastics (Figure 2).[10,20,21] Though the necessary infrastructure is a significant investment, chemical recycling could theoretically process mixed, contaminated, and end-of-life plastics not suited for mechanical or dissolution recycling.[1,20] State-of-the-art chemical recycling employed at the industrial scale is typically a high temperature and pressure process, made more favorable by the presence of an inorganic solid or solvent-based catalyst. However, such techniques still require high temperatures (varying between 250−700 °C depending on the plastic) and generate more acidification and air polluting gases than mechanical recycling, including NO_x (0.49 kg/ton of plastic waste), SO_x (0.09 kg/ton of plastic waste), and pollutant organic gases (1.42 g/kg of plastic processed).[1,22] Although dissolution and mechanical recycling remain more environmentally and economically friendly options *at the moment*, the unusable physical properties of end-of-life plastics demonstrates the need for a catalytic depolymerization process, which generates value-added, upcycled plastic products from plastic waste.[1] Thus, chemical recycling has become a focus of academic and private research and development in recent years.[4,5,10,22−25]

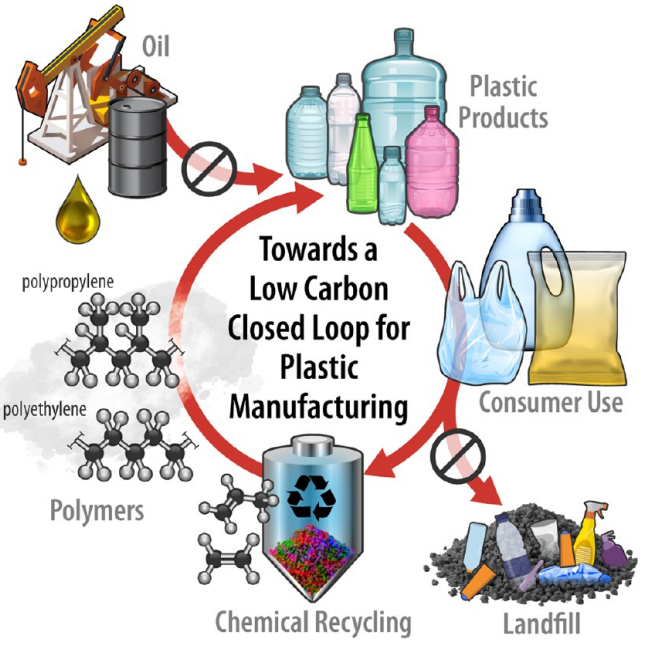

Figure 2. A representation of an ideal closed-loop polyolefin plastic economy, in which end-of-life plastics are kept in circulation by being chemically recycled into monomer and repolymerized into virgin plastics, eliminating petroleum consumption and mismanagement of plastic waste.

Compared to other major plastics in production, PET, polystyrene (PS), and polyvinyl chloride (PVC), polyolefins

https://doi.org/10.1021/acs.langmuir.3c03966
Langmuir XXXX, XXX, XXX−XXX

Pursuant to the DOE Public Access Plan, this document represents the authors' peer-reviewed, accepted manuscript.
The published version of the article is available from the relevant publisher.

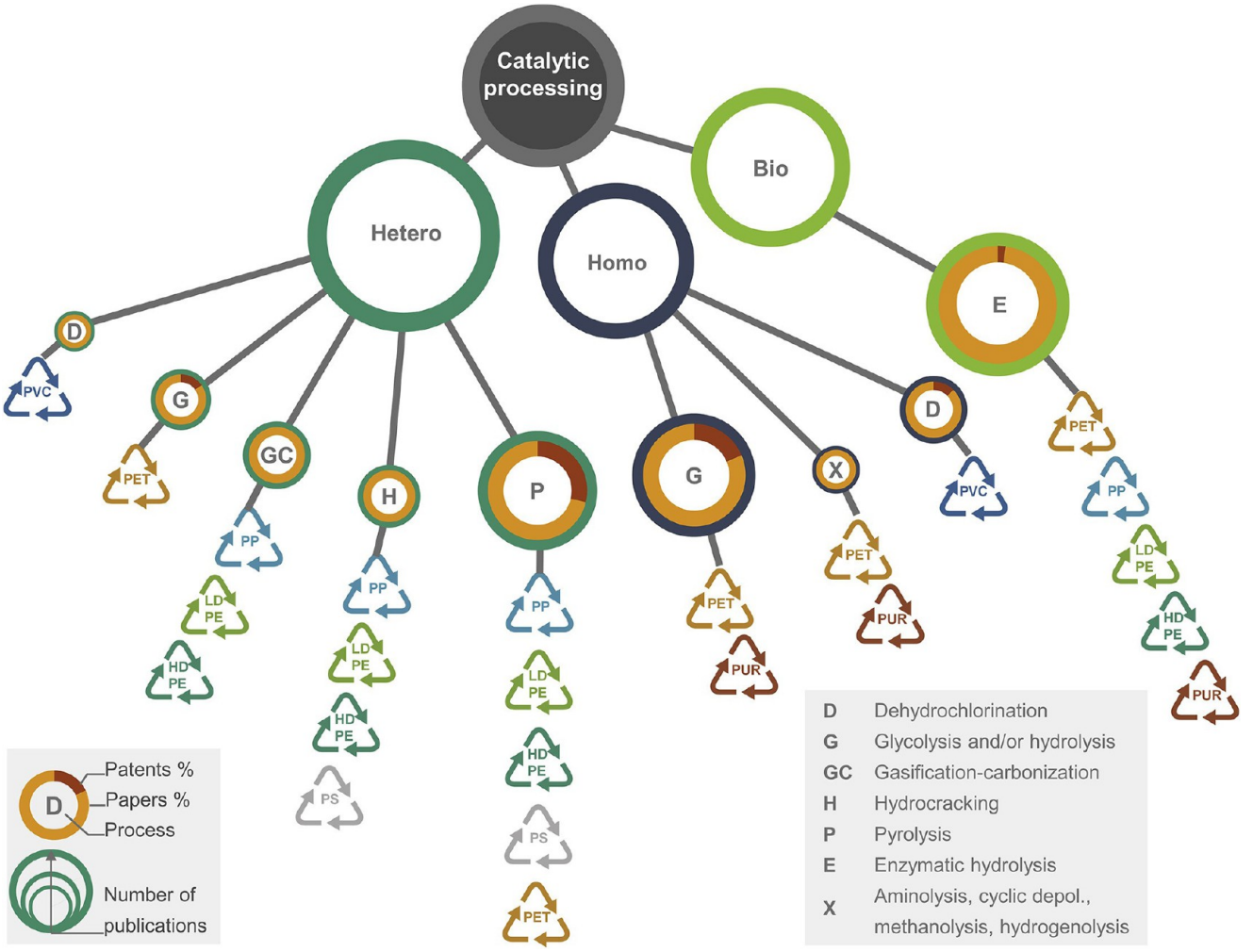

Figure 3. Patents and publications for chemical recycling of various plastic grades as of 2020. Reprinted with permission from ref 22. Copyright 2021 Elsevier.

(POs) are relatively low in cost, have sturdy and modulable properties, and emit less greenhouse gases during manufacturing. As a result, POs drive 48% of global plastics demand and >20% of single-use plastics demand in the form of polyethylene (PE) and polypropylene (PP).[1,2,26] As of 2017, PP and high- and low- density grades of PE represented 21% and 36% of all nonfiber plastics ever made, respectively.[3] Despite their abundance and continued use, no process is currently able to efficiently chemically recycle POs efficiently into their monomers.[1,3,26] The saturated C−C bonds linking the monomers of PO polymers are comparatively harder to cleave than the unsaturated or heteroatom-based bonds linking the polymers that compose most other commodity plastics. For example, thermal pyrolysis of PP, PE, PS, or PET, induces radical-based decomposition at high temperatures, generating a lower molecular weight but uncontrolled product mixture known as pyrolysis oil that must undergo further steam or catalytic cracking to generate small-chain aromatics and olefins.[22,24] While the polarizable bonds of plastic polymers like ester-linked PET allow bond activation at temperatures below 250 °C, PO pyrolysis demands temperatures above 600 °C for conversion to liquid paraffins and aromatic products best suited for use as combustible fuels.[1,27] While the federal Clean Air Act would normally apply strict regulations to the incineration of plastic waste, the indirect incineration of single-use fuels produced by pyrolysis subverts the same degree of regulation. As a result, many, including United States lawmakers, associate the limitations of pyrolysis with chemical recycling as a whole.[1,28,29] Liquefaction and gasification alleviate the high temperatures needed for pyrolysis by pressurizing the system but generate noxious byproducts and corrosive supercritical solvents that damage infrastructure.[1,22,30] To reduce the environmental and financial burden of the chemical recycling techniques articulated above, conceptually similar polymer deconstructions are increasingly performed in the presence of catalysts.[1,31−33]

Despite decades of study, process patents for catalytic depolymerization, which indicate industrial viability, are limited to dehydrochlorination (PVC), heterogeneous pyrolysis (PE, PP, PS), and hydrolysis/glycolysis (PET, PC, PUR) (Figure 3).[1,22,33,34] The temperatures needed to pyrolyze POs can be significantly lowered (<450 °C) by strongly acidic catalysts (i.e., HZSM-5).[30,33,35,36] However, even with extensive heating, most pyrolysis catalysts generate products limited to use as single-use oils and waxes or fuel-grade hydrocarbons.[25,31,37] Solvolysis (e.g., hydrolysis/glycolysis, methanolysis) and similar enzymatic methods (e.g., hydrolysis/glycolysis, aminolysis) are only successful with PET, polycarbonate (PC), polyurethane (PUR), and other heteroatom-linked polymers.[22] Although PET accounts for <10% of

https://doi.org/10.1021/acs.langmuir.3c03966
Langmuir XXXX, XXX, XXX−XXX

Pursuant to the DOE Public Access Plan, this document represents the authors' peer-reviewed, accepted manuscript.
The published version of the article is available from the relevant publisher.

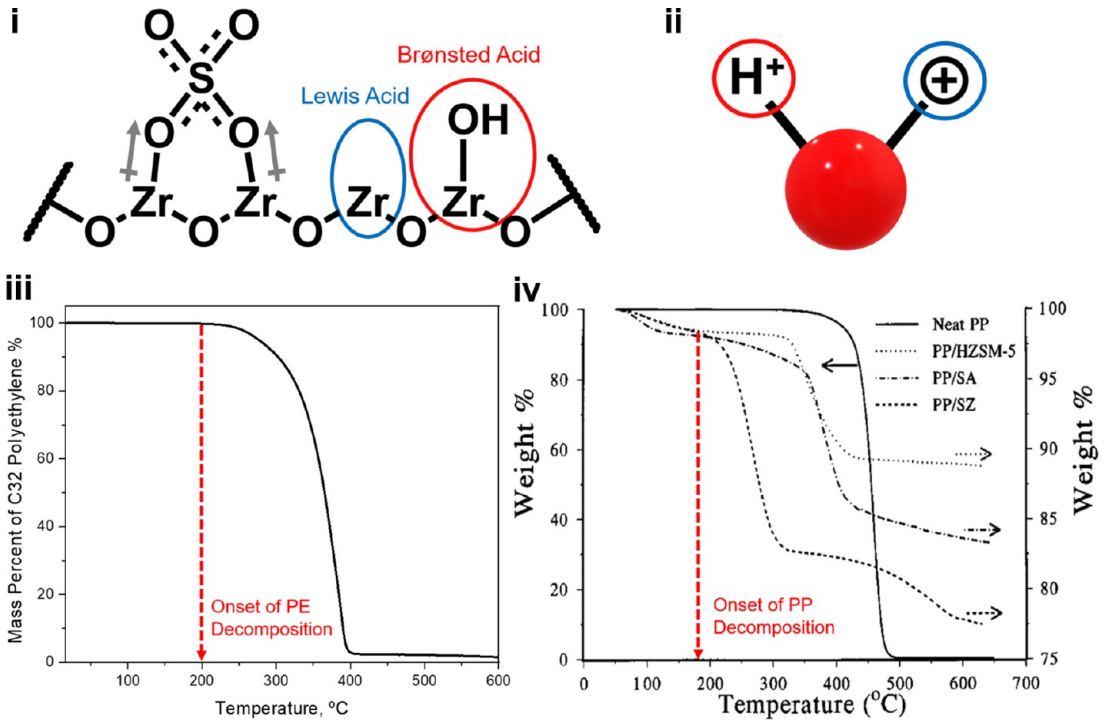

Figure 4. (i) A hypothesized representation of sulfated zirconia based on the reviewed literature. It is generally agreed that the inductive effect of a proximal surface sulfate enhances the Lewis acidity of Zr(IV) atoms (blue) and Brønsted acidity of hydroxyl groups (red). (ii) A simplified representation of a sulfated zirconia active site containing a Brønsted acidic proton (red) and a Lewis acidic site (blue). (iii) Our TGA-IR (N_2 flow and 1 °C/min) results for dotriacontane decomposition over 50 wt % Luxfer MEL Technologies sulfated zirconia activated at 300 °C for 30 min and (iv) White et al.'s TGA-MS (He flow and 10 °C/min) results for decomposition of "neat" polypropylene over 15 wt % sulfated zirconia (SZ), HZSM-5, or an amorphous silica−alumina (SA). Adapted by moving the key to allow addition of the approximated, red "Onset of PP Decomposition" line with permission from ref 37. Copyright 1998 John Wiley & Sons, Inc.

plastics, PET depolymerization has become a benchmark for economically and environmentally sustainable chemical recycling.[1,3] Prior to 1997, it was deemed profitable enough for commercialization by DuPont, leading to PET chemical recycling plants opening in Japan, Canada, Sweden, the United States, France, and Italy.[1,22,34] PET solvolysis boasts an impressive >95% conversion to monomer within 3−24 h at low pressures (1.4−4 MPa) and temperatures (180−300 °C). The low cost and complexity of homogeneous catalysts is counterbalanced by the energetically costly regeneration of the solvents and more challenging product separations.[1,34] With proper feedstock controls and infrastructure, PET plastics could be infinitely recyclable. While solvolysis may be extended to PC, polyester, and other vinyl or heteroatom-linked polymers, commercial PO recycling remains limited to pyrolysis, dissolution, and mechanical recycling to produce single-use oils and waxes or plastics with finite recyclability.[1,30] Thus, to enable a cost-effective chemical recycling process to upcycled quality materials for POs, a process would ideally achieve catalytic depolymerization to ethylene and propylene monomers at pressures <4 MPa and temperatures <300 °C by a catalyst of low cost and complexity.

Polyolefin Chemical Recycling. Beyond acid-catalyzed pyrolysis, chemical depolymerization of POs can be performed by a variety of homogeneous and heterogeneous catalysts to improve conversion rates, control selectivity, and lower temperature and pressure inputs toward efficiency comparable to modern PET depolymerization techniques. Notable recent reports of homogeneous deconstruction methods have utilized organozirconium-catalyzed β-alkylelimination to initiate C−C bond cleavage, with early reports focused on polymers containing C═C double bonds (e.g., polybutadiene, polyisoprene, polycyclooctene) as the initial site for cleavage. The reaction can be performed at relatively mild temperatures (e.g., ambient to 100 °C) in typical organic solvents (e.g., tetrahydrofuran), albeit under air- and moisture-free conditions. The promising aspects of these homogeneous catalysts prompted an investigation of heterogenized Zr sites on a silica−alumina support to perform comparable chemistry, with an alkylaluminum cocatalyst.[38,39] The combination of supported-Zr and alkylaluminum facilitated PE C−C bond cleavage to shorter parrafins, and functionalized products could be accessed through the appropriate quenching reagent. For example, quenching with methanol gave saturated hydrocarbons, iodine gave alkyl iodides, and carbon dioxide gave fatty acids.[40]

Compared to homogeneous catalysts, heterogeneous catalysts that operate without solvents can offer particularly facile product separation and catalyst reactivation. However, product selectivity and deactivation issues present major hurdles to their industrial employment.[18,37,41] For many of these catalysts (e.g., hydrocracking, dehydrogenation, hydrogenolysis), selectivity cannot be easily steered toward production of readily repolymerized olefin monomers. Thus, novel catalytic PO waste management techniques tend to target a means of making POs easier to decompose or other reuse applications for their products.

To enable PO cracking under mild conditions, POs can be modified with more easily activated linkages through dehydrogenation, sometimes paired with secondary metathesis

https://doi.org/10.1021/acs.langmuir.3c03966
Langmuir XXXX, XXX, XXX−XXX

Pursuant to the DOE Public Access Plan, this document represents the authors' peer-reviewed, accepted manuscript. The published version of the article is available from the relevant publisher.

of functionalized olefins. Still, dehydrogenation catalysts tend to suffer from low per-mass conversion rates without overoxidation into CO or employ increasingly precious noble metal catalysts (e.g., Ir). Subsequent metathesis would also require additional feedstocks, pressurized hydrogen, and high temperatures (350 °C), while also increasing the number of catalytic steps.[1,42−44] Although telechelic polyolefins, POs with functional groups at each end, produced by tandem dehydrogenation and metathesis could improve the future recyclability or biodegradability of end-of-life POs, their physical properties struggle to compete with those of virgin PO plastics without additional catalytic modification.[44] Thus, a single-step and energetically efficient approach to generating olefin monomers from PP and PE plastics is needed. Still, products other than small olefins, like those created by hydrogenolysis catalysts (e.g., cyclized aromatics, fuel-grade paraffins), have economic value.

Hydrogenolysis of POs into valuable fuels and oils cleavage of PO C−C bonds can be achieved at appreciably lower temperatures (250−300 °C) in the presence of a catalyst. However, hydrogenolysis catalysts tend to generate a large distribution of wax/liquid paraffins and have low per-mass conversion rates without excess cracking into undesirable gaseous paraffins.[41,45−47] Instead, POs can be upgraded by tandem approaches to alkylaromatics. A recent report demonstrated conversion of PE to alkylbenzenes and alkylnaphthalenes by Pt/Al_2O_3 catalysts through combined dehydrogenation (metal sites) and cyclization (acid sites).[48,49] Still, such catalysts employ precious noble metal nanoparticles (e.g., Pt, Ru) and high pressures of H_2 (1.38−0.89 MPa) to generate hydrogen radicals, prevent coking, and promote product desorption.[41,45−47] The use of hydrogen is undesirable for two reasons: (i) hydrogen is currently produced by CO_2-emitting steam reforming of methane, and (ii) reactions between olefins and hydrogen over the catalytic metal convert the otherwise easily repolymerized olefin products into paraffins.[50−53] While not useful for olefin production, hydrogenolysis catalysts have been used to eloquently demonstrate that pore-confinement can improve product selectivity, namely for fuel-grade liquid paraffins.[41,46,47] Similar to how the micropores of zeolites shift selectivity toward lower molecular weight gasoline-grade oils during pyrolysis,[30,32,35,36] physically confining hydrogenolysis catalysts in mesoporous silica forces chain-end activation of POs and processive hydrogenolysis of smaller molecular weight products. Additionally, active site sintering is eliminated and coking over the active sites is reduced, improving recyclability and long-term activity.[41,46,47] Perhaps, the benefits of confinement could be extended to other catalytic active sites that favor production of olefin monomers at lower temperatures and pressures.

In particular, heterogeneous superacids are a promising avenue to efficient PO decomposition.[54] By the original definition, superacids are capable of activating saturated, heteroatom-free hydrocarbons with better efficiency than typical mineral acids (e.g., nitric acid, sulfuric acid), which typically translates to rapid conversion rates at temperatures <250 °C and atmospheric pressures.[54,55] For example, sulfated zirconia (Figure 4i) is an industrial staple solid superacid employed in the isomerization of *n*-butane to isobutane at comparably low temperatures, though its strong Brønsted acids can also catalyze alkylation and C−C bond cracking.[50,56,57] Hydrocracking performed by acidic supports like sulfated zirconia (SZrO) doped with hydrogenolysis metal nanoparticles can aid cracking POs into liquid products, but the high pressures of hydrogen necessary likely reduce the desired olefin yield.[1,32,58] Without modification, SZrO's unique expression of both Brønsted and Lewis acid sites, which may be modulated for each application by synthetic controls, make it a desirable platform for the study of superacids as depolymerization catalysts.[57,59,60] To test if an unmodified superacid's propensity for C−C bond activation extends to the cracking of large POs, we examined an industrially employed SZrO standard prepared by calcining a sulfated precursor provided by Luxfer MEL Technologies in air at 620 °C, a calcination temperature described in literature.[61] We observed that the onset of decomposition of dotriacontane (C32) PE over SZrO occurs at temperatures near 200 °C (Figure 4iii). The corresponding Fourier transform infrared (FT-IR) spectroscopy data (Figure S10) suggests the PE broke down into smaller, gaseous hydrocarbons near 190 °C. It is worth noting that Andresen's group reported a higher onset decomposition of PE (337 °C) when heating at a faster ramp rate (10 °C/min) over less SZrO (10 wt %) calcined at 550 °C that was also supplied by MEL Chemicals.[62] However, White's group demonstrated an onset decomposition temperature of PP and PE for SZrO below 200 °C by thermogravimetric analysis and mass spectrometry detection (TGA-MS) at a similar catalyst wt % and ramp rate to Andresen's study. Concurrently, they demonstrated that the prototypical porous acid catalyst, HZSM-5, and amorphous silica alumina required higher temperatures to decompose PP than SZrO (Figure 4iv).[35,37] The White group's study of PE decomposition by HZSM-5 and SZrO demonstrated that SZrO produces nearly double the relative abundance of alkene products compared to HZSM-5.[35] However, MS results also indicate the majority of PP reduced mass species produced by SZrO are still heavy paraffins. Also, SZrO's activity drops rapidly due to coke build up on its strong acid sites for both polymers.[35,37] Still motivated by the low onset decomposition temperatures of this heterogeneous catalyst, we began to investigate solid superacids as a potential solution to the inefficiencies of modern PO plastic recycling.

Toward this goal, this critical review seeks to define common pitfalls in the synthesis, characterization, and application of solid acidity by analyzing the archetype heterogeneous superacidic catalyst, SZrO, particularly as it pertains to interactions with and degradation of POs. SZrO will be used as an example to discuss the common misconceptions surrounding acidity and superacidity, highlighting limitations in structural and acidity characterization of complex, porous solid acid surfaces. Standard acidity characterization techniques[63−68] and staple strong solid acids (zeolites, metal oxides, MOFs, etc.)[69−74] have been thoroughly reviewed elsewhere; however, factors pertinent to the mischaracterization of SZrO will be identified. This analysis is then applied to identify the gaps in knowledge that limit SZrO's value as an acid catalyst and its potential in the catalytic depolymerization of POs.

OVERVIEW OF SOLID ACIDS

History of Acid Catalysts. Acid-mediated catalysis was first demonstrated in 1552 with the conversion of alcohol to ether by sulfuric acid.[75] Today, many hydrocarbon conversions are designed around aluminosilicate acid catalysts for their low cost, ease of reactivation, and low operating temperatures.[50,76,77] Although engineering controls, activation and synthetic procedures, and environmental regulations have

https://doi.org/10.1021/acs.langmuir.3c03966
Langmuir XXXX, XXX, XXX−XXX

Pursuant to the DOE Public Access Plan, this document represents the authors' peer-reviewed, accepted manuscript. The published version of the article is available from the relevant publisher.

continued to shape these processes, the core components of the catalysts employed have largely remained the same since the 1950s: heterogeneous acidic oxide supports with promoter species.[71,78−80] These catalysts have found far-reaching value as bifunctional acid−base/redox catalysts capable of multistep syntheses including: aldol condensation, esterification, isomerization, alkylation, cyclization, and fuel refinment. However, the complexity of heterogeneous acid surfaces and the application-driven development of acid catalysts has led to limited mechanistic and structural understanding.[71,78] Because minute changes to solid acid synthetic protocols alter acid−base and redox properties, expanding fundamental atomic-level understanding of acidity and superacidity is critical to sustainable chemical manufacturing.[59,71,78] By furthering these fundamental insights, we may enable thermally efficient, selective, recyclable, and solvent-free acid-mediated PO cracking. One possible approach to improving efficiency is the use of extremely strong acids, namely superacids.

Superacidity. Superacids, first defined as acids stronger than typical mineral acids (e.g., sulfuric acid, nitric acid, etc.), significantly reduce the energy required to activate the C−C bonds of saturated carbon centers. This translates to room-temperature protonation events and conversions below 250 °C. Superacidity was first observed in liquid acids in 1927 by Hall and Conant, but the definition was updated by Ronald Gillespie in 1971 to include a quantitative metric for Brønsted superacid strength.[55,59] As the pH scale was designed only for dilute aqueous environments with H_3O^+ acid species, the strength and concentration of such strong acids invalidates the Henderson−Hasselbalch approximation. A more accurate approximation for Brønsted superacid strength is the Hammett acidity function (H_0) (eq 1).[55,76,81]

$$H_0 = -\log(a_{H^+}) - \log\left(\frac{\gamma_B}{\gamma_{BH^+}}\right) \quad (1)$$

The Hammett acidity function is analogous to the Henderson−Hasselbalch equation, but it uses the negative log of the equilibrium constant (pK_{BH^+}) for the dissociation of the conjugate acid (BH^+) of a very weak base (B) in place of pK_a. As hydrogen ion activity (a_{H^+}) changes more rapidly than concentration in concentrated liquid acids, activity is used for the calculation of pK_{BH^+}. Activity coefficients are used for B and BH^+, whose individual concentrations are assumed to be equal after titration. Thus, Hammett acidity measures Brønsted acid strength in place of concentration alone and is ideal for quantifying the acidity of homogeneous liquid acids.[55,76,81,82] Doing so appears to extend the pH scale to very negative values, that is, superacidic levels of acidity. However, the true meaning of a $H_0 = -12$ is not −12 pH but a protonation strength theoretically equal to an unrealistic $[H_3O^+] = 10^{12}$ M, recently equated to a proton affinity ≥250 kcal/mol.[83] Hammet superacids are stronger than pure sulfuric acid ($H_0 \geq 12$), and the H_0's of stronger acids decrease logarithmically, with the strongest known acid being fluoroantimonic acid ($HF\text{-}SbF_5$, $H_0 < -25$).[54,55,78,82]

Liquid superacids protonate species that otherwise do not exhibit acid−base properties by generating very inert conjugate Brønsted bases that distribute their charge across conjugated and electronegative groups. Additionally, Lewis acids form acid−base adducts with these Brønsted bases, that further enhance conjugate base stability and Brønsted acidity.[55,76,82] The majority of superacids are generated by Brønsted and Lewis acid pairs that produce superacidity in otherwise nonsuperacidic Brønsted acids.[57,76] First observed in the 1960s with $HSO_3F\text{-}SbF_5$, also known as "magic-acid" ($H_0 = -19.2$), liquid superacidity is often achieved by a fluorinated Brønsted acid (HF, HSO_3F, CF_3SO_3H, etc.) forming an anionic adduct with a strong Lewis acid (SbF_5, TaF_5, AsF_5, etc.) upon deprotonation.[55,76,78,84] In $HF\text{-}SbF_5$, stoichiometrically more of the Lewis acidic species generate larger anionic adducts, $(SbF_5)_xF$ increasing the conjugate base stability and the Brønsted acid strength. Thus, electron-withdrawing groups and Lewis acidic species seem critical to the expression of Brønsted superacidity.[76,78] The existence of Brønsted superacidic species that do not require promotion by a Lewis acid led to the development of definitions for isolated Lewis superacidity. Lewis superacids exceed the fluoride ion affinity value of what was once considered the strongest Lewis acid, antimony pentafluoride (120 kcal/mol). However, acid strength scales differently with soft and hard base probe molecules. Thus, soft Lewis superacids are those with a stronger hydride ion affinity in the gas phase than tris(pentafluorophenyl)borane (115 kcal/mol), while hard Lewis superacids retain the fluoride ion affinity definition.[85] Several classes of Lewis superacids have been identified, typically small, poorly shielded Group III or transition metal cores with electron-withdrawing organic ligands.[85] For our purposes, "Lewis superacidity" will be specified while Brønsted superacidity may be referred to as simply "superacidity", as most superacids and relevant reactions are tied to the Brønsted acidic definition.

Liquid superacids were once valued for their low temperature activity in ethylene glycol synthesis, benzene alkylations, and isobutylene hydration; however, the corrosiveness of boiling and supercritical liquid acids means they have a narrow range of operating conditions (10−85 °C).[76,78] Thus, selectivity cannot be well controlled by altering temperature, pressure, or other reaction conditions. Additionally, superacidic liquids are prone to oxidizing, coking, and generating toxic reaction fumes, which complicates product separation, corrodes industrial infrastructure, and makes regeneration challenging, typically recovering <50% of spent catalyst. Though the reduced volatility and corrosiveness of alternatives like superacidic ionic liquids is promising, global legislation now restricts the use of hazardous superacidic liquids.[76,78,84,86] Thus, liquid superacids have been replaced in many applications by heterogeneous catalysts.

Heterogeneous superacids allow efficient chemical manufacturing with reduced harm to infrastructure (i.e., fixed bed reactors that restrict contact), easier phase separation, and simpler reactivation procedures. Additionally, their stability allows selectivity to be shifted based on a broad range of temperatures (>800 °C) and pressures.[54] Some solid superacids, such as SZrO and certain zeolites, were originally considered superacidic based on their ability to isomerize *n*-butane below 250 °C, propelling their use in a variety of reactions.[50,57,87] However, inconsistency in the evaluation of solid acidity has generated doubt in whether SZrO, zeolites, and all solid acids actually qualify as superacidic in terms of acid strength. In fact, despite several decades of industrial deployment and development, the means by which SZrO and other solid acids activate saturated hydrocarbons is still not well understood.[59,60,88−90] To begin to decipher the nature of solid superacidity, we must identify the features of staple solid acids.

https://doi.org/10.1021/acs.langmuir.3c03966
Langmuir XXXX, XXX, XXX−XXX

Pursuant to the DOE Public Access Plan, this document represents the authors' peer-reviewed, accepted manuscript. The published version of the article is available from the relevant publisher.

Heterogeneous Acids. Industrial solid acids typically derive their catalytic properties from a surface featuring Brønsted acidic hydroxyl groups and Lewis acidic coordinatively unsaturated metals.[71,76] While both acid types (i.e., Brønsted or Lewis) can exist on solid acid surfaces, they are often physically separated and cannot engage in the same cooperative Brønsted and Lewis acid interactions that increase Brønsted acidity in liquid acids. Instead, the depth of solid beneath the Brønsted acidic surface helps maintain acidity through sequential deprotonation events and stabilizes the conjugate base in a similar manner to liquid superacids.[76,91] Still, the substantial alkane bond cracking capability of highly acidic surfaces means they are prone to rapid deactivation by coking and active-site poisoning.[56,92] Though weaker acids operate for weeks or years without reactivation, coking causes deactivation of the strongest acid sites on solid superacids on a scale of seconds to hours. As only weaker acids remain, this also causes a shift in selectivity without extensive engineering controls.[56,82,92] Higher temperatures and pressures will shift selectivity due to both reaction thermodynamics and the rate of coke build up. Long-term activity can be retained by pressurization with H_2 and doping with metal nanoparticles that remove coke from Lewis acid sites, but these nanoparticles also block access to the surface's existing active sites.[50,51] Alternatively, selectivity on solid acids can be controlled by synthetically altering the expression of Brønsted or Lewis acidity, acid strength, and acid density.[59,60,93] For example, in isobutene alkylation with SZrO, cracking products are observed during reaction onset as a result of SZrO's strong Lewis acid sites. However, the yield of cracking products rapidly decreases with time on stream, as coking that blocks acid site accessibility shifts selectivity to alkylation catalyzed by weaker acids. SZrO's stronger, Lewis acidic sites seem particularly sensitive to coking and are rapidly deactivated in the presence of an alkene feedstock.[56,94] Thus, the desired PO conversion to small olefins over solid superacids will be in competition with events like coking, polymerization, or cyclization of reactive intermediates generated by initial cracking reactions.[56,92] While the elimination of the additional costs, hazards, and complex separations of liquid acids make the drawbacks of solid acidity easy to overlook, coking and selectivity issues for these strong acids may be reduced or eliminated by confinement in porous architectures.[18,41,46]

The Role of Porosity in Solid Acids. Porosity provides a variety of benefits, including increased surface area, reduced active site sintering, selectivity controls, and resistance to deactivation from coke, water, and impurities. For example, solid porosity allows control of stereo- and regioselectivity not available in liquid acids through effects influencing substrate orientation, reactive intermediate size, mass transfer, and intermediate stabilization.[76] The classic example is the shape selectivity associated with zeolite catalysts of varying pore dimensions and pore connectivity.[50,95,96] These principles have been extended to polymer deconstruction reactions using supported metals in the zeolite pores, with recent examples employing dehydrogenation to initiate C−C bond cleavage and C−H borylation reactions.[97−99] Zeolites can both naturally and synthetically occur as 2D sheets (e.g., MMT) and/or 3D interconnecting porous networks (e.g., HZSM-5).[90,100] As previously discussed, acid-catalyzed depolymerization of PP generates an uncontrolled mixture of primarily paraffin products on solid acids with little pore volume (e.g., SZrO). However, the ordered, 0.55 nm, high-volume pores of HZSM-5 promote chain-end β-scission and sterically impede formation of the bulky intermediates produced by SZrO that generate heavier paraffin products.[37] Enhanced selectivity control has been demonstrated with various reactants in the micropores of zeolites, including decomposition of 100 kDa PE near 400 °C with greater selectivity for short-chain olefins compared to nonporous heterogeneous acids of similar strength.[35,36,101,102]

Diffusion of hydrocarbons in zeolites is influenced by the pore dimensions as well as the density of sorption sites lining the pores. More polar surfaces facilitate rapid diffusion of reactants, reduce dwell time on active sites, and impede coking, driving remarkable catalytic activity through mass transfer even with relatively weak acidity.[90,93] At the melt temperature, the weak intermolecular forces that hold POs together are broken, and diffusion into polar pores becomes favorable.[41,100,103] While large-molecular-weight species like straight-chain POs diffuse rapidly due to abundant interactions with pore walls that promote continued feeding of the untangled polymer into the pore, low molecular weight species diffuse slowly.[46,100,103] Slower diffusion of cracked products facilitates secondary cracking events, coking, and a slower turnover rate as products impede the rapid diffusion of larger molecular weight reactants. To enable cracking of PE to small olefins by acidic zeolites, short pores and temperatures exceeding 300 °C are needed, as well as high H_2 pressures to break up coke.[100,103] In terms of pore diameter, narrow pores not only prohibit large intermediate and product formation but also interactions with branched or bulky reactants. Therefore, narrow pores will facilitate external coking and are easily blocked by a single coking event.[37,50,90] Modification of microporous zeolites to secondary mesopore shapes ($2 < x < 50$ nm) improves conversion rate and selectivity, suggesting that mesopores have superior mass transfer. Catalyst lifetime is also extended because coking primarily occurs in the mesopores of catalysts with multiple pore sizes, extending their lifetime.[50,71] The numerous, weak adsorption sites lining the pores of metal oxide supports also provide electrostatic stabilization of high-energy intermediates.[104] While acidity characterization results suggest the acid sites located deep within the smaller pores of zeolites are stronger, more precise characterization indicates that these acid sites are not significantly stronger than acid sites on the exterior. Instead, the catalytic activity observed in these smaller pores is the result of confinement effects that shape the interactions of these strong, but not superacidic, acid sites with reactant molecules. The delayed desorption of analytical probe molecules from deep within pores, alongside other confinement effects, explains the numerous measurements that overestimate acid strength.[63,68,104,105] Therefore, it is more likely that the density of adsorption sites generates better activity inside the pores by stabilizing reactive intermediates and promoting mass transfer. The combination of strong, but not superacidic, acidity and these confinement effects likely explains the superacid-like activity of some solid acids.[104]

Many porous architectures are hierarchical, expressing different domains of acidity on the surface and within one or more domains of pore sizes. Therefore, the acidity of the exterior is just as important to consider as the acidity within the pores. For example, MFI zeolites have an abundance of strong acid moieties on their exterior that crack POs to enable diffusion of smaller products inside pores where secondary cracking to C_1−C_7 molecules occurs; however, these acidic exteriors also coke rapidly, blocking pore access and

https://doi.org/10.1021/acs.langmuir.3c03966
Langmuir XXXX, XXX, XXX−XXX

Pursuant to the DOE Public Access Plan, this document represents the authors' peer-reviewed, accepted manuscript.
The published version of the article is available from the relevant publisher.

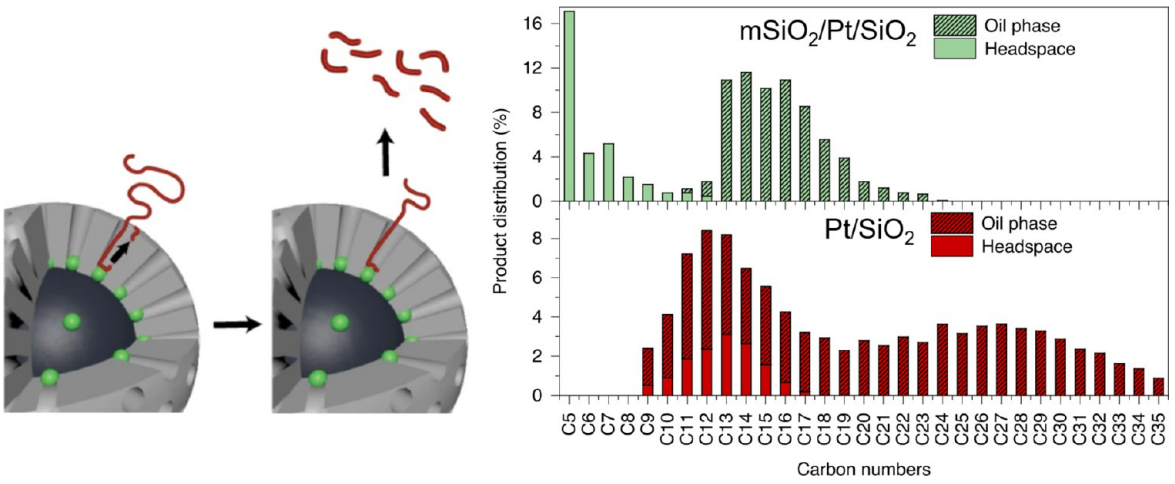

Figure 5. Models of mesoporous silica core@shell architectures that confine Pt nanoparticle active sites and corresponding product data for 130 kDa polyethylene hydrogenolysis over catalysts at 250 °C and 1.38 MPa H_2 after 6 h for the complete core@shell ($mSiO_2/Pt/SiO_2$) and without the mesoporous shell (Pt/SiO_2). Adapted by combining portions of two figures and adding the $mSiO_2/Pt/SiO_2$ and Pt/SiO_2 labels with permission from ref 41. Copyright 2020 Springer Nature.

deactivating the catalysts from the outside.[100] On the other hand, the low acid density of HZSM-5′s exterior experiences little to no surface coking and allows diffusion of precracked reactants into its micropores. Hierarchical design of porous systems that confine the majority of strong acid sites inside pores should facilitate high rates of PO cracking and longer catalyst lifespans.[90,100] Beyond coking, lining the exterior of porous materials with lower acid strength and density zeolite or silica also generates a somewhat hydrophobic exterior that impedes water uptake and deactivation of hydrophilic Lewis acid sites.[104,106,107] Hydrophobic porous exteriors should also impede diffusion of bulky and polar plastic additives like antioxidants (chloroaromatics and alkylated phenols), flame retardants (chloroalkylphosphates, chloro- and bromo-paraffins, bromoaromatics), and plasticizers (adipates, phthalates).[16,17] Thus, many catalyst design studies emulate the benefits of pore confinement by placing active sites more prone to deactivation inside less polar mesoporous architectures. For PO cracking, the value of this concept has already been modeled using hydrogenolysis catalysts.

Tennakoon et al. demonstrated that confining Pt active sites at the bottom of 1D silica mesoporous core@shell architectures eliminates nanoparticle sintering, extends catalyst life-span, and shifts PE depolymerization selectivity to lower molecular weights (Figure 5).[41] A lower average product weight can be obtained while maintaining activity with smaller pore diameter so long as the pore diameter still bares the entire exposed face of the nanoparticle and allows substrate diffusion.[41,47] The diffusion of PE into mesoporous silica has also been confirmed by ^{13}C-labeled PE probes and solid state nuclear magnetic resonance (ssNMR) spectroscopy, as PE unravels to maximize van der Waals interactions with the pore walls in a quasi-equilibrated anti conformation.[41] Kinetic models predict that there is an appreciable enthalpic barrier to breaking these noncovalent interactions, and POs are likely to engage in multiple interactions with the active site before diffusing out of the pore.[45,47] The majority of these interactions with the active site do not cause C−C bond cleavage by hydrogenolysis catalysts.[45] Coarse-grained molecular dynamics simulations and in situ ssNMR spectroscopy results indicate that larger polymer lengths, smaller pore diameters, and deeper pores facilitate longer PO residence time, allowing more interactions with the active site and more opportunities for chain-end cleavage.[45,47] Population balance models have also identified the features of processive PE hydrogenolysis, product release, and chain repositioning by core@shell confined active sites to predict turn over frequency within different pore dimensions.[108] Evidence suggests that hydrogenolysis activity is not limited by mass transfer of reactant POs in the porous media, as POs extend and equilibrate with the pore walls faster than C−C bond hydrogenolysis.[45−47] The same is likely true for acid-catalyzed carbenium formation, which appears to limit the rate of zeolite- and SZrO-catalyzed alkane conversions.[50,76,87] In fast-rate reactions, slow exit diffusion of small product molecules slows the conversion rate. Zeolites with smaller crystallites, and thus shallow pores, can promote faster conversion rates by reducing product residence time, but these small catalysts are also difficult to separate from products.[109,110] Sadow's group successfully mediated this issue using larger catalysts by replacing the nonporous core of their previous core@shell catalyst (Figure 5) with porous MCM-48 nanoparticles with 2.2 nm mesopores, creating channels through the center of the particle. With an exit diffusion pathway that does not compete for pore wall interactions with incoming reactants, product residence time is reduced, conversion rates improve, coking and H_2 consumption are reduced, and the molecular weight of the hydrogenolysis products increase.[46] While these ordered 3D architectures with 1D pores are a desirable research model for acid-catalyzed PO depolymerization, 2D sheet architectures and 3D architectures with multidimensional, interconnecting pores may provide superior catalytic value.

Confinement effects influence the functional strength (i.e., bond activation capability) of an acid site. For example, the strongest analytically determined Brønsted acid strength for a solid was reported by Liu et al. for a sulfonated polymer packed between aluminosilicate clay sheets (MMT@PAN[C_3N]-[SO_3CF_3]). This structure's pores are lined with numerous hydrogen bonding groups that enhance mass transfer and should elongate reactant C−H bonds to ease hydride protonation by a Brønsted acid. These pore walls also stabilize high-energy intermediates and transition states.[63,90] However,

https://doi.org/10.1021/acs.langmuir.3c03966
Langmuir XXXX, XXX, XXX−XXX

Pursuant to the DOE Public Access Plan, this document represents the authors' peer-reviewed, accepted manuscript.
The published version of the article is available from the relevant publisher.

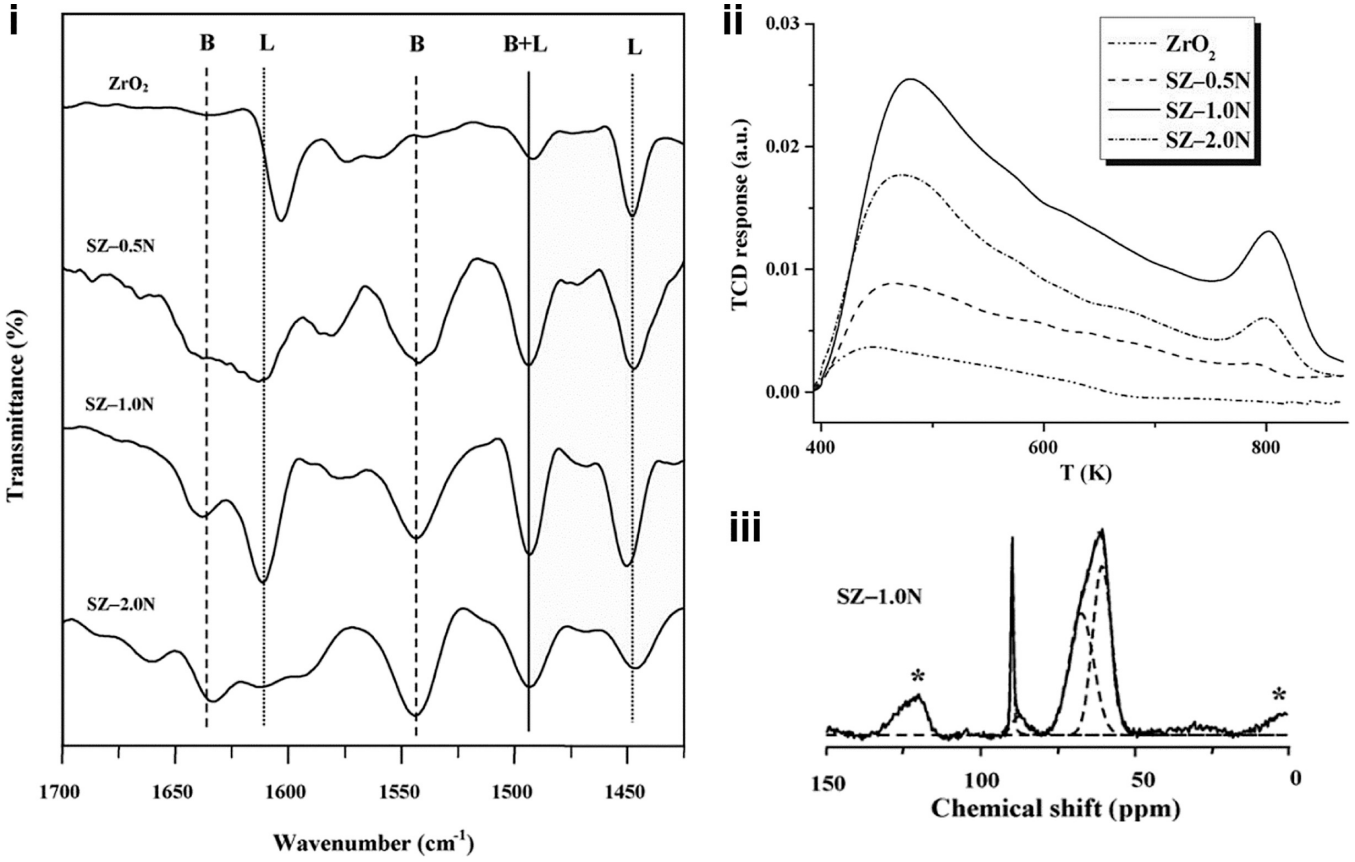

Figure 6. Zirconia and sulfated zirconia treated with a range of sulfating agent concentrations, 0.5−2 M, prior to calcination and analysis by (i) FT-IR spectroscopy of adsorbed pyridine and (ii) temperature programmed desorption of NH_3. (iii) ^{31}P ssNMR spectra of trimethylphosphine oxide adsorbed on dehydrated sulfated zirconia treated with a 1.0 M sulfating agent prior to calcination. Adapted by combining the three figures and modifying (iii) to not show spectra of several other samples with permission from ref 64. Copyright 2006 Elsevier.

strongly acidic functional moieties (e.g., acidic polymers, metal nanoparticles, oxyanions, etc.) distort sheet structures, generating disordered and obstructed pores that are difficult to characterize and synthesize reproducibly.[90,111] Thus, ordered pores in 3D architectures remain a more tenable platform for the study of superacid confinement. However, for these architectures, the dimensionality of the pores themselves must also be considered. When coking occurs in zeolites with small-diameter, 1D pores (i.e., mordenite and zeolite-β), it may block an entire channel of active sites and cause rapid deactivation. Multidimensional, interconnecting porous networks are generally less prone to coking deactivation and can facilitate reaction pathways with larger intermediates. Although HZSM-5 has smaller pore sizes than mordenite, its larger interpore junctions allow larger species to form.[50] Additionally, since ideal chemical depolymerization products are small olefins that can contribute to coking, porous architectures must also be designed to promote the rapid diffusion of small products away from the active site.[18,50,112] In summary, while pore confinement substantially improves mass transport, selectivity, and long-term activity, the pore width, depth, dimensionality, and surface energy must be carefully controlled. Moreover, given the influence of pore confinement effects and the numerous domains of acid strength, structure, and accessibility found in solid acids, accurate characterization of acidity remains challenging.

Challenges in Evaluating Solid Acidity and Superacidity. Characterization of a solid surface requires skilled analysis and data interpretation of the abundance, strength, and accessibility of individual acidic surface structures. In liquids, superacidity is the result of the intrinsic protonation ability of the Brønsted acid, the stability of its conjugate base, and that base's adduct formation with a Lewis acid.[55,76,82] While all of these factors contribute directly to Brønsted acid strength in the form of H_0 in liquid acids, many factors that contribute to a solid acid's catalytic activity are not accurately quantified by metrics that only characterize Brønsted or Lewis acidity. This is because the definitions for acidity and superacidity were designed for liquid systems and measurement of homogeneous Brønsted acidity.[55,59,81,113] However, heterogeneous surfaces typically have multiple "active sites" of varying acidity and strength, that are impacted by their chemical environment, physical confinement, and spatial proximity to other surface features. Thus, acidity on solid surfaces fundamentally differs from liquids.[76] For example, the stabilization of reactive intermediates is driven by the density and strength of *proximal* surface features on solid acid surfaces.[59,102] The diversity of acid strength, type, proximity, and accessibility of acid sites on solid surfaces, as well as the more complex role of Lewis acidity, make evaluating solid acidity much more challenging.[71,76,85] Though mischaracterization issues abound in the literature, when the individual acid strength of common solid acids is isolated, it is not clear if any have a Brønsted acid strength greater than sulfuric acid, meaning they are not superacidic according to classic definitions.[63,89,90] However, there is no denying that staple

https://doi.org/10.1021/acs.langmuir.3c03966
Langmuir XXXX, XXX, XXX−XXX

Pursuant to the DOE Public Access Plan, this document represents the authors' peer-reviewed, accepted manuscript. The published version of the article is available from the relevant publisher.

solid acids like HZSM-5 and sulfated zirconia are capable of performing low-temperature hydrocarbon conversions.[50,57] Thus, proper characterization of strong solid acids demands extensive analytical and catalytic analysis that targets both Brønsted and Lewis acidity, while considering additional effects from the active site environment.

The limitations of solid acid characterization are discussed thoroughly elsewhere;[63−68,74] thus, we will identify only the most relevant factors that impact evaluation of functional acidity (i.e., acidity valued in terms of catalytic performance) in SZrO. Hammett acidity was designed to quantify the strength of a single, concentrated, homogeneous Brønsted acid species in liquids by colorimetric titration of weakly basic amine and aromatic probes.[113] Such titrants are not reliable solid acid probes, as not only will hydration and size-exclusion of the bulky aromatic probes impede accuracy but also color-indication will be impacted by a variety of acid strengths.[67,81,113] Thus, a solid superacid's catalytic potential cannot be defined by a single numerical value like Hammet acidity. Though modern characterization of solid acids employs spectroscopic techniques to individually probe Brønsted and Lewis acidity with better accuracy, these techniques generally still rely on weakly basic probe molecules that experience similar diffusivity and sensitivity issues.[67] The techniques discussed below are the most widely accessible tools for the characterization of solid acids.

Spectroscopic Evaluation of Acidity. While direct analysis of O−H bond vibrations with FT-IR spectroscopy can approximate the strength, relative abundance, and coordination mode of hydroxyl moieties (Brønsted acidity) and surface-bound sulfates (bridging, chelating, etc.), indirect analysis through basic surface adsorbents allows identification and quantification of both Brønsted and Lewis acid sites.[67,114] However, factors like probe basicity and diameter can impact the accuracy of acidity profiling. While weak bases like pyridine (pK_a = 5.23) only chemisorb at strong Brønsted or Lewis acidic sites (Figure 6i), stronger Lewis bases like CO interact with weaker acids but only Lewis acid sites.[105,114−116] As even weak acids contribute to catalytic driving forces, very basic probes may be necessary to fully characterize a surface.[117] Additionally, basicity expressed on certain amphoteric metal oxide acid catalysts may still contribute catalytically, demanding characterization with acidic gas probes (CO_2, SO_2, etc.).[71,116,118] The dimensions of the probe molecule should also be capable of probing active sites accessible to expected reactant and intermediate molecules. For example, pyridine's kinetic diameter (KD = 0.54 nm) and rigid structure limits its access in micropores (<2 nm) compared to CO (KD = 0.38 nm).[67,116] Varying probe KD, typically by functionalizing a basic probe (e.g., pyridine, acetonitrile) with sterically bulky alkyl groups, can help characterize active site accessibility.[67,110] Sensitivity can be enhanced by techniques like UV−Visible spectroscopy, Raman spectroscopy, and diffuse reflectance infrared Fourier transform spectroscopy (DRIFTS), but these methods still only provide a description of acid type and acid strength.[67,74,114,116,117]

Sensitivity to acid strength and density can be enhanced by pairing techniques (e.g., FT-IR spectroscopy) with calorimetric desorption analyses like temperature-programmed desorption (TPD) or microcalorimetry. While microcalorimetry yields similar information about acidic solids, TPD of a small, volatile, very basic probe (typically NH_3) stands as the lowest complexity method of determining abundance and strength of acid sites.[68,119−121] The temperature at which a particular amount of NH_3 desorbs (Figure 6ii) can be correlated to the quantity of sites with a particular binding energy, acid strength, or even approximate H_0 using Katada et al.'s model. However, Brønsted versus Lewis acidity cannot be distinguished, and this strongly basic probe can reabsorb during exit-diffusion, form secondary adsorption layers, and may undergo disproportionation, impeding accuracy.[59,67,114,120,122] Similarly, bulkier probes can experience slower diffusion and reabsorption in small pores. Additionally, pyridine's low volatility and overlap of Brønsted and Lewis acid signals make binding energy nontrivial to calculate.[68,105,117,120] The density of acid sites must also be considered when selecting a probe. For example, benzene and pyridine's large aromatic rings donate electron density into sulfates that are proximal to SZrO's Lewis acid sites.[112,115] Thus, smaller, softer probe molecules such as CO may be required to measure Lewis acidity without displacing surface structures, though stronger bases may undergo complicating reactions with the surface.[116] Still, weak bases like pyridine can better distinguish the strength of stronger acid sites than very basic probes. For example, theoretical adsorption energies at the strong and weak Lewis acid sites of SZrO for pyridine suggest a significant difference in strength (−25 kcal/mol and −5 kcal/mol), but the difference was relatively more marginal for ammonia (−25.90 kcal/mol to −19.15 kcal/mol).[123] Where many adsorption probes cannot fully distinguish Brønsted from Lewis acidity, reactive probes like isopropylamine, converted into ammonia and propene by Brønsted acids, allow selective acid site quantification but require more complex/costly TGA-MS analysis.[120,124] Rather than analyzing the combination of strong/weak base and small/large probes necessary to characterize all of a solid acid's active sites with TPD and FT-IR spectroscopy, ^{31}P probe ssNMR spectroscopy can more efficiently characterize both acid types, their abundance, and strength.[67]

Similar to FT-IR spectroscopy, acidity characterization by ssNMR spectroscopy is enhanced by indirect analysis of basic probes. While deuterated FT-IR spectroscopy probe molecules can reduce overlap of interfering signals from the probe,[125] solvent and other extraneous signals can be fully eliminated with deuterated molecules in NMR spectroscopy, allowing analysis of better isolated catalyst signals and observation of solvation impacts.[67,74] The nuclei's natural abundance, range and separation of chemical shifts for Brønsted and Lewis acid sites, and sensitivity to acid strength must all be considered in probe selection.[67,74] The 100% natural abundance and chemical shift range (>650 ppm) of ^{31}P probe-based ssNMR spectroscopy (Figure 6iii) make trimethylphosphine (TMP) and trimethylphosphine oxide (TMPO) powerful probe molecules for determining concentration, strength, and location with good discrimination of Brønsted and Lewis acidity. Superior stability and reduced steric bulk around TMPO's (KD = 0.55 nm) oxygen atom compared to the nucleophilic atoms of pyridine and TMP make TMPO and its homologues of larger alkyl/aryl groups (R_3PO) better suited to determine the location of Brønsted and Lewis acid sites in porous solids by size exclusion.[63,67,74,83,110,126] Though deprotonation energy derived from ^{31}P chemical shift only measures Brønsted acidity, multinuclear-2D ssNMR spectroscopy methods (e.g., transfer of populations in double resonance (TRAPDOR), heteronuclear correlation (HETCOR), $^{31}P-^{31}P$ double-quantum (DQ)) can relate Brønsted and Lewis acid sites through cross-polarization and spatial

https://doi.org/10.1021/acs.langmuir.3c03966
Langmuir XXXX, XXX, XXX−XXX

Pursuant to the DOE Public Access Plan, this document represents the authors' peer-reviewed, accepted manuscript. The published version of the article is available from the relevant publisher.

resolution of peak-pairs.[67,74] Still, TMPO, TMP, and pyridine probes are too large for complete characterization of some microporous and high acid density solids.[74,110] Additionally, the likelihood of inaccuracies, particularly for Lewis acids, related to steric repulsion, probe basicity, surface hydration, probe oxidation by air or oxide surfaces, and retention of solvents in probe-based techniques mean secondary verification will always be necessary when profiling solid acidity.[63,65,67,74,85] It is increasingly apparent that most probe-based spectroscopy and calorimetry techniques do not accurately isolate acid strength from other solid surface effects.

The interactions between a solid's surface features and the probe molecule differ with acid strength, density, softness, type, and the active site's accessibility and the probe's interactions with neighboring features of the surface and pore environment. To accurately evaluate surface acidity through ssNMR spectroscopy, FT-IR spectroscopy, and TPD, probe molecules should be chosen to model reactant behavior, and results must always be interpreted with care. Probe selection can be better informed by surface area and pore size distribution determined from physisorption of small, inert gaseous probes (e.g., N_2, Ar). However, Brunauer–Emmett–Teller (BET) analysis of 77 K N_2 or 87 K Ar gas adsorption data cannot accurately define microporous domains, and alternatives like non localized density functional theory (NLDFT) that improve micropore approximations are not accessible or developed enough to easily model hierarchical porosity.[127] To explore the implications of pore dimensions on these analytical probes, Gorte and Parillo performed microcalorimetry of NH_3, pyridine, and isopropylamine adsorption on zeolites of varying pore dimensions and acid site densities (i.e., HZSM-5, HZSM-12, H-Y, H-mordenite). Though the acid sites of these zeolites were theoretically identical in strength, desorption was delayed to different temperatures by different pore dimensions, denser acidity, and other confinement effects.[68,105,114,120] Thus, in experiments like TPD higher desorption temperatures may not be the result of differences in acid strength. Additionally, while heats of adsorption for small probes (ammonia) are similar for all the zeolites, the larger probes (pyridine and isopropylamine) have higher adsorption energies that vary more across the zeolites studied, meaning steric and electrostatic effects also impede diffusion of bulkier or more polar probes.[68,78,105] In fact, the extended alkyl groups of R_3PO and derivatives of other probes appear to have additional interactions with the environment surrounding the active site. Where higher chemical shifts indicate stronger Brønsted acidity, Mafra's group identified that the highest ^{31}P ssNMR spectroscopy shift (>86 ppm) observed for TMPO adsorbed on HZSM-5 is not due to stronger acidity.[63] Instead, pore-confined active sites appear stronger due to van der Waals interactions promoting diffusion of the protonated probe away from the Brønsted acidic hydroxyl group, elongating its O–H bond so it appears at a higher chemical shift.[63,83] As further evidence, the highest reported ^{31}P chemical shift for TMPO adsorbed on a solid acid was for the previously discussed 2D architecture synthesized to maximize mass transfer, MMT@PAN[C_3N][SO_3CF_3]. However, TMPO chemical shifts for the vast majority of solid acids, including HZSM-5 and SZrO, do not have a TMPO ^{31}P chemical shift greater than sulfuric acid and would not be considered superacidic even with these mass transfer effects (Figure 7).[83,90] Though this does not match the classic definition of superacidity or explain all solid superacid-like activity, like the relatively shallow pores and impressive functional acidity of SZrO, high mass transfer and other confinement effects may be the source of superacid-like activity in some solids. However, it is apparent that these probe molecule-based analytical techniques do not isolate Brønsted or Lewis acid strength from other interactions between the probe and the surface. While confinement effects and other factors that influence these probes are catalytically relevant, many are not accounted for by Hammett acidity and other definitions for superacidity that were designed for liquid acids.[76,81]

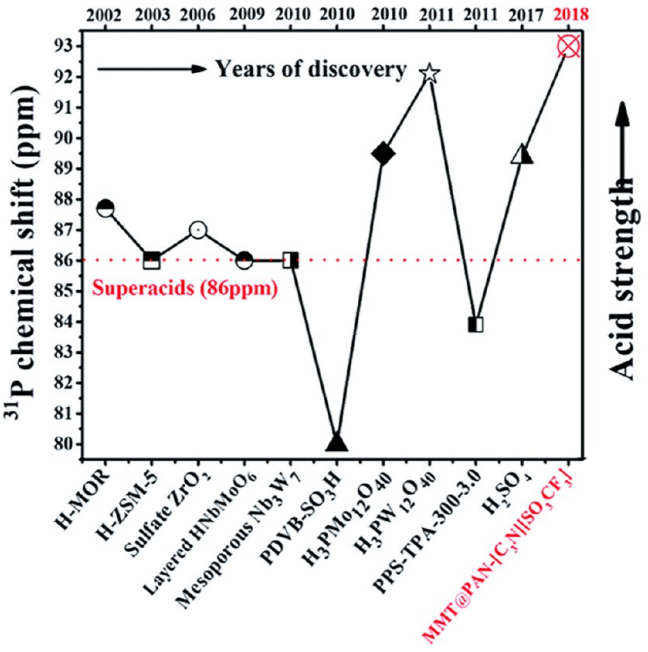

Figure 7. ^{31}P ssNMR spectroscopy chemical shifts for trimethyl phosphine oxide chemisorbed by acid catalysts ordered by year reported. Reprinted with permission from ref 90. Copyright 2019 the Royal Society of Chemistry.

Probes that resemble reactant molecules should better reflect relevant surface–reactant interactions. Analysis of deuterated alkanes dissolved in liquid superacids by NMR spectroscopy has previously proven useful in analyzing reaction kinetics based on hydrogen/deuterium (H/D) exchange rate.[55,76,78,128] H/D exchange also allows comparison of solid to liquid acids, but results still indicate that solid "superacids" resemble weaker liquid acids rather than superacids.[76] Confinement effects clearly impact this event, as smaller pores in zeolites with similar acidity promote H/D exchange.[128] Interestingly, H/D exchange on alkanes in the presence of strong acids occurs at temperatures lower than the C–C bond cracking reactions, suggesting that protonation of alkanes is more favorable than the subsequent hydrocarbon cracking via C–C bond scission.[76] Thus, it is apparent that the elements of solid superacidic expression cannot be fully evaluated with the aforementioned probe-based analytical techniques alone. While these techniques prove useful in comparing solids of similar acid density and hierarchical porosity, solid and liquid acid catalysts may only be accurately compared based on their functional acidity in catalytic testing, in which the turnover rate, life span, and selectivity of the catalyst are emphasized and acid site strength metrics are secondary.

https://doi.org/10.1021/acs.langmuir.3c03966
Langmuir XXXX, XXX, XXX–XXX

Pursuant to the DOE Public Access Plan, this document represents the authors' peer-reviewed, accepted manuscript.
The published version of the article is available from the relevant publisher.

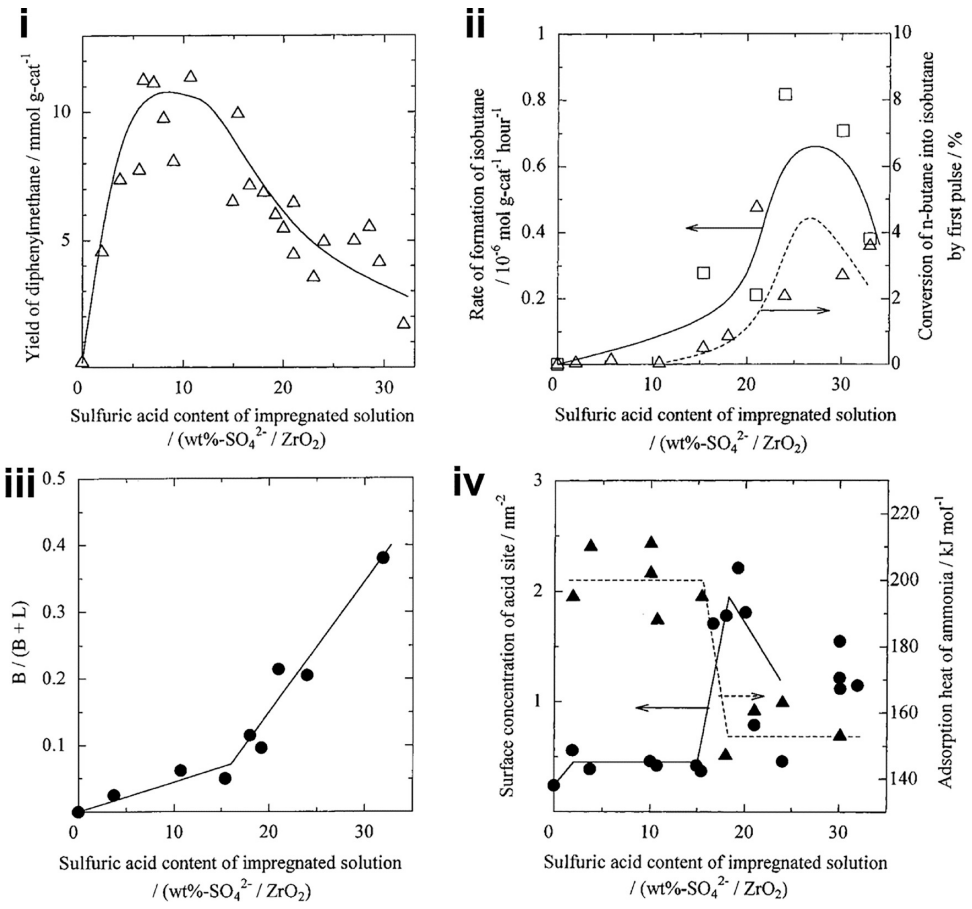

Figure 8. Performance of sulfated zirconia catalysts in the (i) alkylation of benzene and (ii) isomerization of *n*-butane (solid and dashed lines represent closed circular and pulse reaction experiments, respectively), their (iii) relative expression of Brønsted and Lewis acid sites based on pyridine-FT-IR spectroscopy, and (iv) the concentration and strength of these acid sites according to NH_3-TPD. The various sulfated zirconia samples were prepared using a range of sulfuric acid concentrations (0.26−4.4 M in 100 mL) to deposit sulfates prior to calcination. Adapted by combining four figures with permission from ref 59. Copyright 2000 American Chemical Society.

Catalytic Evaluation of Acidity. Catalytic testing is imperative to accrediting solid acids with superacid-like behavior that may not be detectable by analytical characterization methods, particularly for SZrO. Certain hydrocarbon conversions have even proven to be valuable in selectively evaluating Brønsted and Lewis acidity.[50,56,57,59] Though it is impossible to unambiguously distinguish the acid type responsible for catalyzing the reaction from the role of confinement effects and other surface interactions, the product distribution and kinetics of a test reaction can provide an estimation of type, density, and strength of the accessible acid sites. For example, even though sulfated tin oxide has greater Brønsted acidic strength, SZrO's expression of an abundance of both Brønsted and Lewis acid sites generated superior selectivity for cracking products in the alkylation of 2-butene. Thus, the potential of solid acids that express primarily Brønsted or Lewis acid sites and the cooperative benefits of Brønsted−Lewis pairs may only be observed catalytically in some cases.[56,89,129] Test reactions can also be useful in distinguishing the impact of synthetic conditions on a catalyst's expression of acid strength and acid density, such as identifying that SZrO has two catalytically valuable forms: one that expresses both strong Brønsted and Lewis acid sites and another that expresses little to no Lewis acidity but a high density of relatively weak Brønsted acid sites. For SZrO, when more concentrated impregnation solutions of sulfating agent (e.g., dilute H_2SO_4, which is discussed in detail in the Impregnation Sulfation section) are used, the sulfate loading on the resulting SZrO increases (to an uptake limit). While sulfate loading progressively increases the Brønsted acid site density, Lewis acidity is progressively eliminated and the strength of all Brønsted acid sites decreases. Two test reactions were needed to distinguish these catalytically valuable forms of SZrO.[59,130] The isomerization of *n*-butane has two reaction pathways: a monomolecular pathway driven by isolated strong acid sites at high temperatures and a bimolecular pathway driven by dense, weaker acid sites at lower temperatures.[50] It seems SZrO's *n*-butane isomerization follows the bimolecular path catalyzed by weaker acids, as its activity is insensitive to acid strength and the expression of Lewis acidity, increasing with continued sulfation and Brønsted acid density (Figure 8ii). On the other hand, benzene alkylation is sensitive to acid strength and Lewis acid expression. SZrO's benzene alkylation activity increases with surface area and the less abundant, stronger acid sites that are expressed at lower sulfate loadings (Figure 8i).[59] Thus, test reactions can be useful in validating analytically determined acidity as well as identifying which of the factors that define functional acidity is most important in a targeted application.

Test reactions can also be used to investigate the implications of porosity in conjunction with expressed acidity. The dimensions of the reactants and intermediates drive

https://doi.org/10.1021/acs.langmuir.3c03966
Langmuir XXXX, XXX, XXX−XXX

Pursuant to the DOE Public Access Plan, this document represents the authors' peer-reviewed, accepted manuscript. The published version of the article is available from the relevant publisher.

selectivity and activity in porous systems. Even some of the strongest zeolites like mordenite do not have strong enough acid sites to catalyze the monomolecular *n*-butane isomerization pathway.[50,59] Mordenite's narrow, 1-dimensional pores are also incompatible with the bimolecular pathway's bulky intermediates, causing a slow bimolecular conversion to isobutane. Although H-ZSM5 has weaker acid sites and more narrow pores than mordenite, wider junctions in its 3-dimensional porous network permit bulky intermediate formation, facilitating its better isomerization activity. However, by dealuminating to introduce mesopores, *n*-butane isomerization in mordenite can more easily follow the bimolecular pathway and has greater activity than the weaker acid sites of HZSM-5.[50]

Analysis of a solid acid's product distribution when informed by analytical acidity characterization can also be useful in predicting its surface features. For example, methylbutynol (MBOH) could potentially probe the presence of proximal Brønsted−Lewis acid pairs, as peak expression of both Brønsted and Lewis acid sites on SZrO and sulfated alumina maximizes prenal production, a product not typically observed on primarily Brønsted or Lewis acidic solids. MBOH can also generate other unique products over basic, amphoteric, and acidic surfaces, allowing it to screen numerous surface properties at once.[131,132] Thus, test reactions for a specific application can be a more efficient catalyst screening tool than analytical probe-based methods. For novel catalysts, it is critical to analyze the material's performance in multiple test reactions, particularly those that can probe the acid type, strength, density, and impacts of the surrounding architecture.[50,57,132]

However, there is a core concern with such strong acids, namely that rapid coking and deactivation leads to changes in selectivity and activity as only weaker acid sites remain after an "incubation period". For example, the impressive cracking ability of the most strongly acidic form of SZrO generates a large number of olefins on its surface, causing rapid coking and deactivation of strong acid sites, particularly Lewis acids.[18,50,59,112] While pore-confined derivatives could prolong strong acid expression, SZrO is extremely challenging to synthesize with stable and ordered mesoporosity and limited exterior acidity without modifying it with support materials.[50,133−135] Instead, the initial activity and selectivity can be extended by using pulse-reactions to reduce the coking/deactivation rate, wherein small doses of reactants are delivered instead of a dense reactant stream. Pulse reactions, like those performed by Katada et al. (Figure 8ii), allow analysis of the selectivity and activity driven by strong acid sites and should better reflect the activity and slower coking of strong acids that are confined in pores.[59,79,94,136] As pore-confined acids have additional kinetic limitations regarding diffusivity, pulse-reactions are best suited for systems with negligible restraints on diffusion. Still, pulse dosing could allow comparison of bulk catalysts with pore-confined derivatives to distinguish the influence of pore diameter, depth, dimensionality, and confinement effects. Verifying the successful development of a catalyst suited for the efficient depolymerization of POs requires an improved standard in the characterization of solid acid catalysts; one that relies on detailed screening of reactant and product interactions with the surface and is informed by robust structural and acidity analysis.

Recommended Standards in Solid Acid Characterization. To this end, we propose the following protocols to guide the study of solid acidic materials. (i) Reactions for which acidity is being probed as a catalytic tool should be screened over a variety of discrete Brønsted (e.g., $Cs_2HPW_{12}O_{40}$) and Lewis (e.g., tungstated alumina) acid expressing solids of similar surface features, and in protic and aprotic solvents where necessary, to illuminate their mechanistic roles.[50,130,137] Probing a variety of the previously discussed test reactions initiated primarily by Brønsted or Lewis acids or a particular acid strength can also be valuable.[50,112,130] (ii) An even more direct comparison of the role of Brønsted and Lewis acidity is the modification of known catalysts to enhance or repress a specific acid type/strength, such as doping with Lewis acidic metal nanoparticles or selective deactivation with Brønsted or Lewis basic probes. Indeed, targeted poisoning with analytical basic probes molecules (e.g., NH_3, pyridine) and alkali metals has been demonstrated.[92,138−140] For example, the number of strong acid sites on a SZrO sample (25 μmol/g) was determined by NH_3 microcalorimetry and then poisoned with an excess of NH_3 (30 μmol/g) to observe the impact of deactivating its strong acid sites. This method eliminated the incubation period in which strong acid sites are progressively deactivated by coking during *n*-butane isomerization.[92] (iii) One should probe the reactivity of the individual components of complex catalysts. For example, in a core@shell architecture, test reactions should be performed on the isolated core and pore shell support, bulk catalyst, core loaded with the acidic active sites, and the pore-confined catalyst.[41] Pore depth, pore diameter, support surface energy, and polymer melt temperature should be considered to effectively facilitate mass transfer and selectivity. For depolymerization in porous materials specifically, testing alkanes of various length can elucidate reaction and mass transfer rates for POs of target molecular weight and cracked products. (iv) Finally, activation procedures must be optimized for each catalyst, since more ionic oxides require a more thorough outgassing step to desorb water and express Lewis acidity.[60,121]

Confining strong catalysts inside porous supports is an increasingly popular technique that without significant structural characterization may instead generate a physical mixture of the two materials instead of sterically confined active sites.[141] These issues are particularly prevalent in the evaluation of solid acids, which are often composed of mixed oxides and nanoparticle dopants.[51,69,142−144] Thus, guidelines for the characterization of pore-confined catalyst systems have been proposed, including: (i) rigorous analytical analysis of the bulk catalyst, porous support, and the composite (powder X-ray diffraction (PXRD), FT-IR spectroscopy, scanning electron microscopy (SEM)/transmission electron microscopy (TEM) with energy dispersive X-ray spectroscopy (EDS), TGA, and N_2 77 K physisorption); (ii) characterization over a range of values relevant to all structural components; and (iii) identification and attempts to prove/disprove a theory explaining inconsistencies that arise.[141] Analytical characterization with the previously described chemisorbing probes should be performed with a range of molecules, with particular considerations for their stability and diffusivity. Adsorption assumes that an isolated acid site is analyzed with a standard orientation of the probe; however, on a heterogeneous surface, the proximity of other acidic structures can cause migration and unique probe orientations due to hydrogen bonding and other interactions with neighboring species.[63,105,116,123] The interactions between sulfates and probe molecules (e.g.,

https://doi.org/10.1021/acs.langmuir.3c03966
Langmuir XXXX, XXX, XXX−XXX

Pursuant to the DOE Public Access Plan, this document represents the authors' peer-reviewed, accepted manuscript. The published version of the article is available from the relevant publisher.

ammonia, acetonitrile, pyridine) on SZrO may even cause sulfate desorption and lower sulfate decomposition temperatures.[96,140] Thus, post-mortem acid catalysts should not be reused between multiple modes or rounds of characterization outside of catalyst recylability studies. Employing probes with a range of basicity, Lewis or Brønsted selectivity, and kinetic diameters will allow identification of ambiguities related to the individual probes and a more complete profile of solid acidity.[64] Still, other variables that influence the diffusion and interactions of probe and reactant molecules with the surface result in variability that can make kinetic and activation energy measurements inaccurate, particularly when small gaseous molecules are consumed or produced.[96,140] Thus, specifying the *apparent* or *functional* acidity based on catalytic function is a more feasible means of representing solid acidity and comparing acids of different phases/architectures.

We strongly emphasize that at all steps of synthesis, characterization, activation, and catalytic testing extremely thorough procedure reporting is necessary due to the sensitivity of solid acids. The Supporting information for acid catalyst development articles must be detailed enough to allow minor alterations to procedural variables to be diagnosed as the root cause of differences in expressed acidity. Despite these complicating factors, the value of solid acidity and superacid-like acidity have not been completely overlooked.

Solid Superacids. Solid superacidity is often associated with the protonation ability of zeolites. Though zeolites express Brønsted acidity comparable to the weakly acidic form of SZrO (i.e., with a sulfate-saturated surface), heterogeneous surface effects like mass transfer and intermediate stabilization drive their impressive protonation ability not just pure Brønsted acid strength.[63,74,104] Other reported superacid-like solids are generally a combination of porous supports that compose typical solid acids (e.g., zeolites, transition metal oxides, hydroxyapatite) with electron-withdrawing groups that make up strong liquid acids (e.g., phosphates, sulfates, chloric acids, transition metal−halogen salts).[71,78,145] Supports are generally affordable, earth-abundant materials with tunable porosity and high surface energy/acidity that enhance the porosity and surface area of more expensive catalysts. The thermal stability and uniform porosity of synthetic silica, alumina, and aluminosilicates make them ideal architectures for pore-confinement.[77,146] Though generally less stable, polymeric membranes (i.e., sulfonated tetrafluoroethylene) and carbonaceous supports have an impressive number of hydrogen bonding functionalities that promote mass transfer and can enable superacid-like activity.[90,145] Deposition of stronger acidic species on the support, such as metal−halogen salts, single-site organometallic catalysts, heteropolyacids, ionic liquids, transition metal oxides, Lewis acidic metal nanoparticles, and oxyanions, can further increase acid strength and density.[57,71,78,79,86,145,147] Other materials known to generate particularly strong, even superacidic, solid acidity include carborane clusters, heteropolyacids, and metal−organic frameworks (MOFs); however, their relative instability, cost, and/or complexity cannot compete with superacids derived from earth-abundant metal oxides.[72,73,145,148,149] Specifically, the strongest and most stable solid acids are historically metal oxides functionalized with oxyanions, such as B_2O_3, WO_4^{2-}, MoO_4^{2-}, PO_4^{3-}, and, of course, SO_4^{2-}.[70,79]

While most metal oxides are basic and there are many exceptions to the following trends, relatively more electronegative metals often form more acidic oxides, and transition metals with intermediate oxidation states are generally amphoteric oxides, capable of expressing both acid and base behavior. Metal oxides typically terminate with surface O^{2-} anions but are prone to defects that enhance their surface energy. Upon exposure to water, surface hydroxyl groups are generated that can behave as Brønsted acids or bases, while coordinatively unsaturated oxygens and metals can act as Lewis bases and Lewis acids, respectively. These amphoteric metal oxides will act as acids toward strong bases and will act as bases toward strong acids.[54,70,71,114,150] Without modification, earth-abundant, amphoteric, transition metaloxides like zirconia exhibit weak acid/base sites, while more electronegative metal oxides like alumina and silica exhibit stronger acidity.[54,71] Although pure metal oxides make useful catalysts (e.g., for isomerization, epoxide synthesis, aldol condensation),[71,77] the inductive effect of surface-deposited electron-withdrawing groups polarize the surface and draw electron density away from the surface structures. This enhances the Brønsted acidity of hydroxyl groups by stabilizing their conjugate bases and the Lewis acidity of coordinatively unsaturated metals by making them more electropositive. Particularly, the sulfated Sn, Fe, Zr, Hf, Ti, and Al oxides (sometimes with promoter metal nanoparticles) demonstrate superacid-like protonation capabilities, create minimal damage to reactor infrastructure, and have impressive stability under reaction conditions.[55,79,151] Sulfation of metal oxides not only generates new Brønsted acid sites and increases acid strength but also stabilizes the metal oxide crystal phase during catalytic use and regeneration (e.g., higher zirconia crystal phase transition temperatures as discussed in the Sulfation and Crystallization During Calcination section).[57,152] Other oxyanion treatments may produce zirconia with higher (e.g., WO_4^{2-}) or lower (e.g., B_2O_3, PO_4^{3-}) surface area, but they also generally yield lower acid strength and acid density than sulfation.[57,70,137,152] SZrO is a particularly effective acid catalyst as zirconia is a relatively more ionic amongst amphoteric metal oxides, has high surface energy facets, and retains its sulfate loading at higher calcination and reaction temperatures than other sulfated metal oxides.[56,112,121]

The density of both SZrO's Brønsted and Lewis acids appears to play a central role in its observed C−C bond cracking ability.[56,112] For comparison, sulfated SnO_2 has the strongest Brønsted acidity among sulfated metal oxides but no significant Lewis acidity. In reactions driven by Brønsted acid strength (e.g., phenol tertbutylation, toluene benzoylation, *n*-pentane isomerization) sulfated SnO_2 outcompetes SZrO. Since even sulfated tin oxide does not have Brønsted acid strength equal to H_2SO_4 (i.e., superacidic) according to ^{13}C acetone-ssNMR spectroscopy, SZrO's weaker Brønsted acid sites must not be particularly strong.[89,129,153] However, in the conversion of isobutene and 2-butene, SZrO produces a higher amount of cracking products than sulfated SnO_2 prior to the deactivation of its strong Lewis acids, suggesting that SZrO's expression of both strong Brønsted and Lewis acid sites facilitates more efficient C−C bond cracking.[56] On the other hand, pure zirconia and the other group IV metal oxides have a unique density of Lewis acids that are strong enough to bind the CO probe, greater than even the principle Lewis acidic metal oxide alumina. Zirconia also has a higher fraction of highly coordinatively unsaturated cations on its surface than TiO_2 and HfO_2.[60,121] Though the strength of these Lewis acids increases when zirconia is sulfated, they are still much weaker in strength than sulfated and even unsulfated alumina. Still,

https://doi.org/10.1021/acs.langmuir.3c03966
Langmuir XXXX, XXX, XXX−XXX

Pursuant to the DOE Public Access Plan, this document represents the authors' peer-reviewed, accepted manuscript. The published version of the article is available from the relevant publisher.

SZrO has more Brønsted acid sites and a number of Lewis acid sites detectable by pyridine-FT-IR spectroscopy comparable to sulfated alumina. Since the sulfated catalysts have comparable alkylation abilities, a reaction sensitive to Lewis acidity, SZrO's weaker Lewis acids are still strong enough to be catalytically valuable.[60,112,121] However, alumina is not Lewis superacidic, so SZrO's weaker Lewis acids cannot explain its superacid-like activity either.[60,112,121] Though SZrO's Brønsted and Lewis acids are weaker compared to the more strongly acidic sulfated oxides highlighted above, it has a unique density of both Brønsted and Lewis acids among solid acids. Thus, numerous research groups have speculated that SZrO's superacid-like alkane cracking ability arises from cooperativity between proximal Brønsted–Lewis acid pair sites.[50,60,92,112,131,151] The synthetic parameters necessary to generating SZrO's Brønsted and Lewis acid sites must be clearly defined to enable its use in PO depolymerization.

SULFATED ZIRCONIA

SZrO was patented in 1962, and by 1979, it had gained attention as a low-temperature hydrocarbon isomerization agent.[154,155] More specifically, SZrO has found industrial use as a fuel-upgrading catalyst, as it can efficiently increase the octane number of gasoline via paraffin isomerization. SZrO's uses also extend to numerous industries (e.g., pharmaceutical, fine chemical synthesis, biomass conversion), a variety of acid and redox reactions (e.g., alkylation, benzylation, condensation, acylation, esterification, methanol reduction, Fischer–Tropsch conversions), and even fuel-cells and photoluminescence.[50,57,133,156] SZrO's worth in oligomerization and cracking reactions has already been demonstrated, though the strong acid sites needed to catalyze these reactions are rapidly deactivated by coking and hydration. Thus, SZrO is primarily employed in forms where its strongest acid sites have been deactivated or replaced with a high density of weaker Brønsted acid sites.[57,157,158] Nonetheless, SZrO's weaker acid sites are still strong enough to catalyze numerous reactions at impressively mild temperatures and pressures. Most prominently, SZrO modified with supports and metal-dopants is currently employed in the isomerization of *n*-butane to isobutane at temperatures as low as 120 °C.[50,158] Yadav and Nair have extensively discussed the selectivity and conversion rates of SZrO in numerous reactions, demonstrating its competitive catalytic capabilities and the potential it had to replace homogeneous catalysts and other solid acids at the turn of the century.[57]

Indeed, superacid-like SZrO is a promising PO depolymerization catalyst capable of solvent-free alkane cracking below 200 °C.[22,35,37,159] Ideally, chain-end activation of POs by the strong acid sites of SZrO should protonate a C–H bond to release H_2 and generate a carbenium. Then, the polymer can undergo unimolecular β-scission along the polymer backbone to yield olefin monomers. However, very strong acids yield very weak conjugate bases that have weaker stabilizing interactions with the generated carbenium. As a result, SZrO's stronger acid sites generate less stable carbenium intermediates than the weaker acid sites found on other industrially employed solid acids (e.g., HZSM-5).[35] These highly unstable carbeniums are therefore likely to undergo intra- or intermolecular hydride abstraction to generate a more saturated carbenium. Additionally, SZrO does not have the porosity of HZSM-5 to promote chain-end activation of POs.[100,103,146] Thus, confinement of strongly acidic SZrO active sites in lower surface energy, mesoporous architectures should promote chain-end activation of POs, inhibit hydride transfer, and may enable small olefin production and efficient circular recycling of PO plastics (Figure 9).[37,41,46]

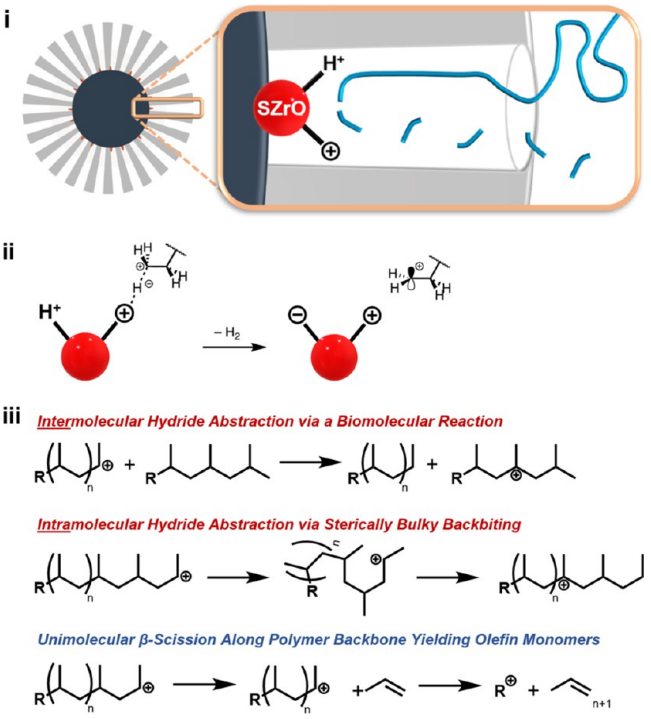

Figure 9. (i) Model of sulfated zirconia (SZrO) embedded at the end of 1D micropores (inset), wherein disaggregated polyolefins diffuse toward the active site and smaller products diffuse out of the pore. (ii) A proposed mechanism for polyolefin C–H bond elongation to ease protonation, release of H_2, and generation of reactive carbeniums over solid superacid-like catalysts. (iii) We hypothesize that carbenium formation in a micropore (≤2.0 nm) will impede hydride abstraction, promote β-scission, and enhance selectivity for olefin monomers.

Intrigued by the catalytic potential of SZrO, we began to study the structural features that define its acidity. The categorization of SZrO as a superacid is widely contested, as, even when considering inaccuracies in analytical characterization, its Brønsted acid sites are substantially weaker than the requisite criteria for superacidity in liquids.[60,89,125] Additionally, SZrO's generally shallow pores are unlikely to generate its superacid-like behavior through the confinement and mass transfer effects that facilitate similar paraffin protonation capability in 2D and 3D porous architectures.[63,90,146] Upon deeper examination of the literature, we made a very surprising realization: despite more than 40 years of industrial use and optimization, the active site structure of SZrO is poorly understood and reported syntheses are widely variable, undetailed, and unreliable.

Substantial ambiguity remains around SZrO's active site structure, the source of its superacid-like activity, and thus how its synthesis can be modulated to control acid density, strength, and catalytic performance (e.g., activity, selectivity, resistance to coking). While the literature of the previous century did much to begin optimization of SZrO's synthesis, its impressive and affordable catalytic function has led many to emphasize study of its application in place of atomic-level comprehension.[50,57,160] As a result, recent study of SZrO

https://doi.org/10.1021/acs.langmuir.3c03966
Langmuir XXXX, XXX, XXX−XXX

Pursuant to the DOE Public Access Plan, this document represents the authors' peer-reviewed, accepted manuscript.
The published version of the article is available from the relevant publisher.

Figure 10. In the synthesis of sulfated zirconia, $Zr(OH)_4$ must first be prepared in a manner that favors formation of a tetragonal crystal pattern upon calcination. Then $Zr(OH)_4$ is calcined at low temperatures to produce amorphous zirconia. Sulfates are then deposited and weakly coordinated to the amorphous zirconia surface and strongly coordinate to the crystalline zirconia surface formed during calcination at high temperatures. The zirconia surface then forms acidic hydroxyl groups upon room temperature (RT) air exposure. We hypothesize that the strong active site is composed of a Brønsted acidic site proximal to a coordinatively unsaturated Lewis acidic Zr(IV) site and a sulfate. The bonding structure is drawn with purposeful ambiguity.

largely generates more inconsistency than clarifying information. Most troublesome is the wide variability of its reported Brønsted acid strength. SZrO's acid strength and catalytic performance has demonstrated capabilities similar to both nonsuperacidic sulfuric acid ($H_0 = -12$) and competitive with some of the strongest liquid superacids ($H_0 = -19$).[59,70] In tandem with insufficient and improper use of the previously described acidity characterization tools, this expansive range of acid strengths stems from the sensitivity of sulfated metal-oxides to numerous synthetic variables that alter the expression and physical proximity of surface Brønsted and Lewis acid sites. Minor adjustment of synthetic variables like calcination temperature, sulfation conditions, and surface hydration expose different zirconia crystal phases/facets and unique active site structures.[59,64,161,162] Additionally, insufficient reporting of synthesis and activation conditions prior to analysis plagues the field of solid superacidity. Therefore, the remainder of this review will identify common sources of error in the synthesis of SZrO, critical synthesis and structural insights, and the knowledge gaps impeding the potential of SZrO as a PO depolymerization catalyst.

Ambiguity Surrounding Sulfated Zirconia. *Synthesis Procedures.* The standard synthetic procedure for SZrO can be summarized as the calcination of a $Zr(OH)_4$ precursor to tetragonal ZrO_2 in the presence of a SO_x source (Figure 10). Of particular importance is the method by which the $Zr(OH)_4$ precursor is generated. Though numerous syntheses are in circulation, the most common method is base precipitation of $Zr(OH)_4$ from a zirconyl salt, typically $ZrOCl_2$ or $ZrO(NO_3)_2$. The zirconyl source is dissolved in water and crashed out with concentrated NH_4OH via hydroxylation of the Zr(IV) salt. After either aging or reflux of the suspended solid to promote complete hydroxylation, the solid is washed and dried.[61,163−167] Previous reports have described the significance of a heating step prior to sulfation at a temperature below the transition point from amorphous to tetragonal crystalline zirconia, known as precalcination.[146,168] Thus, the procedure can be further deconstructed to include precalcination of the $Zr(OH)_4$ to amorphous zirconia, sulfation and calcination to form sulfated tetragonal phase zirconia, and rehydration to generate the majority of SZrO's surface hydroxyl groups. As the literature discussed below and our empirical evidence suggest, any modulation of the variables that compose these steps, from the rate of base addition to the composition of the calcination vessel, can significantly alter the resulting structure, and thus acidity, of SZrO.

Investigators identified as early as 1996 that the comparatively weak strength of SZrO's Lewis and Brønsted acid sites must have some cooperative behavior not seen in other forms of solid superacids that enables its catalytic performance.[60,92] Though studies during the first few decades of SZrO's prominence aimed to elucidate the nature of its structure−acidity relationship, these works and their resulting insights are largely overlooked by the subsequent era of studies screening potential applications toward industrial adoption. As a result, the 21st century's literature on SZrO is hampered by mischaracterization and deleteriously ambiguous reporting that does not build off the foundation of the previous century. Still, there is some fundamental knowledge that is agreed upon: (i) sulfation of zirconia's surface reduces the density of Lewis acid sites but dramatically increases the strength of those that remain; (ii) sulfation facilitates the expression of Brønsted acidity through hydroxyl, bisulfate (HSO_4^-), and pyrosulfate ($S_2O_7^{2-}$) moieties; (iii) increasing the sulfate loading to near surface saturation continues to increase the number of Brønsted acid sites, though these acid sites typically outnumber the sulfur atoms/nm^2; and (iv) completing or exceeding a monolayer of sulfates produces relatively weak Brønsted acid sites and no accessible Lewis acidity.[59,169]

Though many reaction rates increase with the number of Brønsted acid sites regardless of the SZrO's expression of Lewis acidity, paraffin cracking below 250 °C is most effective when stronger Brønsted and Lewis acid sites both contribute to its functional acidity.[59,112,131] The fact that two catalytically valuable forms of SZrO exist that increase activity in different types of reactions has contributed to conflicting reports of SZrO's most active phase either exhibiting less than superacidic protonation energy (i.e,. weaker than 100% sulfuric acid) or acidity 2−7 orders of magnitude stronger than the threshold for superacidity.[50,59,79] Thus, it became clear that the conditions under which SZrO is prepared significantly alter the expression of its Brønsted and Lewis acid sites, and both are ultimately necessary for its superacid-like low temperature C−C bond cracking ability. These are not tandem or bifunctional catalytic sites that perform separate reactions to generate one desired product.[170−173] Rather, SZrO's superacid-like activity is speculated to stem from cooperativity between the Brønsted and Lewis acid sites working together to

https://doi.org/10.1021/acs.langmuir.3c03966
Langmuir XXXX, XXX, XXX−XXX

Pursuant to the DOE Public Access Plan, this document represents the authors' peer-reviewed, accepted manuscript.
The published version of the article is available from the relevant publisher.

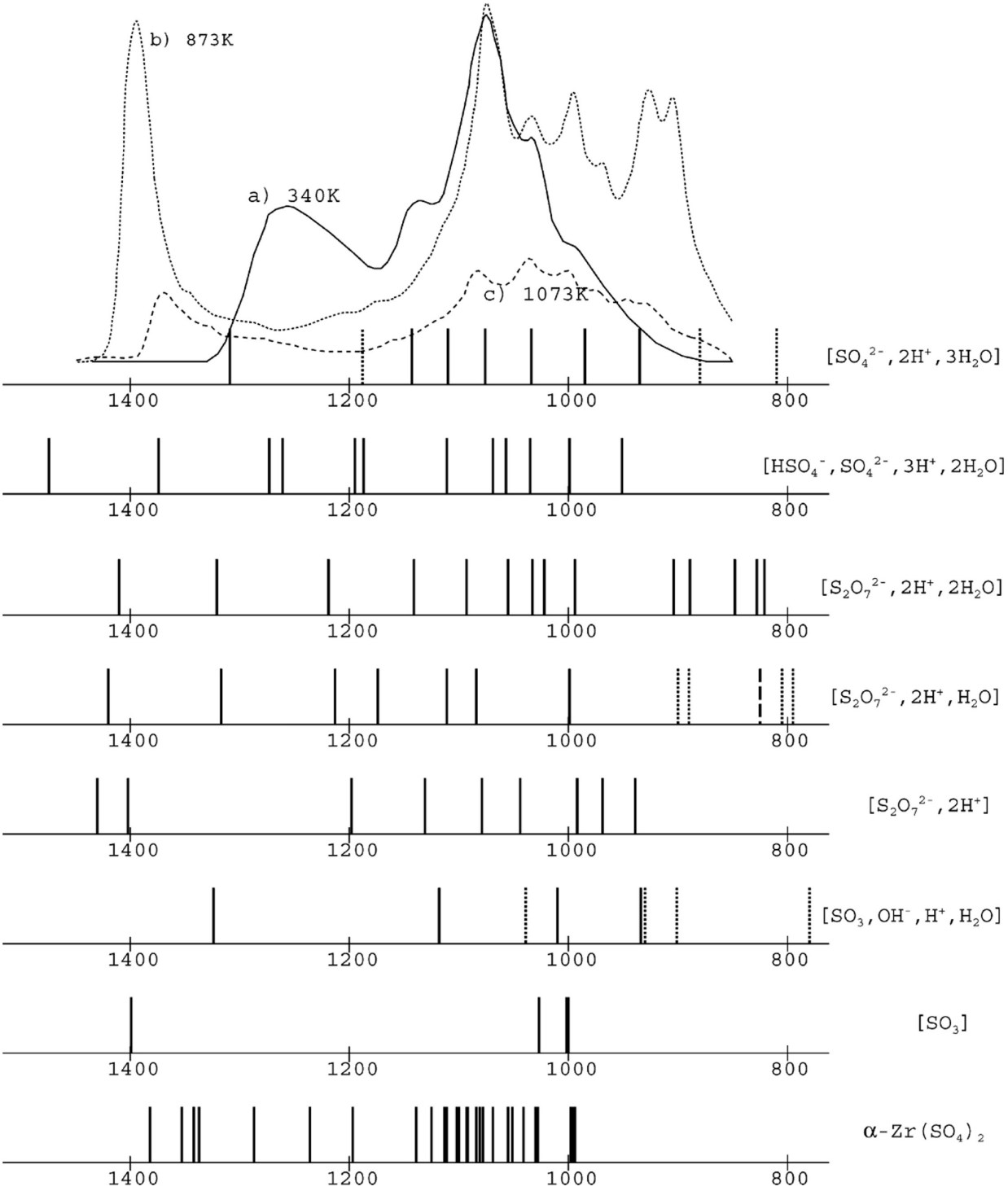

Figure 11. Simulated FT-IR spectroscopy vibrations relevant to expected SO_x species generated by sulfation of zirconia. The dotted lines correspond to hydroxyl groups, the dashed lines correspond to surface zirconia vibrations, and the solid lines correspond to the SO_x species. Reprinted with permission from ref 154. Copyright 2004 American Chemical Society. The experimental spectra at the top demonstrate the signal overlap observed for sulfated zirconia activated at different temperatures and were reproduced from refs 177 and 178.

protonate even the weakest bases, such as saturated hydrocarbons. Specifically, it is believed that a Lewis acid promotes elongation of a saturated carbon center's C−H bond to ease hydride protonation by a proximal Brønsted acid (Figure 9ii).[50,60,92,112,131,151] As protonation occurs at lower temperatures than cracking according to H/D exchange experiments, these Brønsted−Lewis pairs or nearby sulfates may also catalyze cracking by stabilizing the resulting carbenium group.[76] To clearly define the active site structures of the strongly and weakly acidic forms of SZrO, common pitfalls in the synthesis and characterization of SZrO must be reviewed to identify areas demanding computational and laboratory study.

The Role of Water and Surface Activation. Like many heterogeneous inorganic catalysts, lack of detailed reporting of SZrO's synthesis plagues the literature. As SZrO is so sensitive

https://doi.org/10.1021/acs.langmuir.3c03966
Langmuir XXXX, XXX, XXX−XXX

Pursuant to the DOE Public Access Plan, this document represents the authors' peer-reviewed, accepted manuscript.
The published version of the article is available from the relevant publisher.

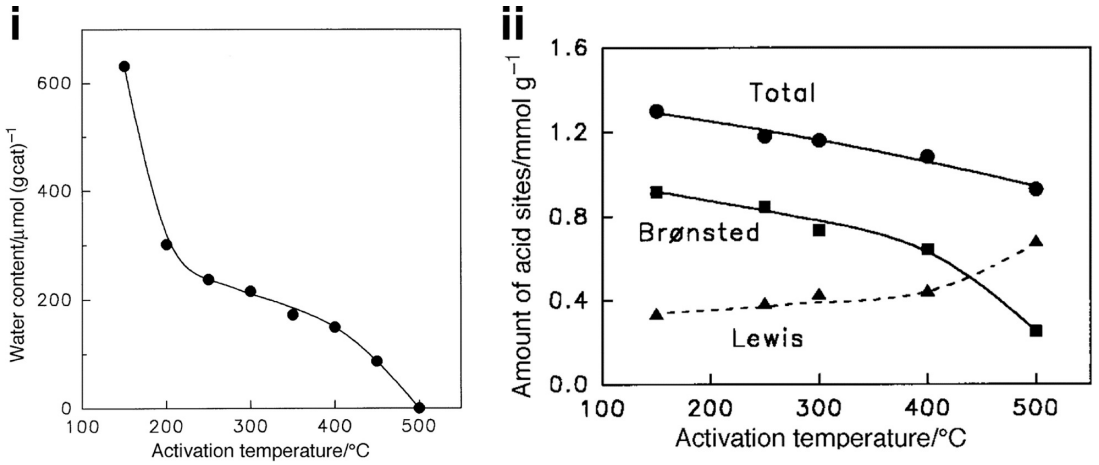

Figure 12. (i) Water content and (ii) expression of Brønsted and Lewis acid sites on sulfated zirconia according to pyridine-FT-IR spectroscopy as a function of activation temperature. Adapted by combining two figures and removing an "A" used to identify the figure from ii with permission from ref 162. Copyright 1998 the Royal Society of Chemistry.

to minor adjustments to its synthetic conditions, alteration to seemingly inconsequential variables may alter the resulting sulfate loading and crystallinity, yielding catalysts with very different functional acidity. In a similar manner, insufficient reporting on the hydration and activation prior to characterization of hydroscopic materials like SZrO is detrimental to reproducibility. Excess hydration of the catalyst depolarizes the surface and deactivates the zirconia's Lewis acid sites; however, some hydration is critical to the expression of Brønsted acidity on SZrO.[125,157,162] Sulfate chemisorption is generally more favorable than water on the zirconia facets.[174] Thus, crystallization of SZrO generates a surface generally free of surface hydroxyl groups, but water is adsorbed upon cooling and exposure to air. Samples that are not cooled and hydrated by atmospheric water were found to exhibit almost no activity in the primarily Brønsted-acid-catalyzed isomerization of *n*-butane, suggesting that the majority of Brønsted acidic hydroxyl groups are formed by hydration.[162] At low loadings, water is chemisorbed to generate hydroxyl groups, but an excess saturates the surface with physisorbed water. Though hydration increases the amount of Brønsted acid sites, Lewis acidity is eliminated and the strength of the Brønsted acids is reduced.[125,162] In the same way that dehydration increases the expression of Lewis acidity on SZrO, Lewis acidic sites are converted into Brønsted acidic sites as water is chemisorbed in small amounts on the activated surface. After nearly eliminating *n*-butane isomerization activity by activating SZrO at 500 °C, rehydrating with ∼75 μmol/g of water decreased catalyst deactivation rate and maximized activity compared to other water loadings.[59,162,175] This change in deactivation rate could be attributed to a reduction in the number, strength, or accessibility of SZrO's strong Lewis acid sites and the rapid coking known to occur over them.[18,50,59,112] Although selectivity is fully restored by rehydration, the maximum *n*-butane activity of the rehydrated SZrO is 60% that of SZrO simply activated at lower temperatures that do not eliminate Brønsted acidity.[175] Thus, surface hydration and activation conditions influence the expression of both acid types, and a delicate balance is needed for optimal functional acidity.

The conditions under which SZrO is handled before use (i.e., activation) readily control surface hydration and influence surface sulfate stability and structure. For example, a significant mass of water is desorbed when SZrO is heated from 40 to 350 °C.[162] While water desorption is reversible, sulfate desorption is not and may irreversibly alter zirconia crystallinity if enough sulfates are lost. At temperatures above 400 °C, sulfates begin to desorb as SO_2, or SO_3 at high sulfate loadings, alongside water.[88,131,162,175] As computational studies suggest, adsorbed water and hydroxyl groups participate in hydrogen bonding interactions with surface sulfates. Thus, water desorption above 400 °C may influence sulfate stability on certain zirconia facets.[123,131,174] To characterize the interactions of water and sulfate species with the zirconia surfaces and their behavior in response to sulfate loading and thermal activation conditions, the FT-IR spectroscopy signals of surface-bound hydroxyl, water, and SO_x species have been computationally predicted (Figure 11).[154] Although unique FT-IR spectroscopy vibrations can be observed for tetragonal (578 and 502 cm^{-1}) and monoclinic (751 and 413 cm^{-1}) zirconia, their signal intensity decreases on the sulfated catalyst, particularly for the monoclinic phase.[131] H_2SO_4 and other SO_x sources undergo dissociative chemisorption on zirconia into sulfates or bisulfates that are chelating, bridging two metal sites (μ_2), or bridging three metal sites (μ_3), SO_3, pyrosulfate, and hydroxyl or water species depending on their surface loadings and the temperature.[154,174,176] Note that in this field, bridging binding modes like μ_2 and μ_3 are sometimes referred to as bidentate or tridentate, respectively. For the purposes of this paper, we will refer to these bridging modes by the terminology typically used in coordination chemistry. The diagnostic FT-IR spectroscopy signals on hydrated SZrO for a μ_3-sulfate are 1142 cm^{-1} for the S═O bond and 1040 and 960 cm^{-1} for the S−O bonds, while μ_2-sulfate/bisulfate signals are 1240 cm^{-1} for the S═O bonds and 1076 cm^{-1} for the S−O bonds. The emergence of broad signals from 1000−1300 cm^{-1} at higher sulfate loadings are associated with pyrosulfates. Still, these species and their coordination to the surface are difficult to distinguish by bulk characterization due to signal overlap, particularly in the region of S−O bonding (Figure 11).[131,154,177] Excess physisorbed water has a similar effect to basic probe molecules that red-shift surface sulfate S═O bond vibrations, converting normally covalent sulfates into more ionic species and transforming strong Lewis acid sites into Brønsted acid sites.[50,57,125,162] Thus, S═O vibrations can be useful in diagnosing the

https://doi.org/10.1021/acs.langmuir.3c03966
Langmuir XXXX, XXX, XXX−XXX

Pursuant to the DOE Public Access Plan, this document represents the authors' peer-reviewed, accepted manuscript. The published version of the article is available from the relevant publisher.

presence of different sulfate species, but only when SZrO is sufficiently dehydrated.

To isolate the bond vibrations of a SO_x species from those of adsorbed water, Babou et al. observed FT-IR spectra of conventionally prepared SZrO that was activated and exposed to increasing D_2O loadings. Clear shifts in the sulfate bond vibrations indicated the simultaneous existence of several SO_x species at intermediate hydration levels. As D_2O was added, the band at 1393 cm^{-1} transformed into the species corresponding to 1368 cm^{-1}, 1322 cm^{-1}, and 1207 cm^{-1}.[125] On the dehydrated surface, the S═O bond vibration near 1393 cm^{-1} corresponds to μ_3-sulfates.[125,179] As hydration increases, this signal is diminished, and new resonances analogous to μ_2-sulfates with varying degrees of protonation at 1368 cm^{-1} and below emerge.[125,140] At very high sulfate loadings, frequencies near 1400−1420 cm^{-1} may also emerge corresponding to pyrosulfate on dehydrated SZrO.[140,154] When the surface is not activated or is activated below 150 °C, the large density of retained water diminishes all S═O bond signals.[125,140] However, hydration does not permanently alter sulfate structure or stability at lower activation temperatures. Moreover, hydrated SZrO can be reactivated to desorb water and shift S═O bond signals back to higher wavenumbers.[57,125,162] The effect of numerous variables (e.g., hydration, oxidation of the SO_x source, coordination number of surface Zr^{4+} atoms, etc.) make it difficult to unambiguously define the abundance of each sulfate species under the various synthetic and activation conditions that alter SZrO's surface. Such details have been better computationally and experimentally discussed elsewhere (see refs 123, 125, 131, 140, 154, 158, 174, and 176), but it is apparent that hydration impacts the SO_x structures present on the surface. The hydration-dependent presence of SO_x and hydroxyl/water species define SZrO's expressed acidity in terms of activation conditions.

Physisorbed water is rapidly desorbed by thorough heating up to 220 °C, followed by slower dehydration that results in the loss of Brønsted acid sites from 220−400 °C (Figure 12).[162] At higher temperatures, Brønsted acid site loss continues as water desorption becomes more rapid again.[57,162] Though sulfated MOF-808 has weaker acid sites ($H_0 \leq -14.5$) and less thermal stability than SZrO, its sulfated zirconium-based clusters experience similar phenomena during activation. According to Rietveld refinement of PXRD data and single-crystal X-ray diffraction of sulfated MOF-808 activation at 120 °C shifts surface sulfates from a bridging to a chelating coordination structure. These chelating sulfates are key to its superacid-like catalytic activity.[72,180] Thus, similar to sulfated MOF-808, dehydration-induced sulfate rearrangements on SZrO may enhance their electron-withdrawing nature, and thus the acidity of proximal surface structures. This study also demonstrated that complete dehydration eliminated the sulfated MOF-808's strongest Brønsted acid sites. Yaghi's team determined via 2D ssNMR spectroscopy and computational modeling that either a bound water or hydroxyl group has its O−H bond elongated and its Brønsted acidity enhanced by proximity to a chelating sulfate's oxygen on sulfated MOF-808.[180] Though their model does not account for a mechanistic role for Lewis acid sites, the implication that an optimal hydration level and proximity of surface structures are responsible for strong Brønsted acidity corroborates the hypothesis that cooperativity between surface species is the source of SZrO's superacidity.

Certain acid catalysts function well in aqueous conditions, such as zeolites with hydrophobic pores that impede diffusion of water and better retain the Lewis acidity of confined Ti nanoparticles.[93,104,106,107] However, SZrO's Lewis acid sites are very hydrophilic, and the amount of water desorbed below 300 °C increases with sulfate loading. Thus, optimal activation conditions are impacted by sulfate content.[131,140,162,176] Without thorough desorption of excess water, the surface energy is lowered, Lewis acid site accessibility is diminished, and cooperative interactions with Brønsted acids would be impeded. However, the optimal activation temperature and duration of heating is not a preset value, as the degree of hydration will vary by application and the desired Brønsted:-Lewis acid site ratio. Optimal SZrO activation for *n*-butane isomerization, which favors dense Brønsted acidity, occurs near 250 °C where all physisorbed water is lost, some Lewis acidity is expressed, but 67% of Brønsted acid sites are retained.[50,162,175] However, a reaction that demands stronger acidity (e.g., paraffin cracking) may require further activation to generate stronger and more abundant Lewis acid sites.[57,125,162]

Indeed, studies that do not explicitly define the conditions under which the sulfated zirconia samples were activated and transferred for analysis contribute to inconsistent characterization. Despite effort to avoid atmospheric exposure, hydration during transfer, condensation within instrument chambers used for characterization, hydrated reactants, and water produced during reactions are likely to impact SZrO's expressed acidity.[51,96] Even a seemingly pure *n*-butane feedstock was shown to steadily increase the O−H bond FT-IR spectroscopy signal on the catalyst.[51] The onset decomposition temperature of POs heated over SZrO near 190 °C may be related to the temperature at which water desorbs or dissociates to either expose Lewis acid sites or increase the availability of acidic hydroxyl groups. Additionally, changes in reaction selectivity and activity over time may also be related to water in a similar fashion to coking, with water in the feedstock or generated during the reaction increasing the degrees of saturation of Lewis acid sites.[51] Thus, activation conditions and hydration prior to and during the reaction must be more carefully recorded and reported in the study of SZrO. Still, the surface and crystal phase beneath these surface structures is just as critical to the acidity they express.

Crystal Phases and Facets. Zirconia exhibits three crystalline phases, monoclinic, tetragonal, and cubic,[58,116,181] but the following discussion will focus on the monoclinic and tetragonal phases, shown to be more catalytically active than cubic zirconia.[116] Though the two are distinguishable by Raman spectroscopy, it is worth noting that the PXRD pattern of cubic zirconia has only small differences in its reflection angles and is nearly indistinguishable and often confused with tetragonal zirconia.[136] The two phases are similar fluorite structures, but where all Zr−O bond lengths are equivalent for cubic zirconia (223 pm), tetragonal zirconia is a slightly distorted structure with one tetrahedra of short Zr−O bonds (210 pm) and another tetrahedra with weaker, longer bonds (243 pm).[140,154] The literature highlighted below demonstrates that tetragonal zirconia's distortion yields the most acidic SZrO surface.

In zirconia ceramics, precursors sinter and transition first from amorphous to monoclinic zirconia, then to large particles of the tetragonal phase during calcination. However, in catalytic applications, high surface area nanoparticles are

https://doi.org/10.1021/acs.langmuir.3c03966
Langmuir XXXX, XXX, XXX−XXX

Pursuant to the DOE Public Access Plan, this document represents the authors' peer-reviewed, accepted manuscript. The published version of the article is available from the relevant publisher.

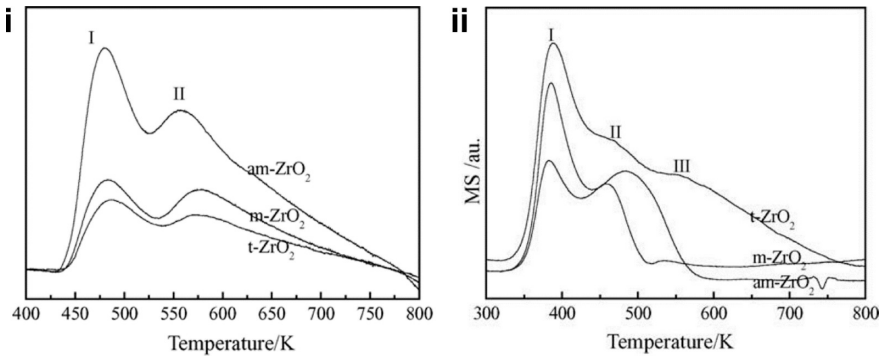

Figure 13. (i) NH_3 temperature programmed desorption and (ii) CO_2 temperature programmed desorption profiles of amorphous (am), monoclinic (m), and tetragonal (t) unfunctionalized zirconia. Adapted by combining two figures with permission from ref 116. Copyright 2005 Elsevier.

desirable for the exposure of more coordinatively unsaturated atoms and high surface energy facets. When a fine polycrystalline powder containing very small grains is heated above 250 °C, it transitions from the amorphous phase into metastable tetragonal zirconia nanocrystals.[123,182] At 400 °C and higher temperatures, these particles begin to sinter beyond a critical nanoparticle size (~20 nm) and transition into the monoclinic zirconia phase.[182,183] Unfunctionalized zirconia is typically most valuable for acid catalysis in the monoclinic phase, as the monoclinic phase exhibits Brønsted acid sites strong enough for detection by FT-IR spectroscopy with weakly basic pyridine. This and the greater abundance and strength of acid sites detected by NH_3-TPD on unsulfated monoclinic zirconia (Figure 13i)[116] lead many to assume that monoclinic SZrO will be more acidic than tetragonal SZrO. Indeed, the Brønsted acid sites detectable by NH_3-TPD on unfunctionalized tetragonal and amorphous zirconia are very weak, as they are undetectable by pyridine-FT-IR spectroscopy.[116] The coordination of hydroxyl groups to the surfaces of these crystal phases differ, though this cannot explain the difference in their Brønsted acid strength. While tetragonal zirconia has terminal, μ_2- and μ_3-bridging hydroxyl groups, monoclinic zirconia has only terminal or μ_3-hydroxyl groups.[88,116] In terms of Lewis acidity in the absence of sulfation, the abundance and strength of acid sites is greater on monoclinic zirconia than the tetragonal phase, but the strength and abundance of Lewis acid sites is greatest for the amorphous phase. Though too thermally unstable for practical use, the abundance of coordinatively unsaturated Zr^{4+} sites on amorphous zirconia yields a density of Lewis acid sites that exceeds both crystalline phases.[116,184] Thus, between the two acidic crystalline phases, unsulfated monoclinic zirconia has a greater abundance of and stronger Brønsted acid sites; however, amphoteric oxides like zirconia express their surface energy through basic behavior as well.

Normally, more electronegative metals generate more acidic metal oxides.[54,70,71,114] The transition from tetragonal to monoclinic is associated with surface facet rearrangements as the saturated zirconium coordination number in the bulk reduces from eight to seven.[183] Perhaps the lower coordination number of the monoclinic phase zirconium atoms increases the oxide's acidity. Regardless, this coordination number difference causes the tetragonal phase to generally have higher surface energy facets than the monoclinic phase when computational slab models of the unsulfated facets are analyzed.[174,185,186] As such, although the Lewis acid sites of the unsulfated monoclinic phase are more abundant, the Lewis acid sites of the unsulfated tetragonal phase have CO heats of adsorption 10 kJ/mol that are greater than those of the monoclinic phase.[121] In the presence of a weak base like ammonia, the surface moieties of amphoteric oxides like zirconia should behave like acids. But in the presence of a weak acid like CO_2, zirconia's surface features should behave as bases.[54,70,71,114] When CO_2-TPD is observed, the higher surface energy of the tetragonal phase manifests as an abundance of strong basic sites, four times the number of sites observed on monoclinic zirconia (Figure 13ii).[116] While zirconia is amphoteric, it seems the tetragonal phase is more prone to basic character. But upon sulfation, the inductive effect of surface sulfates causes most of the zirconia surface sites to act as acid sites, as seen in the NH_3-TPD of tetragonal SZrO (Figure 6ii).[64] Therefore, the greater density and strength of active sites, surface area (i.e., smaller particle size), and sulfate loading of tetragonal phase zirconia make it a more functionally acidic SZrO catalyst.[64,134,160] Sulfate surface interactions begin upon sulfation of the amorphous phase prior to calcination, evidenced by a diminished number of amorphous zirconia's basic sites upon sulfation.[123] Although sulfation eliminates some of the coordinatively unsaturated sites that could become Lewis acid sites, the remaining Lewis acid sites and new Brønsted acid sites become stronger, though some basic behavior is retained.[64,88,116,169] The lower coordination number of the tetragonal phase's exposed zirconium atoms also means more Lewis acid sites and acid strength is retained on the tetragonal phase through sulfation. Still, the superior unsulfated Brønsted acidity and stability under reaction conditions of the monoclinic phase has facilitated extensive study of the less acidic sulfated monoclinic zirconia.[174,185,186] Though reports that argue no catalytic activity exists on sulfated monoclinic zirconia have been disproven, the lower sulfate loading and surface area of monoclinic SZrO certainly has a less polar surface, fewer acid sites detectable by pyridine-FT-IR spectroscopy, and lower acid site density than tetragonal SZrO.[160,174,187] Thus, as the monoclinic and tetragonal phases of SZrO are often conflated, this contributes to underestimations of SZrO's functional acidity.

Sulfation and Crystallization During Calcination. Sulfation not only enhances the acidity of the tetragonal phase but also dramatically increases its thermal stability, promoting growth of small nanoparticles and higher surface energy facets that are desirable for heterogeneous catalytic activity.[61,64,123,152,169] Computational models have supported

https://doi.org/10.1021/acs.langmuir.3c03966
Langmuir XXXX, XXX, XXX−XXX

Pursuant to the DOE Public Access Plan, this document represents the authors' peer-reviewed, accepted manuscript.
The published version of the article is available from the relevant publisher.

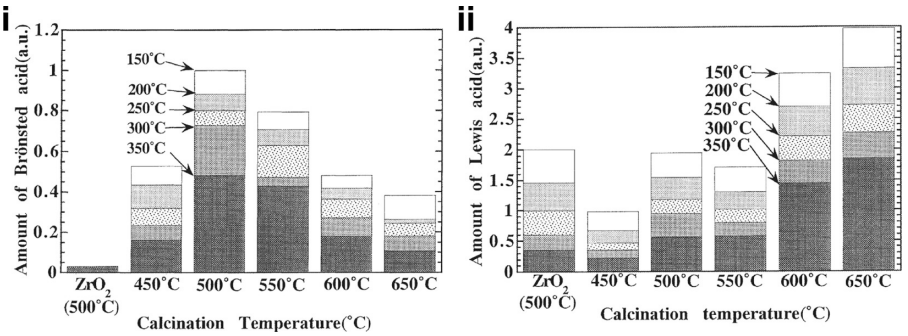

Figure 14. Quantity of (i) Brønsted acid sites and (ii) Lewis acid sites detectable by pyridine-FT-IR spectroscopy across a range of calcination temperatures (450−650 °C) of sulfated $Zr(OH)_4$ activated at 350 °C, loaded with pyridine, and analyzed while heating from 150 to 350 °C. Adapted by combining two figures with permission from ref 161. Copyright 1998 Springer.

speculation that the presence of sulfates during calcination promotes tetragonal phase stability as sulfates adopt more stable surface structures on the tetragonal phase than the monoclinic phase.[123,174,187] Afanasiev et al. validated these predictions when they observed that normally spherical unsulfated zirconia clusters (62 m^2/g) instead grow as higher surface area rod shapes (108 m^2/g) with a higher relative amount of the tetragonal phase when sulfated prior to calcination at 600 °C.[152] Sulfation after calcination also results in diminished surface area, and is thought to lower sulfate loading and acid density.[158,174,187] Given these events and the meta-stability of the unsulfated tetragonal phase, it is critical to sulfate the amorphous zirconia or $Zr(OH)_4$ prior to calcination.

Calcination thermally anneals and crystallizes the amorphous phase, shifts weakly coordinated sulfates into stable surface structures, and desorbs excess water and sulfates.[61,94,96,161] During calcination, physisorbed water molecules desorb first, then at higher temperatures neighboring hydroxyl groups combine to release water and expose Zr^{4+} and O^{2-} surface atoms. As less proximal hydroxyl moieties combine, the strain on surface Zr−O bonds increases and so does the surface energy.[61] Though this process substantially reduces the surface area compared to amorphous zirconia, this reduction is noticeably lessened when sulfates are present and is necessary for crystallization and superacid-like activity.[94,152] The thermal stability enhancements offered by sulfation increase the tetragonal to monoclinic crystal phase transition from below 600 °C to temperatures ≥650 °C, which also enhances stability under reaction conditions. Near 700 °C, the complete transition of sulfated tetragonal zirconia to the monoclinic phase occurs; this conversion is coupled with a large loss of sulfur wt % (representing surface bound SO_x species), surface area reduction, pore collapse, and a loss of the majority of Lewis acid sites.[64,152]

Yet, optimal calcination conditions are not met by merely generating tetragonal SZrO. Shimizu et al. used pyridine probes to demonstrate that calcination temperature alters the expression of Brønsted and Lewis acidity across the range of temperatures normally used to generate tetragonal zirconia, as seen by PXRD. Calcination of sulfated $Zr(OH)_4$ up to 650 °C increases the abundance of Lewis acid sites, including the strongest Lewis acids, but also progressively decreases the number of strong Brønsted acid sites at temperatures >500 °C (Figure 14).[161] As previously discussed, excess sulfates are labilized above 400 °C, and up to 500 °C sulfate loss increases the density of strong acid sites, particularly Lewis acid sites. However, higher temperatures begin to desorb chemisorbed sulfates that contribute to catalytic activity, suggesting that within a range of 500−650 °C the desired calcination temperature is defined by the application's preference for Brønsted and Lewis acidity.[88,131,161,162] For example, at peak weak:strong Lewis acid site ratios, high benzene alkylation activity is achieved, as weak Lewis acid sites appear to remove small olefin impurities from cyclized aromatic feedstocks.[160] Thus, in ideal PO depolymerization where olefin monomer is generated, a low weak:strong Lewis acid site ratio may be necessary.

Though calcination temperature alters acid site density and strength, the functional acidity of SZrO is also closely linked to its crystallinity prior to calcination. Sulfation prior to crystallization at high calcination temperatures allows retention of smaller (<10 nm), tetragonal, faceted nanoparticles with more coordinative unsaturation at facet edges/stepped terminations.[167] While industrial SZrO manufacturers are likely to obviate additional synthetic steps in favor of sulfating the $Zr(OH)_4$ precursor, precalcination into amorphous zirconia prior to sulfation and subsequent calcination appears to promote uniform crystallization for higher functional acidity and surface area. But there is limited study on the impact of precalcination.[79,134,146,168] Sulfate anions interact with the abundant Lewis acid sites of the amorphous zirconia surface better than $Zr(OH)_4$.[116,123] It has been suggested that the weak coordination of sulfates to the precursor prior to calcination are hydrogen bonds to the surface and direct contacts to zirconium atoms form during zirconia crystallization.[96] These hydrogen bonding interactions should be stronger with the amphoteric, amorphous metal oxide than with the hydroxide, promoting more sulfate coordination prior to heating. Therefore, it is possible that the smaller crystallites of precalcined SZrO are the result of surface sulfates reducing zirconia crystallite sintering during calcination.[96,123]

Using precalcination to retain a larger surface area particle to distribute sulfates upon may also impede formation of $Zr(SO_4)_2$. $Zr(SO_4)_2$ arises at excessively high sulfate loadings to $Zr(OH)_4$ and requires higher temperatures to form crystalline zirconia than sulfated $Zr(OH)_4$.[166,188,189] As a result, nonuniform crystallization occurs in which portions of the oversulfated zirconia remain amorphous at the temperatures of the sulfated $Zr(OH)_4$'s tetragonal-to-monoclinic phase transformation. For example, Signoretto et al.'s one-step generation of a sulfated aerogel via hydrolysis of alkoxides (e.g., zirconium isopropoxide) in the presence of a sulfate source generates different SZrO crystal phases depending on

https://doi.org/10.1021/acs.langmuir.3c03966
Langmuir XXXX, XXX, XXX−XXX

Pursuant to the DOE Public Access Plan, this document represents the authors' peer-reviewed, accepted manuscript.
The published version of the article is available from the relevant publisher.

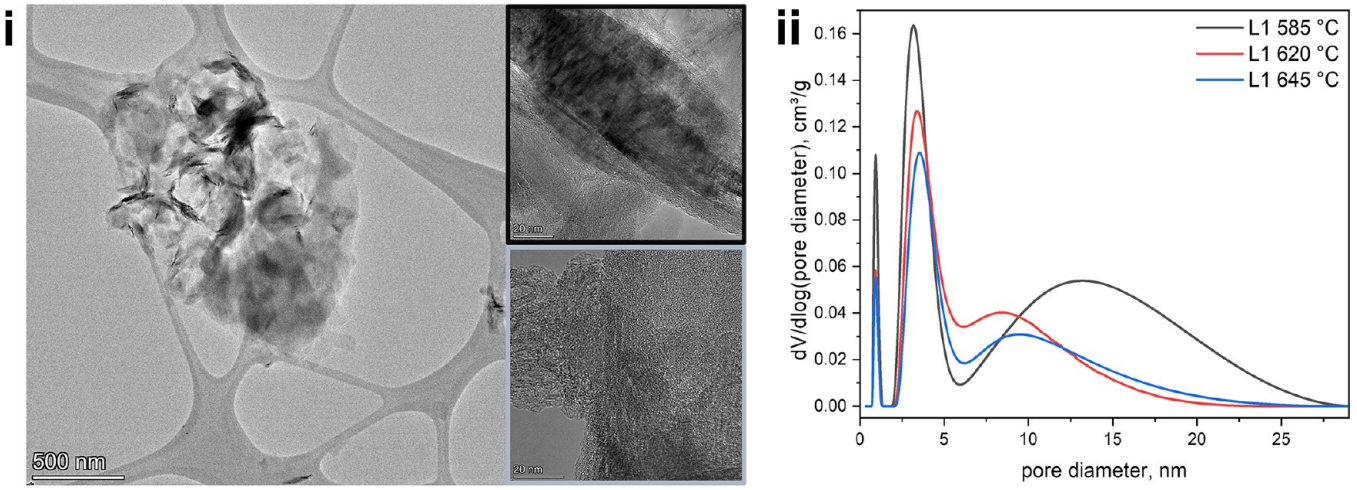

Figure 15. (i) High-resolution bright field TEM images of a representative sulfated zirconia particle, including higher magnification regions of high (black) and low (gray) crystallinity, prepared by calcination of Luxfer MEL Technologies sulfated precursor at 620 °C. (ii) Pore size distribution data determined by NLDFT analysis of N_2 77 K isotherms for the same Luxfer MEL Technologies sulfated precursor calcined at different temperatures.

the sulfate loading. Tetragonal SZrO was generated at low sulfate concentrations, but at higher sulfate loading temperatures that fully crystallize the zirconia yield a mixture of monoclinic and tetragonal SZrO. This is likely due to the nonuniform crystallization of $Zr(SO_4)_2$ and the sulfated hydroxide.[51] The crystallinity of the SZrO is clearly sensitive to $Zr(SO_4)_2$ formation and the concentration of sulfates on the hydroxide precursor. A high SO_4^{2-}:Zr^{4+} ratio generates very acidic salts that impede crystallization, while basic salts that form at lower SO_4^{2-}:Zr^{4+} ratios form infinite sheets via sulfate bridging.[135,189] Thus, the formation of a long-range ordered crystal lattice depends on a low SO_4^{2-}:Zr^{4+} ratio and the amount of amorphous zirconia formed prior to sulfation.

The central benefit of precalcination prior to sulfation is the production of more abundant and stronger acid sites on SZrO, but acidity is particularly sensitive to the precalcination temperature. Though assessed with the Hammett indicator method, Guo et al. found the acid strength of SZrO that was calcined at 650 °C was seemingly more superacidic for samples precalcined between 110−400 °C prior to sulfation ($H_0 \leq -16.2$) than samples precalcined at high temperatures 500−800 °C ($H_0 \leq -13.75$).[57,168] These higher precalcination temperatures likely crystallize the zirconia prior to sulfation. Thus, the optimal precalcination temperature is likely near 300 °C, a temperature that allows only small amounts of amorphous zirconia to form and exposes Lewis acid sites prior to sulfation.[146,168] Syntheses that require complete zirconia crystallization prior to sulfate impregnation (e.g., nanosheets) are more likely to generate monoclinic SZrO, but even sulfation of precystallized tetragonal zirconia yields lower sulfate loadings, less abundant and weaker acid sites, and substantially less surface area than conventionally prepared SZrO.[158,174,187,190] Aside from minor surface atom rearrangements that occur when heating crystalline metal oxides (e.g., Cu_2O) in reducing or oxidizing atmospheres, the crystal phase and facets exposed as $Zr(OH)_4$ transforms into crystalline zirconia are irreversible in most contexts.[174,187,191,192] Thus, as sulfates stabilize certain high energy zirconia facets, complete crystallization prior to sulfation likely reduces the expression of higher surface energy facets.

Arata et al. found the benefits of precalcination extend to both synthesized sulfated $Zr(OH)_4$ and a standard sulfated $Zr(OH)_4$ from MEL Chemicals, increasing conversion of *n*-butane to isobutane by ∼25%. Though the $Zr(OH)_4$ preparation method alters the optimal precalcination and calcination temperature, ranging between 200−300 °C and 525−600 °C respectively, precalcination ubiquitously improved catalytic function and lowered the optimal calcination temperature.[79] A lower necessary temperature for optimal crystallinity supports the idea that precalcination reduces $Zr(SO_4)_2$ formation. Still, the limited study of precalcination, variance of other synthetic conditions, and inconsistent characterization of samples highlights the difficulty of comparing SZrO across different publications to identify the influence of a single variable. If we do indeed attempt to identify the influence of precalcination on calcination temperature by comparing two studies, Shimizu et al. observed optimal *n*-butane isomerization activity without precalcination of SZrO at a 550 °C calcination temperature, and Guo et al. observed optimal isobutane alkylation activity for precalcined SZrO when calcined at 650 °C. But the impact of precalcination cannot be isolated when the test reaction and numerous synthetic and catalytic variables are also altered: sulfuric acid concentration (1.0 M vs 0.5 M), period of calcination (3 h vs 4 h), and reaction temperature (100 °C vs 150 °C).[161,168] Even seemingly minor differences in the conductivity of an oven's surface to the calcination vessel in which the sample is heated may shift the optimal calcination temperature by as much as 50 °C.[79] In summary, detailed reporting of synthetic variables and screening a range of (pre)calcination temperatures to verify results is critical to acid catalyst optimization and reproducibility. These sensitive synthesis parameters define crystal growth, acidity, and surface area, and insufficient characterization increases the difficulty of identifying trends.

The Role of Amorphous Zirconia. Though unstable and not well studied, the highly Lewis acidic surface of amorphous zirconia may contribute to catalytic activity in partially crystallized SZrO. We have identified that many nonoptimized synthetic parameters generate a mixture containing distinct regions of the crystalline and amorphous phases of SZrO. This

https://doi.org/10.1021/acs.langmuir.3c03966
Langmuir XXXX, XXX, XXX−XXX

Pursuant to the DOE Public Access Plan, this document represents the authors' peer-reviewed, accepted manuscript. The published version of the article is available from the relevant publisher.

means reported particle sizes that are not verified with microscopy are likely larger than crystallite size due to physical contributions of amorphous zirconia.[51,135,189] Particle and crystallite sizes of conventionally prepared SZrO have rarely been verified with high-resolution TEM; instead, they are approximated by dynamic light scattering or from PXRD peak width using the Scherrer equation.[53,187,193] However, neither of these techniques can be accurately applied to samples that do not have uniform crystallinity. For example, the SZrO we synthesized from the precursor provided by Luxfer MEL Technologies contains a significant volume of less crystalline, amorphous zirconia. The crystallite size of this sample appears to be <10 nm according to its PXRD pattern's peak widths (Figure S2) and the Scherrer equation, but the average particle size observed by TEM (~600 nm) is much larger due to the amorphous phase content that is not easily detected by X-ray diffraction (Figure 15i). Unconventional sulfation techniques, such as sulfation of the basic $Zr(OH)_4$ suspension or using a large excess of sulfates, appear to generate a significant amount of amorphous zirconia according to TEM images.[51,135,160,163] Adding a low but sufficient sulfate loading to amorphous zirconia generated by precalcination should reduce crystallite sintering, promote uniform crystallization, and increase the surface area of the calcined product.[123] Still, amorphous zirconia may be catalytically valuable, as the strong Lewis acid sites of SZrO may be related to amorphous zirconia's strong and numerous Lewis acid sites.[116] Although the Luxfer MEL Technologies SZrO we prepared is a mixture of amorphous and tetragonal phase zirconia (Figure 15i), its ability to decompose POs near 190 °C suggests that the amorphous phase may contribute to its cracking ability. However, a study evaluating the impact of crystallinity prior to sulfation/calcination on SZrO's amorphous phase content and expressed acidity using detailed characterization methods (i.e., TEM and atomic pair distribution function analysis) has to yet to be reported.

Even for appropriately sulfated samples, the increase in the temperature at which zirconia crystallizes induced by sulfation has caused study of less-crystalline materials that are unlikely to reflect the acidic potential of crystalline SZrO. For example, in a study intending to compare tetragonal and monoclinic SZrO, the broadness of the reflections of the monoclinic sample's PXRD pattern suggest it is largely amorphous. Thus, the catalytic function the authors attribute to monoclinic SZrO may instead stem from amorphous zirconia or loosely coordinated H_2SO_4.[193] No standard for calcination conditions (i.e., an optimal tetragonal/amorphous zirconia phase ratio) has also caused detailed study of insufficiently calcined tetragonal SZrO that has little Brønsted acidity. For example, pyrosulfate formation is associated with a densely Bronsted acidic surface, but pyrosulfates can only form when two SO_x species adsorb in close proximity to one another on a fully crystallized zirconia surface. Breitkopf et al. and Li et al. both found that their SZrO catalysts could not form pyrosulfates on an insufficiently calcined zirconia surface with a relatively low sulfate loading.[94,140]

When we studied the influence of a small range of calcination temperatures (585−645 °C) on the SZrO precursor provided by Luxfer MEL Technologies, crystallinity was impacted in ways that are difficult to detect by bulk characterization methods. Though the PXRD pattern of the Luxfer sulfated tetragonal zirconia is largely unaltered across the range of calcination temperatures studied (Figure S2), the surface area (Table S1), pore size distribution (Figure 15ii), and likely other surface features are significantly altered. Note that while mesoporous domains are shown in the pore size distributions, these volumes are still very low and unlikely to contribute catalytically in the same manner to the large pore volumes of zeolites and other supports. The TEM images also show a lack of ordered porosity, and much of this volume could be attributed to unstable void space in amorphous SZrO. Still, this demonstrates the sensitivity of SZrO's crystallinity in catalytically valuable forms. Therefore, the Scherrer equation should only be applied to SZrO to estimate crystallite size not particle size, and reports that determine optimal calcination conditions based on catalytic activity better reflect the density and strength of SZrO's acid sites.[161,168,194]

So far, we have identified that hydration, retention of primarily tetragonal phase zirconia, the timing and degree of sulfation, calcination temperatures, and the expression of both Lewis and Brønsted acid sites generated by these variables are critical to SZrO's superacid-like behavior. While misconceptions surrounding these details continue to impede progress, key synthetic and structural features have indeed been defined by studies that understand the sensitivity of SZrO's expressed acidity.

Recommendations in the Synthesis of Sulfated Zirconia. *Synthesis of Zirconium Hydroxide.* The two most active forms of SZrO, the strongly acidic and densely acidic derivatives, both require a partially dehydrated surface with a specific sulfate loading on tetragonal phase zirconia. Synthesis of such a material is sensitive to numerous variables which will be outlined here for a typical synthesis of SZrO. To begin, there are numerous variables in the preparation of the $Zr(OH)_4$ precursor that control the crystal phase of the final product. Efforts to synthesize SZrO by directly calcining $Zr(NO_3)_4$ or $ZrCl_4$ salts typically generate monoclinic zirconia. The same is true for direct calcination of $ZrO(NO_3)_2$ and $ZrOCl_2$, which form when their unoxidized precursors are exposed to air or dissolved in water.[135,146,182,195] Synthetic routes that first hydroxylate these salts more successfully yield primarily tetragonal SZrO with a high surface area. Typically, the suspended $Zr(OH)_4$ solid is then isolated via filtration and washed to remove lingering anions using water and/or a dilute base.[57,61,94,96,163−167,189,196,197] However, poor control of the factors involved in hydroxylating the zirconyl precursor can predispose the $Zr(OH)_4$ to favor formation of monoclinic zirconia, not due to particle size but the incomplete hydroxylation of each zirconium atom.[198]

When a zirconyl salt is dissolved in water, it will begin to hydrolyze into poly-zirconium species that contain a small number of zirconium ions, not much larger than the zirconyl chloride tetramers of the solid. Zirconyl chloride tetramers are composed of four Zr(IV) atoms arranged in a square-like fashion, linked by two bridging hydroxyl groups to two other zirconium atoms. The outward-facing sides of these zirconium atoms have four waters, forming the complete zirconyl cation, $[Zr_4(OH)_8(H_2O)_{16}]^{8+}$. This cation is charge-balanced by an outer coordination sphere of two chloride atoms per zirconium atom.[198,199] As base is added to the zirconyl solution, these small poly-zirconium species polymerize into larger species by forming two hydroxyl bridges to other zirconium atoms that displace the water and chloride in their coordination spheres.[189,196] Complete hydroxylation should produce a zirconium hydroxide precursor that resembles a zirconium atom's coordination number in the tetragonal phase and can be

https://doi.org/10.1021/acs.langmuir.3c03966
Langmuir XXXX, XXX, XXX−XXX

Pursuant to the DOE Public Access Plan, this document represents the authors' peer-reviewed, accepted manuscript. The published version of the article is available from the relevant publisher.

readily calcined into tetragonal zirconia. However, modulation of variables involved in hydroxylation like the suspension's pH prior to filtration, base addition rate, and other factors that influence the complete exchange of chloride atoms with hydroxide groups control the crystal phase formed.[196,198]

The zirconium source can alter how sensitive the zirconia phase formed is to these variables. While the anion (e.g., Cl^-, NO_3^-) of the zirconium source does not impact the zirconia phase generated by this method, it is generally agreed that polymerization of the zirconyl species in solution controls the crystal phase produced.[196,198] The size of the poly-zirconium seed particles in solution prior to hydroxylation likely varies across chemical manufacturers and the synthetic conditions used to prepare the zirconyl source.[198] Regardless, $ZrO(NO_3)_2$ and $ZrOCl_2$ should theoretically yield identical zirconia products. To discuss the variables involved in hydroxylation, a $ZrOCl_2$ reagent will be used as an example.

Dissolving $ZrOCl_2$ causes polymerization to begin among the zirconyl cations. As two waters combine to generate a new hydroxyl bridge between zirconium atoms, H^+ and Cl^- are also released into solution.[198] Ideally, the zirconyl tetramers will be fully hydroxylated and polymerize into ordered polymeric sheets that can come together to form an ordered three-dimensional structure.[189,196] Similar trends in polymerization are observed for other zirconyl salts like zirconium alkoxides and even $ZrO(NO_3)_2$, despite its initial chain-like structure of ZrO_8 dodecahedra.[94,96,189] The size of these poly-zirconium species in acidic solutions should increase at elevated concentrations of zirconyl chloride (i.e., 0.5−2 M).[198] However, at the acidic pHs generated by zirconyl salt dissolution, the polymerization process is limited and reversible. Base addition causes hydroxides to displace both chloride and water from the zirconium atoms at random points on the poly-zirconium clusters, in a seemingly irreversible manner, and precipitates an amount of zirconium hydroxide that increases with pH.[196,198] Still, at low pH (i.e., pH 2−7) the randomness of these hydroxylation events causes some anions to linger on the precipitate. Thus, there are numerous zirconium atoms within the bulk that have an incomplete number of hydroxyl bridges to nearby zirconium atoms. As a result, the zirconium hydroxide product is largely amorphous, washes are less effective at removing anions, and the resulting zirconia phase will be mostly monoclinic.[163,189,196,198,200] This could be explained by the lower number of oxygens coordinated to zirconium atoms in the bulk of the monoclinic phase compared to the tetragonal phase.[185,186] Though small amounts of tetragonal zirconia can form at lower pHs, the amount steadily increases to 100% as pH increases from 9 to 14. Because pH greater than ∼10.4 cannot be achieved with NH_4OH, higher pHs necessitate an alkali base. Still, the ammonium chloride/nitrate generated by ammonium hydroxide basification has a superior buffering capacity that improves as pH increases compared to alkali bases (e.g., NaOH, KOH). While a pH greater than 13 appears to generate primarily tetragonal zirconia regardless of base addition rate, at pHs of 10.4 and lower the rate at which this base is delivered to the zirconyl solution defines the percentage of tetragonal phase zirconia in the product.[189,196,198]

While larger poly-zirconium $Zr(OH)_4$ species in solution are an ideal precursor for stable tetragonal zirconia nanoparticles, the growth of these poly-zirconium species must be controlled to allow complete hydroxylation of the zirconium atoms in the bulk. It is apparent that rapid base addition adds hydroxyl groups to random points on the zirconium clusters, causing random polymerization in many directions and formation of an amorphous zirconium hydroxide gel instead of dense, ordered sheets. In this case, particle growth from polymerization occurs faster than zirconium atom hydroxylation, resulting in large particles that cannot be penetrated to complete hydroxylation. For similar reasons, amorphous zirconium hydroxide particles cannot be easily washed to remove the anion, and monoclinic zirconia is generated upon calcination.[196,198] Slowing the rate of base addition allows complete hydroxylation prior to polymerization and yields a zirconium hydroxide that forms tetragonal phase zirconia upon calcination. While this $Zr(OH)_4$ is more ordered, these samples still appear amorphous to PXRD analysis.[196,198] The increased density of crystallites formed by slow base addition suggests that complete hydroxylation is achieved prior to polymerization into large particles.[189,196,198] While a pH between 7 to 9 will generate a mostly monoclinic sample regardless of base addition rate, Srinivasan et al. found that prolonging addition of NH_4OH up to pH 10.4 from 1 to 8 h increases the tetragonal phase content of their zirconia product from <60% to nearly 90%. This study demonstrates that both pH and base addition rate play an important role in generating tetragonal phase zirconia.[198] Higher pHs (e.g., pH ≥ 13) cause $Zr(OH)_4$ to become slightly soluble, allowing cycles of dissolution and precipitation that allow even amorphous $Zr(OH)_4$ to transform into more ordered sheets over time regardless of base addition rate.[196,198] Still, the alkali bases needed to achieve these pHs introduce small metal cations (e.g., Na^+, K^+) that may linger on the surface oxygen atoms of the SZrO product, altering its surface chemistry and acidity.[140] Instead of alkali bases, other factors can aid slow base addition of ammonium hydroxide in repeatably synthesizing a zirconium hydroxide precursor that transforms into tetragonal zirconia upon calcination.

Refluxing solutions of zirconyl chloride promotes a slow hydrolytic polymerization process in a similar manner to slow base addition that allows amorphous zirconium hydroxide to reform into the tetragonal zirconia precursor. Thus, reflux may replace amorphous $Zr(OH)_4$ formed by rapid base addition with a tetragonal pattern over time.[196] Heat is necessary for this rearrangement to occur. Srinivasan et al. found that aging zirconium hydroxide prepared by rapid base addition in a pH of 10.4 solution for 3 days generated 90% monoclinic zirconia upon calcination.[198] However, the phase formed by reflux is still sensitive to the suspension's pH. The pH of the solution must be greater than 7, or HCl displaced into the boiling solution will lower the pH and zirconium hydroxide predisposed to form a mixture of monoclinic and tetragonal zirconia will form.[196] Generally, higher pH values achieved prior to reflux (i.e., 9.2 or greater) increase the tetragonal phase content and decrease the monoclinic phase content, but it is difficult to reform a fully amorphous sample into a tetragonal pattern by reflux alone.[163,189,196,200] Therefore, reflux of $Zr(OH)_4$ of pH 9.2 or greater reached by slow addition of ammonium hydroxide should eliminate the need for alkali bases while repeatably producing tetragonal SZrO. Still, excessive reflux may cause the pH to drop again and the monoclinic phase to form.[182,189,196] The reflux period, base addition rate, and zirconyl precursor concentration all alter the dimensions of the $Zr(OH)_4$ particle, which grow as extending 0.7 nm diameter rods. In concentrated suspensions (i.e., 0.5 M), reflux promotes polymerization to longer rod lengths,

https://doi.org/10.1021/acs.langmuir.3c03966
Langmuir XXXX, XXX, XXX−XXX

Pursuant to the DOE Public Access Plan, this document represents the authors' peer-reviewed, accepted manuscript. The published version of the article is available from the relevant publisher.

while reflux in more dilute solutions (i.e., 0.05−0.1 M) causes crystallite clusters to expand in diameter as well.[189,198] An excess of heat applied to the suspension is also likely to cause zirconia to form, but the numerous other variables at play during incubation/reflux make precalcination a more straightforward means of controlling crystallinity prior to sulfation.[189,196] A balance of zirconyl precursor concentration, base addition rate, pH achieved prior to reflux, and reflux period/temperature must be struck to fully hydroxylate the sample and produce high surface area tetragonal SZrO. However, a thorough study of the relationship between these four variables has not been reported to our knowledge.

It is also worth noting that Srinivasan et al. found that $Zr(OH)_4$ precipitated from $ZrOCl_2$ and $ZrO(NO_3)_2$ stored in concentrated hydrochloric acid and nitric acid, respectively, formed tetragonal zirconia regardless of pH. Perhaps the abundance of the anion being displaced by hydroxides in solution slows hydroxylation of the zirconium atoms and polymerization.[198] However, the large amount of base required to alter pH, increased volume of washes required to remove the anion, and hazardous nature of such strong acids make this synthesis route less desirable for scale-up.

Sulfation is typically performed after drying the $Zr(OH)_4$, as optimal hydroxylation conditions are impacted by the presence of sulfates in the solution. Ivanov et al. found that by briefly aging sulfated $Zr(OH)_4$ suspensions, the tetragonal phase formed even with relatively rapid base addition at pH 7 or greater. Although the surface area of the sample increased with basicity up to the highest pH studied (a pH of 9), the sulfur content of the product SZrO decreased as well. This could be remedied by increasing the sulfating agent concentration beyond the 0.25 M $(NH_4)_2SO_4$ used. Further study of how hydroxylation and polymerization of zirconium precursors occurs in the presence of sulfates could reduce the number of synthetic steps required to obtain industrially valuable SZrO.[163,196]

Finally, we found a previously unreported trend in the leaching of silica from glassware employed when refluxing basic $Zr(OH)_4$ suspensions. Even with leach-proof glassware, we (via FT-IR spectroscopy and EDS analysis (Figures S5−S9 and Luxfer MEL Technologies (≥2 wt % silica via X-ray fluorescence analysis) observed significant silica leaching when refluxing in a glass apparatus. Longer reflux periods increased silica content in the final SZrO product. This silica content increased the thermal stability of the SZrO's tetragonal crystal phase to above 1000 °C and likely impacts its acidity (Figures S3, S4). Thus, plastic (PTFE, perfluoroalkoxy (PFA), etc.) or other leach-proof apparatuses should be considered when generating $Zr(OH)_4$. Careful attention to the variables surrounding the hydroxylation and incubation of the suspension should yield a tetragonal zirconium hydroxide precursor ready for sulfation and crystallization.

Sulfation and Expressed Acidity. Of course, there are significant nuances to consider when sulfating the $Zr(OH)_4$, or amorphous zirconia if the sample was precalcined. First, let us discuss how surface sulfation influences the acidity of SZrO. Sulfation effectively eliminates the expression of basicity normally observed on calcined zirconia, and it is not recovered when excess sulfates are labilized during calcination. In its place, sulfate exposure generates new acidic behavior and structures on the tetragonal SZrO produced.[169] It is generally agreed that tetragonal zirconia retains both bridged and terminal hydroxyl groups upon sulfation, though Lónyi et al. found sulfation eliminated the terminal hydroxyl species that Bolis et al. believe are the source of any lingering basicity on SZrO.[142,169,174] Though the strong Brønsted acid sites on SZrO are primarily generated by hydration and greatly outnumber the sulfur atoms/nm^2, the concentration of Brønsted acid sites increases with higher sulfate loadings.[59,131,140,162,201] While tetragonal zirconia has no Brønsted acid sites capable of *n*-butane isomerization, tetragonal SZrO's weakest Brønsted acid sites have demonstrated impressive catalytic activity below 100 °C.[59,169] Increasing sulfate loadings up to at least 12 wt % also increases the thermal stability of the tetragonal phase, reducing the surface area, pore size, and pore diameter that is lost under calcination and reaction conditions.[59,61,88,96] Sulfation also substantially reduces the abundance of Lewis acid sites on tetragonal zirconia, but the strength of those that remain is increased. Two Lewis acid sites with unique strengths can be detected on unsulfated zirconia, but only one remains post-sulfation. While sulfate proximity to the Lewis acid sites impacts accuracy, heats of CO adsorption suggest the strength of the Lewis acids on SZrO (>80 kJ/mol) are not much stronger than those on the unsulfated tetragonal phase (70 kJ/mol).[121,169] Though acidity is stronger after sulfation, neither of the individual Lewis and Brønsted acid sites of SZrO are strong enough to be considered superacidic.[60,89] Thus, defining the structure to function relationships between these acid sites and surface SO_x species is critical to explaining SZrO's superacid-like activity. It is probable that the electron-withdrawing nature of the sulfate oxyanion reduces the electron density of proximal oxygens and coordinatively unsaturated zirconium atoms to make the hydroxyl groups better proton donors and increase the electrophilicity of the metal centers (Figure 4i).[79,96] Because of this, the unique active sites of the two catalytically valuable forms of SZrO, strong but isolated acid sites and weaker but dense acid sites, are defined by the surface sulfate loading.

The expression of weak but abundant Brønsted acid sites occurs at high sulfate loadings that approach saturation of the zirconia surface with a sulfate monolayer, while sulfate loadings associated with the expression of both strong Brønsted and Lewis acid sites partially cover the surface with 1−2.5 sulfur atoms/nm^2.[59,131,202] Near half-monolayer (∼2.5 sulfur atoms/nm^2) coverage of a tetragonal zirconia surface with sulfates, the strongest but low-density (0.5 acid sites/nm^2) acid sites on SZrO have NH_3 heats of adsorption of 200 kJ/mol. While the weaker, more densely packed (2 acid sites/nm^2) acid sites of SZrO saturated with a full sulfate monolayer have 40 kJ/mol weaker NH_3 heats of adsorption, their strengths are competitive with the strongest acid sites of typical zeolites (110−170 kJ/mol).[59,105] Although more detailed spectroscopic characterization has verified SZrO's acid sites are not strong enough to be considered superacidic, Katada's team devised a conversion for the isolated NH_3 heats of adsorption to Hammett acidity values. They found these heats of adsorption values agree with the strongest (H_0 = −19.1) and weakest (H_0 = −12) reported Hammett acidity values for SZrO, demonstrating the relationship between acid strength and sulfate loading.[59] These high heats of adsorption are likely related to effects that impede the accuracy of NH_3 desorption from solid acid surfaces (e.g., diffusivity in pores, disproportionation, reabsorption, multiple adsorption layers).[67,114,120,122] The acid sites of zeolites are generally stronger when the total surface acid site density is below 500 μmol/g, as the Al^{3+} atoms that generate its acid sites have a greater polarizing effect when

https://doi.org/10.1021/acs.langmuir.3c03966
Langmuir XXXX, XXX, XXX−XXX

Pursuant to the DOE Public Access Plan, this document represents the authors' peer-reviewed, accepted manuscript. The published version of the article is available from the relevant publisher.

isolated from one another.[203] Similarly, the stronger acid sites expressed at lower sulfate loadings could be explained by a stronger electron-withdrawing effect when sulfates are isolated from one another on the surface.[59]

The coordination modes of these sulfates are also likely to influence their inductive effect, but given the inconsistency of synthesis and activation conditions across SZrO's literature, sulfate coordination structures on tetragonal zirconia have not been unambiguously defined.[57,125,154,158] Still, spectroscopic analysis has revealed several structural insights: (i) below 1.7 sulfur wt %, isolated μ_3-sulfates dominate, (ii) the strongest acid sites stem from μ_2-bisulfates whose expression is maximized at 1.7 sulfur wt %, and (iii) higher sulfate loadings cause proximal bisulfates to merge into pyrosulfates.[131] The stability of μ_3-sulfates depends on the facet's arrangement of zirconium atoms, but this coordination mode forms more bonds to surface zirconium atoms and reduces their degrees of unsaturation (i.e., Lewis acid strength) compared to the μ_2-coordination mode.[174] Near or beyond completion of a sulfate monolayer, the coordination modes as well as the SO_x species begin to change, as pyrosulfates form on the densely covered zirconia. While pyrosulfates exhibit significant Brønsted acid strength, these species are more prone to decomposition, and their appearance is tied to the complete loss of SZrO's Lewis acidity.[123,140,154] As individual sulfate/bisulfate species coexist on SZrO depending primarily on hydration, distinguishing them from pyrosulfates is critical to validating a desirable sulfate loading.[125,131] Although some believe pyrosulfate should be experimentally distinguishable by its S═O vibration between 1400−1420 cm^{-1} on activated SZrO, pyrosulfate and S═O bonding vibrations are not detectable without in situ analysis of the activated catalyst in a dry atmosphere.[125,140,154] Alternatively, since isolated surface sulfates decompose into SO_2 at high temperatures, $S_2O_7^{2-}$ can be identified by the release of SO_3 at lower temperatures.[88,131] Also, UV−visible spectroscopy can discriminate pyrosulfate signals, as the HOMO (highest occupied molecular orbital)−LUMO (lowest occupied molecular orbital) gap is higher for isolated sulfates than the delocalized electron density of pyrosulfates.[158] Sulfate loadings can be increased further to a maximum concentration at which no new Brønsted acid sites appear, and excess sulfates are desorbed during calcination or may linger as $Zr(SO_4)_2$.[57,59] As they decompose and desorb, sulfates and other oxyanions are believed to contribute to oxidation of the zirconia surface and eliminate anionic defects.[88,136,152] To examine the structure−function relationships of the sulfate species that form at different sulfate loadings, we must define the synthetic variables of sulfation.

Impregnation Sulfation. Sulfation is typically performed by impregnation, where $Zr(OH)_4$ or amorphous zirconia is submerged in a 0.5−2 M solution of $(NH_4)_2SO_4$ or H_2SO_4 for 1−24 h followed by decanting the liquid and drying the solid at temperatures as high as 100 °C.[59,61,204] Several liquid sulfation alternatives to impregnation have been reported, but each has significant drawbacks. Sulfation may be carried out by washing and filtering the zirconia precursor with very concentrated sulfate solutions. But, this method provides poor control of sulfate loading, and substantially higher sulfate loadings may be achieved by impregnation with less waste.[61,204] The number of synthetic steps can be reduced by sulfating the $Zr(OH)_4$ suspension instead of the dry solid, though the presence of oxyanions is likely to impact the $Zr(OH)_4$ polymerization process.[196] These one-pot syntheses have even generated amorphous or monoclinic SZrO with significant, though often lessened, catalytic function. However, Cl^- and NO_3^- cannot be easily removed from these mixtures without the loss of weakly coordinated sulfates prior to calcination, and the zirconia proves difficult to crystallize without forming the monoclinic phase. Since samples prepared by sulfating suspended $Zr(OH)_4$ or mixing the zirconyl salt with a solid sulfating agent tend to require higher sulfate concentrations to generate similar loadings to conventional SZrO, these challenges with crystallization may also be related to $Zr(SO_4)_2$ formation.[51,135,163,193,205] The presence of sulfates in the suspension will also alter solution pH and crystallinity in ways that have not been thoroughly studied, and the basic pH values that favor tetragonal crystal growth also generate SZrO with lower sulfate loadings.[163,193] Thus, the well-studied and controlled deposition of sulfates by impregnation is the favored zirconia sulfation technique.

Though the optimal sulfate loadings for zirconia impregnated with either $(NH_4)_2SO_4$ or H_2SO_4 are seemingly identical, the acidity expressed is not.[59,131] For example, some $(NH_4)_2SO_4$ sulfated samples have superior retention of Lewis acidity and require higher calcination temperatures to achieve optimal catalytic activity. This could potentially be explained by sulfation with $(NH_4)_2SO_4$ causing NH_3 to coordinate to amorphous zirconia acid sites and linger until thermally desorbed. NH_3-TPD has demonstrated that a significant amount of ammonia is desorbed from SZrO at temperatures near 620 °C (Figure 6ii), a typical SZrO calcination temperature.[61,64,146,205] Though the SZrO was prepared by washing/filtering the sulfating agent over the zirconia precursor, Parera identified typical S^{6+} sulfate species (e.g., SO_4^{2-}) on samples prepared by $(NH_4)_2SO_4$ sulfation, while H_2SO_4 treated SZrO had relatively more S^{2-} species (e.g., sulfide).[61] Sorption structures of the resulting SO_x species must indeed be different, as impregnation by $(NH_4)_2SO_4$ at concentrations that form more than a half monolayer of sulfates generates a much larger surface sulfur concentration than H_2SO_4.[57] Still, these sulfating agents have not been thoroughly compared. Other liquid sulfating agents include ammonium sulfide ($(NH_4)_2S$) and ammonium thiosulfate ($(NH_4)_2S_2O_3$), but both deposit a much lower sulfur wt % than $(NH_4)_2SO_4$ and were shown to yield SZrO with little *n*-butane isomerization activity.[61] Thus, the safer handling of $(NH_4)_2SO_4$ and seemingly more abundant acid sites of $(NH_4)_2SO_4$-treated SZrO makes it the more ideal sulfation reagent compared to more corrosive sulfuric acid.[131] For both $(NH_4)_2SO_4$ and H_2SO_4, the concentration of this impregnation sulfating agent is the foremost means of controlling sulfate loading.

Katada et al. studied the impact of the concentration of H_2SO_4 (0.26−4.4 M in 100 mL or 2−35 wt % SO_4^{2-}) used during impregnation of $Zr(OH)_4$ precalcined at 400 °C, then calcined at 650 °C to generate SZrO (Figure 8). Interestingly, the product's sulfate loading was largely the same (2.5 sulfur atoms/nm^2 or 1.7 sulfur wt %) for concentrations between 0.26−1.8 M. This suggests that at low sulfating agent concentrations a finite amount of sulfates are chemisorbed at strong adsorption sites and sulfates adsorbed at weaker sites are labilized during calcination.[59] However, H_2SO_4 concentrations exceeding 1.1 M to 3.3 M rapidly increased sulfate loading. Therefore, more concentrated sulfating agents may cause the formerly weakly coordinated sulfates to form more stable surface structures that persevere through calcina-

https://doi.org/10.1021/acs.langmuir.3c03966
Langmuir XXXX, XXX, XXX−XXX

Pursuant to the DOE Public Access Plan, this document represents the authors' peer-reviewed, accepted manuscript. The published version of the article is available from the relevant publisher.

tion.[59,131] When a half-monolayer of sulfates is exceeded using sulfating agent concentrations above ~1.8 M (15 wt % SO_4^{2-}), the surface concentration of acid sites detectable by NH_3-TPD rapidly increased but their strength plummeted (Figure 8iv). Pyridine-FT-IR spectroscopy further identified that while both strongly acidic Brønsted and Lewis sites formed when sulfating agents up to 1.8 M H_2SO_4 were used, the rapid increase in the relative amount of Brønsted acid sites on SZrO prepared by impregnation in >15 wt % SO_4^{2-} is caused by the simultaneous growth of the number of Brønsted acid sites and loss of Lewis acid sites. The progressive loss of acid site concentration when sulfating agents that are more concentrated than 20 wt % SO_4^{2-} are used suggests the increasing relative amount of Brønsted acid sites (Figure 8iii) is not representative of a significant increase in the amount of acid sites but the elimination of Lewis acid sites.[59] Thus, the substantially higher loadings of 10 sulfur atoms/nm^2 or >3.0 sulfur wt % achieved with sulfating agent concentrations above 20 wt % SO_4^{2-} likely induce $Zr(SO_4)_2$ formation, impeding crystallization and reducing the number of strong acid sites.[59,166,188,189] In summary, it is apparent that low sulfate loadings correspond to stronger acid sites and the expression of both Brønsted and Lewis acidity. Additionally, though NH_3 heats of adsorption indicate acid site strength is constant for SZrO prepared with sulfating agents between 0.26−1.8 M H_2SO_4, BET surface area and alkylation activity was highest in a smaller range of 0.54−1.8 M. Katada et al.'s results make it apparent that acid site density alone does not define an optimized sulfation step; the surface area, acid strength, and the relative abundance of acid site types must also be evaluated.[59,131]

Still, it is important to note that Katada et al.'s findings do not consider the relationship between sulfate loading and optimal calcination temperature.[59] Because sulfates stabilize the tetragonal phase, a higher calcination temperature is necessary when higher sulfating agent concentrations are used to remove excess sulfates, expose Lewis acid sites, and crystallize the zirconia.[96] Thus, calcination temperature must be optimized for each sulfating agent concentration. For example, when Nascimento et al. compared SZrO prepared by impregnation in a range of H_2SO_4 concentrations (0.1−1.0 M) and calcination temperatures (500−700 °C) they found that the optimal *n*-butane isomerization rate was achieved when a 0.5 M sulfated sample was calcined at 650 °C. However, a sample sulfated by a lower concentration of H_2SO_4, 0.3 M, had maximum isomerization activity when calcined at 600 °C. Furthermore, although the two catalysts have nearly identical surface areas and minimal differences in their *n*-butane isomerization rates, the 0.3 M and 600 °C SZrO had a higher final sulfate loading (1.99 sulfur wt %) than the 0.5 M and 650 °C (1.33 sulfur wt %).[57,202] Therefore, while sulfating agent concentration has a significant impact on acidity other synthetic parameters need to be adjusted around it, and the resulting sulfate loading is not the defining factor of SZrO's functional acidity. Despite the significance of sulfating agent concentration on the expressed Brønsted and Lewis acidity, other factors that likely impact sulfate loading (i.e., exposure period, perturbation, and volume of sulfating agent per zirconia precursor mass) have not been studied in detail. Insufficient reporting of these parameters has yielded high quality SZrO studies which cannot be replicated or compared against.[59,94,131,161]

Gaseous and Solid Sulfation. Though impregnation provides control of sulfate loading and expressed acidity, liquid sulfation invariably produces large volumes of liquid acid waste; thus, solvent free sulfation approaches are in development. SO_2 or SO_3-saturated air can be useful in regenerating sulfate loadings on spent catalysts, but it has also been demonstrated as the initial sulfur source in SZrO.[96,140,206] Gaseous sulfation, venting sulfur-containing gases over the solid, employs SO_x sources that are generally less oxidized (i.e., $(NH_4)_2S$, SO_3, SO_2, H_2S, CS_2). As a result, the acid/base and redox properties of gas-sulfated zirconia tend to differ from impregenation-SZrO.[140,192,201,206] Unlike liquid sulfate sources, these less oxidized SO_x molecules can be deposited on crystalline, even monoclinic, zirconia in high loadings; however, they are typically weakly-bound to the surface and unstable. The only gaseous SO_x source that forms similar surface species to conventionally prepared SZrO is SO_3, which creates very high sulfate loadings in the form pyrosulfates.[140,192,206] While some SO_3-sulfation studies have reported catalysts with high densities of Brønsted acid sites, the pyrosulfates of SO_3SZrO do not perform acid catalysis. Instead, SO_3-SZrO tends to catalyze hydrocarbon conversions through oxidative dehydrogenation.[140,201,206] Although pyrosulfates are still the catalytic driving force, the pyrosulfates of SZrO prepared by adsorption of SO_3 to unmodified zirconia appear to oxidize reactants much more aggresively than the Brønsted acidic pyrosulfates formed at similar sulfate loadings on impregnation SZrO.[201] These SO_3-SZrO pyrosulfates have been used to catalyze the isomerization of *n*-butane at 100 °C at impressive rates through the dehydrogenation of *n*-butane to butene. Even higher pyrosulfate loadings and higher catalytic activities can be achieved by performing SO_3-sulfation on SZrO prepared by impregnation sulfation. While the butane isomerization activity of these catalysts can exceed that of the acid catalyzed mechanism of conventionally prepared SZrO, each catalytic conversion decomposes a pyrosulfate. As a result, the catalyst is likely to rapidly lose this impressive catalytic function as the pyrosulfate loading is consumed.[140,201,206] For conventionally prepared SZrO, some sulfates are lost during catalysis in liquids, reducing environments, and even polymer pyrolysis. But, this acidity can be easily regenerated for many additional uses by solvent washes, thermal treatments, and re-sulfating the zirconia so long as tetragonal crystallinity is retained with some degree of surface sulfation.[53,96,159,187] SO_3-SZrO has yet to demonstrate its value in other reactions that require stronger catalytic driving forces (i.e., stronger acidity) than *n*-butane isomerization. In comparison, the need to reoxidize and sulfate each active site to recover the easily labilized pyrosulfates of SO_3-sulfated zirconia makes it less desirable than the inherent acidity and recyclability of impregnated SZrO. These gaseous SO_x species may also alter the surface chemistry in interesting ways. For example, SO_3-sulfation can abstract a surface oxygen to replicate SO_4^{2-}-like structures, suggesting SO_3 may change surface oxygen content and thus the availability of Brønsted and Lewis acid sites.[154] Numerous oxygen atom abstraction events may impact the stability of the zirconia, as SO_3-sulfation of thin zirconia films caused holes to form in their surface.[140] To resolve these issues, acidity on zirconia treated with low oxidation number sulfur sources can be induced by heating in O_2 atmospheres. Sohn et al. and Bensitel et al. demonstrated that oxidation of SO_2, CS_2, and H_2S generates FT-IR spectroscopy signals similar to those of conventionally prepared SZrO (Figure 16i).[179,192] While oxidization into SO_4^{2-}-like species induces 1-butene isomerization activity in these gas-sulfated samples,

https://doi.org/10.1021/acs.langmuir.3c03966
Langmuir XXXX, XXX, XXX−XXX

Pursuant to the DOE Public Access Plan, this document represents the authors' peer-reviewed, accepted manuscript. The published version of the article is available from the relevant publisher.

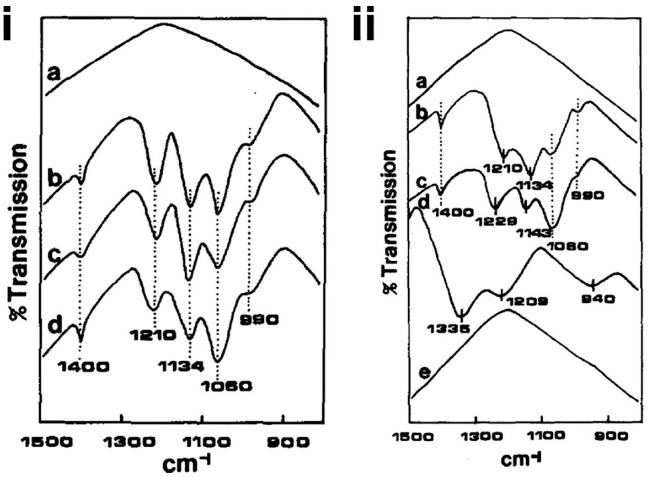

Figure 16. (i) FT-IR spectra in the range of S−O bonding of (ia) $Zr(OH)_{42}$ activated and evacuated at 350 °C, and zirconia oxidized at 400 °C with O_2 after sulfation with (ib) SO_2, (ic) H_2S, and (id) CS_2. (ii) FT-IR spectra in the range of S−O bonding for (iia) $Zr(OH)_4$ activated and evacuated at 350 °C, (iib) impregnated sulfated zirconia, and sample-iib reduced at 500 °C with H_2 for (iic) 0.5 h, (iid) 1 h, or (iie) for 2 h. Adapted by combining two figures with permission from ref 192. Copyright 1989 Elsevier.

conversion rates are still notably slower than SZrO prepared by $(NH_4)_2SO_4$ or H_2SO_4 impregnation.[192] Sohn et al. also verified that catalytic activity is lost if H_2SO_4 impregnated SZrO is reduced with H_2 at 500 °C. The progressive elimination of sulfur−oxygen bonding from FT-IR spectra indicated that SO_4^{2-}-like species are reduced and eventually desorbed in reducing atmospheres (Figure 16ii). This explains the significant sulfate loss observed when Pt-doped SZrO is employed as a hydrocracking catalyst in high pressures of H_2.[51,96,192] These studies demonstrate that prior to sulfur desorption surface SO_x species can be reversibly oxidized and reduced, as well as the significance of the S^{6+} oxidation state in generating acid sites on SZrO.[61,82,192] Reducing environments may still prove useful if used prior to sulfation though, as hydrogenation is believed to generate anionic vacancies and more active sites on metal oxides. Vera et al. successfully increased the expression of acid sites and the tetragonal:monoclinic zirconia phase ratio of crystalline zirconia by heating at 550 °C under H_2 flow, then impregnating with H_2SO_4, and calcining to form SZrO. The authors speculate that the presence of anionic vacancies on amorphous zirconia and reduced crystalline zirconia are needed for sulfates to coordinate to the surface and strong acid sites to form.[136] Atmosphere composition during preparation and use of SZrO is also important to consider, as Zr^{4+} atoms are reduced and surface oxygen and sulfur content is lost during calcination in reducing and even inert atmospheres. On the other hand, calcination in air and other oxidizing atmospheres is thought to enrich the surface oxygen content, limit sulfate loss, and reduce the number of defects in the final product.[61,96,136,162] Kobe et al. found that activation at temperatures above 400 °C results in irreversible surface alternations that reduce *n*-butane isomerization activity unless an oxidizing atmosphere is present.[175] Thus, calcination and activation steps are generally performed in air instead of reducing or inert atmospheres, though the difference between static or flowing air has not been closely studied.[61,96,136,162] The liquid waste of impregnation sulfation has also led to the development of solid sulfating agent alternatives.

Recently, solvent-free sulfation has been demonstrated by the simple calcination of a zirconyl salt ground with solid sulfating agents. Though few solid SO_x sources have been studied, comparison to sulfamic acid (NH_2SO_3H) demonstrated that solid $(NH_4)_2SO_4$ generates a superior sulfate loading, sulfate covalency, thermal stability, and Lewis acid site density.[205] By calcining a large excess (6:1 molar ratio) of solid $(NH_4)_2SO_4$ with $ZrOCl_2$, SZrO with high surface area, sulfur content, and cumene cracking activity at 300 °C was generated. The number of strong Brønsted acid sites detectable by pyridine probing was substantially higher for the dry-SZrO compared to conventionally prepared SZrO. However, as the catalyst had double the sulfur loading of the impregnated catalyst and little Lewis acidity, the activity likely came from more weakly Brønsted acidic pyrosulfate-based acid sites.[135] It is likely that the excess sulfate also generated a large amount of $Zr(SO_4)_2$ in place of sulfated zirconia.[166,188,189] The broadness of the reflections of the PXRD pattern of the dry sulfated sample (Figure 17) suggests the dry-SZrO is largely

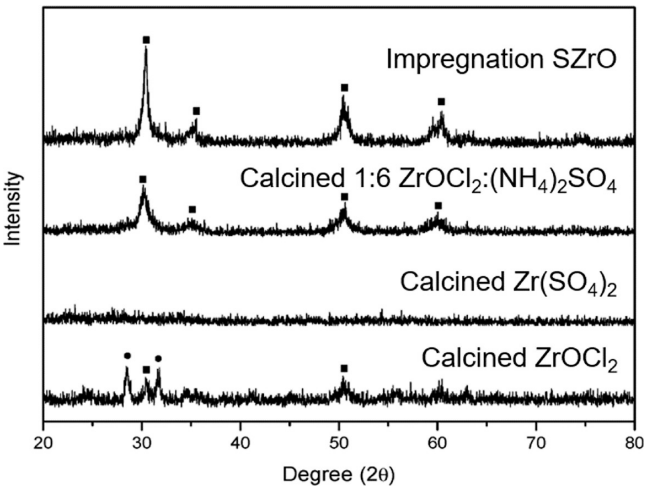

Figure 17. PXRD patterns for impregnation sulfated zirconia and calcined mixtures of ground $ZrOCl_2$ and $(NH_4)_2SO_4$ and other salts. Squares mark the signature tetragonal zirconia reflections while circles mark the signature monoclinic zirconia reflections. Adapted by adding titles over each pattern with permission from ref 135. Copyright 2005 American Chemical Society.

amorphous at typical calcination temperatures due to the presence of $Zr(SO_4)_2$ and unremoved Cl^-.[135] Though Sun et al. observed no crystallinity when calcining $Zr(SO_4)_2$ at 600 °C, other authors have found that $Zr(SO_4)_2$ does crystallize into zirconia. The process just begins at much higher temperatures (~550 °C) than those needed to crystallize $Zr(OH)_4$ into zirconia.[135,166,188] Still, a large excess of the solid sulfating reagent seems critical to the generation of tetragonal SZrO, as dry sulfation by the same method with less excess (2:1 or lower molar ratios) of $(NH_4)_2SO_4$ to $Zr(OH)_4$ generated SZrO with a large amount of the monoclinic phase.[160] While solid sulfation techniques are still in their infancy, with other studies contradicting the need for a high sulfate loading, the lessened complexity and hazardous waste generated suggest it may be valuable in catalyzing reactions driven by weaker Brønsted acid sites.[205]

https://doi.org/10.1021/acs.langmuir.3c03966
Langmuir XXXX, XXX, XXX−XXX

Pursuant to the DOE Public Access Plan, this document represents the authors' peer-reviewed, accepted manuscript. The published version of the article is available from the relevant publisher.

Presently, impregnation of $Zr(OH)_4$ or amorphous zirconia by dilutions of $(NH_4)_2SO_4$ or H_2SO_4 provides the most effective control of sulfation for research applications. Through this literature analysis, we have identified the significance of hydration, crystallinity, and sulfation to the expressed acidity of SZrO, though bulk characterization techniques like those discussed above cannot fully define the structure of its acid sites. Thus, the exact structures that the deposited water and sulfate molecules adopt must be studied at the atomic-level to further define the acidity of SZrO and better intuit its synthesis.

Relationships Between Facet Surface Structures and Acidity. Various sulfate coordination structures have been proposed to explain the high catalytic activity of Brønsted and Lewis acid sites on SZrO. While studies agree that bridging sulfate and hydroxyl species exist on tetragonal SZrO, there is disagreement on whether or not terminal hydroxyl groups are retained and the presence of chelating sulfates at low temperatures.[131,142,169,174] Models have been proposed by Yamaguchi et al., Arata and Hino, Babou et al., Rabee et al., and various other authors in which appropriate oxidation of SZrO prepared with any sulfur source will generate the dehydrated structures that appear at various sulfate loadings (Figure 18).[82,125,131,178,188] Numerous models have attempted

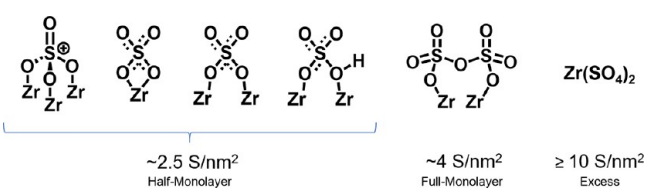

Figure 18. A nonextensive summary of FT-IR spectroscopy and computationally validated sulfate coordination structures for sulfated zirconia across different surface sulfate loadings.

to explain the superacid-like activity of SZrO's Brønsted and Lewis acid sites, but most are based on bulk analysis instead of atomic-level characterization. As previously discussed, multiple Brønsted acidic species and at least one Lewis site of unique strength are present on SZrO, but its catalytic activity cannot be explained by acid strength or confinement effects. Thus, functional acidity is likely impacted by the arrangement, proximity, and structure of the coordinatively unsaturated Zr^{4+} atoms, hydroxyl groups, and sulfate moieties. Many of the previously proposed structures have been critically reviewed by Song et al., Yadav et al., and Yan et al., and they agree that the inductive effect of the surface-bound sulfates enhances acid strength in proximal surface species, Lewis acids are coordinatively unsaturated Zr^{4+} sites, and Brønsted acidity originates from hydroxyl, water, or protonated SO_x species.[57,96,158] The structures of SZrO's active sites can be best defined by modeling the proposed structures of these atomic features on the stable facets of tetragonal zirconia.

Computational Study of Zirconia Facets. Computational modeling of the exposed surface of nanoparticle catalysts is a powerful tool for probing structure−function relationships of unmodified and functionalized inorganic catalysts. Though more prominent for metal nanoparticle design, metal oxide facets may also be probed. Typically, the bond energy of the bisected bonds along a crystal plane of a specified surface area (m^2) provides a good approximation of the facet's surface energy. However, binary oxides like zirconia are more prone to defects (i.e., steps, kinks, vacancies), meaning the stability of a facet is dependent on a variety of synthetic variables. Also, a significant amount of SZrO's Lewis acid sites may arise from defects, facet terminations, or an unpredictable amorphous phase that cannot be easily modeled.[207−209] The oxidizing, reducing, and hydrating atmospheres employed during synthesis and activation will all also contribute to deviations from idealized surface chemistry.[162,192] Thus, computational studies of ideal facets may not elucidate true zirconia behavior or properly predict the growth of particles and their exposed facets. Still, computational slab and cluster models provide a stronger foundation to laboratory studies of SZrO's surface chemistry.

While repeated, symmetric atomic planes do not typically generate a polar, catalytically active metal oxide surface, the slightly distorted structure of tetragonal zirconia has several stable facets with significant dipole moments and surface energy. Still, higher surface energy facets are more unstable, meaning only a select few are likely to be exposed in practice.[140,200,208] The most common nonequivalent facets observed by TEM for unsulfated tetragonal zirconia are (101), (001), and (100), matching Bravais−Friedel−Donnay−Harker theory. Based on computationally determined surface energy determined by Piskorz et al. (Figure 19ii), the relaxed surface energies of the relatively stable tetragonal zirconia facets that could be exposed should be ordered as (101) < (001) < (100) < (111) < (110), with higher-surface-energy facets generally having lower coordination number zirconium and oxygen atoms.[186] For the distorted unit cell of tetragonal zirconia, (001) is not equivalent to (100) and (010).[140,200] Though the rigid, position-locked facets are much higher in surface energy, upon relaxation the lower coordination number Zr^{4+} atoms along the (100) and (111) facets are displaced beneath the top layer of surface atoms to lower their surface energy.[186] The tetragonal zirconia surface also experiences observable reconstructions upon hydration, with hydration stabilizing and relaxing the surface of the facets like (101) and (001).[157] Wulff shapes that predict facet growth of nanoparticles at various degrees of hydroxylation (i.e., water surface coverage) suggest that dehydrated tetragonal zirconia particles primarily express faces of the lowest energy facets, but stabilization from hydration exposes more surface area of the (100), (110), and (111) facets (Figure 19iv). Thus, these models demonstrate that the expression of the higher surface energy (110), (100), and (111) facets should increase in hydrating environments. These results fit well with unsulfated particle shapes observed by TEM.[186] Since water can promote the solvothermal growth of nanoparticles in specific directions by stabilizing high surface energy facets like other chemical additives (i.e., surfactants, ions, polymers) and sulfates enhance thermal stability of tetragonal zirconia, perhaps sulfation promotes growth of the (111) and (110) facets as well.[208,209] Unfortunately, few conventionally prepared, well-faceted SZrO samples have been characterized by TEM. Benaïssa et al. provided some of the highest-resolution TEM analysis of SZrO with well-faceted tetragonal particles and minimal defects at plane terminations, though it appears facet assignments were made based only on crystallographic orientation and *d*-spacing.[167,210] The <10 nm SZrO crystallites exhibited facets primarily in the ⟨111⟩ and ⟨010⟩ orientations, with ⟨111⟩ having long stretches of {110} faces and ⟨010⟩ having regular {101}, {001}, and step-defected {100} faces (Figure 20). Indeed, sulfation exposed large faces of (111) and other high surface energy tetragonal zirconia

https://doi.org/10.1021/acs.langmuir.3c03966
Langmuir XXXX, XXX, XXX−XXX

Pursuant to the DOE Public Access Plan, this document represents the authors' peer-reviewed, accepted manuscript.
The published version of the article is available from the relevant publisher.

i

$$\gamma = (E_{slab} - nE_{bulk})/2A$$

ii

Tetragonal Zirconia Facets

exposed plane	(101)	(001)	(100)	(111)	(110)
$\gamma/(J/m^2)$ rigid surface	1.33	1.21	2.10	3.14	3.18
$\gamma/(J/m^2)$ relaxed surface	1.06	1.17	1.23	1.25	1.77

iii

Monoclinic Zirconia Facets

exposed plane	(−111)	(111)	(−101)	(101)	(011)	(110)	(001)	(010)	(100)
$\gamma/(J\cdot m^2)$ rigid surface	1.34	1.39	1.71	2.37	1.89	2.26	1.97	2.53	1.88
$\gamma/(J\cdot m^2)$ relaxed surface	0.87	1.06	1.23	1.52	1.34	1.42	1.35	1.75	1.47
relative relaxation energy/%	35	24	28	36	29	37	31	31	22

iv

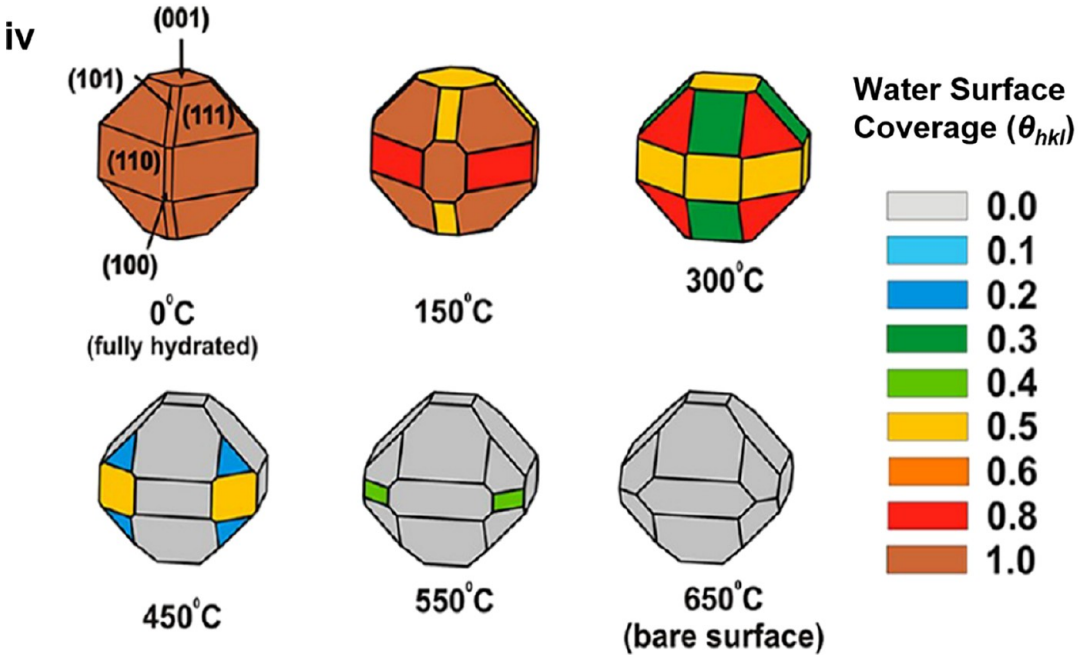

Figure 19. (i) A theoretical surface energy (γ) equation in which the energy of a specified number of units (n) of the bulk (E_{bulk}) is subtracted from the slab model's energy (E_{slab}) over a given surface area (A) of theoretically stable facets of unsulfated (ii) tetragonal and (iii) monoclinic zirconia. (iv) Wulff shapes of tetragonal zirconia nanocrystals as a function of temperature in anisotropic water adsorption at p_{H2O} = 0.01 atm expressed in terms of water surface coverage. Adapted by combining several figures, removing a "relative relaxation energy/%" row and blank space after the units of the two tables, as well as rearranging the Wulff shapes in a horizontal pattern and replacing "θ coding" with "Water Surface Coverage (θ_{hkl})" with permission from refs 185 and 186. Copyright 2011 and 2012 American Chemical Society.

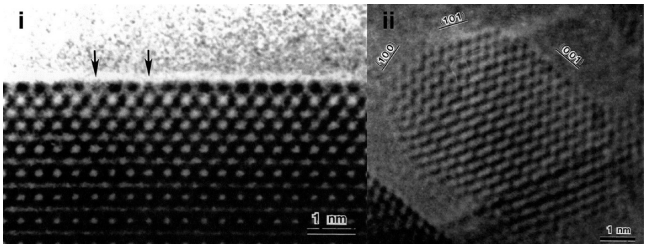

Figure 20. High-resolution TEM images of sulfated zirconia facets in the (i) ⟨111⟩ and (ii) ⟨010⟩ orientations. The (111) facet shows long stretches of the (110) facet with potential defects and a bright surface layer assigned to a monolayer of sulfates. The (010) facet exhibits clean (101) and (001) faces and short, step-defected (100) faces. Adapted by combining two figures and removing a "b" used for identification from figure 20i used for identification with permission from ref 167. Copyright 1996 Elsevier.

facets. Numerous potential defects that contribute to Lewis acidity were also observed. Importantly, while void defects can be seen on the (110) edge, they are less abundant than defects on the edge facets along the ⟨010⟩. Additionally, the authors assign the bright monolayer at the facet edges to a layer of sulfates. The void space between the zirconium atoms is sufficient for these sulfates to assume either a μ_2- or μ_3-coordination structure, in good agreement with spectroscopic predictions (Figure 20i).[167] In spite of these figures being among the highest quality available for faceted tetragonal SZrO nanoparticles, the few images provided have some peculiar qualities that reflect the instrumentation limitations of the time in 1996. Also, since conventional TEM is performed in a vacuum but typically not with activated catalysts, hydration of the facets may impact the atomic arrangements observed on these surfaces, particularly near defect sites.

A similar study of unsulfated monoclinic zirconia by Piskorz et al. (Figure 19iii) demonstrated that the sulfated tetragonal phase's (111) and (110) facets do indeed have higher surface energies than most monoclinic facets.[185,186] The modeled surface energies for the relaxed nonequivalent monoclinic

https://doi.org/10.1021/acs.langmuir.3c03966
Langmuir XXXX, XXX, XXX−XXX

Pursuant to the DOE Public Access Plan, this document represents the authors' peer-reviewed, accepted manuscript. The published version of the article is available from the relevant publisher.

facets follow the trend of (−111) < (111) < (−101) < (011) < (001) < (110) < (100) < (101) < (010). Though Wulf shapes predict the hydroxylated facet growth of the (100) and (101) facets, only the (−111), (111), (011), and (001) facets have been experimentally reported for unsulfated monoclinic zirconia. Assuming growth of higher surface energy monoclinic facets will be favored in the presence of a sulfate source, the difference in the tetragonal and monoclinic facet surface energies is small. Still this small difference manifests as a superior sulfate loading and stronger acid sites on higher surface area tetragonal SZrO nanoparticles.[174,185] Thus, while surface energy influences facet growth in the presence of sulfates, modeling the coordination structures of hydroxyl/water and SO_x groups on the experimentally observed tetragonal facets has provided further insight on the stability and expressed acidity of SZrO's surface.

We previously established that sulfating crystalline zirconia generates SZrO with lower sulfate loadings and acid densities likely impacted by differences in the facets exposed and the sulfate sorption sites available. Thus, the presence of sulfates during calcination is likely to differ from modeling deposition of SO_4^{2-} on already crystalline facets. Even so, computational models of sulfate and water deposition can guide us toward the favored coordination structures on all five predicted tetragonal zirconia facets. Although TEM images indicate sulfation promotes growth of the (111) and (010) facets, expectation that the most stable unsulfated facet would dominate has driven study of the (101) facet.

The (101) Tetragonal Facet. The eight-coordinate Zr^{4+} atoms of the tetragonal (101) facet yields two tetrahedra of strongly (210 pm bonds) and weakly (243 pm bonds) coordinated oxygens surrounding each zirconium atom in bulk zirconia. Cutting along the (101) plane severs one strong or weak bond, with loss of the stronger bond generating stronger Lewis acid sites. Upon hydration of a ten-layer thick DFT slab model of the (101) facet, molecular adsorption of water was observed over the weak Lewis acid sites (−105 kJ/mol), and stronger, dissociative adsorption (i.e., hydroxylation of a zirconium atom and hydrogenation of an oxygen atom) was observed over the strong Lewis acid sites (−194 kJ/mol).[140,176] While other models found dissociative water adsorption over both the weak and the strong acid sites, all predicted water preferentially chemisorbs at the stronger Lewis acid sites first. Also, each successive water adsorption event had a lower adsorption energy, corroborating theories that excess hydration lowers zirconia surface energy.[154,157,211] Another (101) facet slab model explored the proton transfer energies of the hydroxyl groups generated by water adsorption. The extremely weak Brønsted acid sites of the sulfate-free (101) tetragonal zirconia facet had proton transfer energies of 6.14−8.26 kcal/mol, but these energies increased to 100.62 and 101.91 kcal/mol upon sulfation of the slab model. These results verified that the sulfate's inductive effect contributes to Brønsted acid strength in proximal hydroxyl groups.[123] Sulfation of a 2 × 2 × 3 model of the (101) facet revealed its strong and weak Lewis acid sites form two unique hexagonal rings of Zr−O bonds on the surface. One ring is a strong sulfate adsorption site composed of two strong and one weak Lewis acid sites, while the other type of ring is a weak sulfate adsorption site composed of one strong and two weak Lewis acid sites. The strong and weak sulfate adsorption sites alternate, so a strong site is not proximal to another strong site.[123] Similar to water, SO_3 favors adsorption to the stronger sites (−336.6 kJ/mol) over the weaker sites (−258.5 kJ/mol); however, coordination of a second SO_3 is much less favorable (−25.8 kJ/mol).[154] Thus, the expression of a single Lewis acid strength on SZrO is likely explained by the elimination of the stronger Lewis acid site during sulfation and hydration. Because the energetics of water and SO_x species adsorption will change as the strong Lewis acid sites are eliminated, the surface energy is reduced, and interactions form between proximal surface moieties, and coadsorption models must be evaluated as well.

When SO_3 and water adsorb to the slab simultaneously, SO_3 still coordinates to the strong Lewis acid sites while water is displaced to the weaker sites. By far, the most stable sorption structure on (101) is SO_3H^+ and an OH^- species (−370 kJ/mol), facilitated by hydrogen bonding between a bridging hydroxyl group and an S═O bond. Other stable species include $2H^+$ and SO_4^{2-} (−315 kJ/mol) or H^+ and HSO_4^- (−292 kJ/mol).[154] Though Hofmann et al. speculated that the atomically analogous coadsorption of water and SO_3 should resemble H_2SO_4 adsorption, and dissociation of H_2SO_4 into SO_3H^+ and OH^- was not favorable on the (101) facet. Thus, dissociation of H_2SO_4 into $2H^+$ and SO_4^{2-} is more likely to occur; the adsorption of SO_3 differs. While Hofmann et al. found SO_3 treatment generates a μ_2-coordinated SO_4^{2-} by extracting a surface oxygen, Haase et al. found SO_3 has a repulsive interaction with the (101) surface, suggesting there is a high energetic barrier for abstracting a surface oxygen from the (101) facet.[154,176] However, on other facets like the (001) facet oxygen atom abstraction upon sulfation with by SO_3 to form a SO_4^{2-}-like structures is indeed favorable (−467 kJ/mol), more so than the dissociative adsorption of H_2SO_4 $(-408\ kJ/mol)_4$.[176] Since SO_3-sulfation will not generate new Lewis acid sites due to oxygen atom abstraction, the (101) facet should have no Lewis acidity if both water and a SO_x species adsorb. Therefore, facet edges, defects, or amorphous borders may be necessary to facilitate proximity of Brønsted and Lewis acid sites on the (101) facet; still, atmospheric conditions may introduce new surface defects. Haase et al.'s study of H_2SO_4 adsorption also identifies that a μ_3-sulfate is more stable for sulfuric acid adsorption than the μ_2-sulfate that would be produced by SO_3-sulfation of the (101) facet.[176] A theoretically possible μ_3-bisulfate is a far less stable interaction (−243 kJ/mol) than full H_2SO_4 dissociation into a μ_3-SO_4^{2-} and two protons (322 kJ/mol). These protons either protonate both of the strongly basic oxygens neighboring a strong Zr^{4+} Lewis acid or protonate one strong and one weak oxygen. Thus, SO_4^{2-} adsorption with various arrangements of protonation to the neighboring oxygens was investigated.[123,176]

Delarmelina et al. found that the presence of hydroxyl groups on the strong adsorption site of the (101) facet did not impact the sulfate's μ_3-coordination beyond minor bond length adjustments, likely due to hydrogen bonding. Sulfate adsorption at the weaker adsorption site extracts a neighboring hydroxyl group's proton to form bisulfate which can engage in hydrogen bonding to increase its stability. However, this μ_2-bisulfate's hydrogen can engage in hydrogen bonding with either a surface oxygen or the proximal μ_3-sulfate depending on which surface oxygens are protonated.[123] Still, the first adsorption event at the stronger sulfate adsorption site is much more favorable (−66.66 kcal/mol) than adsorption at the weaker site (−37.08 kcal/mol). Thus, the weaker sites are only expected to be sulfated at high sulfate loadings (>2.5 sulfur atoms/nm^2). These weak secondary sulfation events

https://doi.org/10.1021/acs.langmuir.3c03966
Langmuir XXXX, XXX, XXX−XXX

Pursuant to the DOE Public Access Plan, this document represents the authors' peer-reviewed, accepted manuscript. The published version of the article is available from the relevant publisher.

explain why pyrosulfate ($S_2O_7^{2-}$) is only observed at high sulfate loadings: the sulfation of both the strong and weak adsorption sites is necessary for it to form.[123,140]

Particularly water and SO_3- or H_2SO_4-rich structures form highly stable pyrosulfates upon calcination.[154] Physically, pyrosulfates can only form when two surface sulfates are in close proximity, which requires sulfation of the alternating strong and weak adsorption rings on the (101) facet. It is also likely that since sulfate adsorption is more favorable than water, high sulfate loadings that limit hydroxylation may impact hydrogen bonding interactions and lower the stability of isolated sulfate and bisulfate groups. As a result, at high sulfate loadings pyrosulfates formed by connecting sulfates across these adsorption sites may become the more stable structure.[123] A sufficiently crystaline (i.e., thoroughly calcined) surface is also needed for these ordered hexagonal adsorption sites to form. Li et. al. and Breitkopf et. al. prepared high surface area SZrO samples with inferior *n*-butane isomerization activity compared to lower surface area catalysts with identical sulfate loadings. Heating the zirconia further to increase its surface crystallinity/reduce its surface area and increasing the sulfate loading on these samples may have resolved this difference.[94,140] The most recent model of the tetragonal SZrO (101) facet 2 × 2 slab model confirms H_2SO_4's dissociative chemisorption into a μ_3-SO_4^{2-} and two protons which generate two bridging hydroxyl groups. However, Huang et al.'s study also compares sorption of water and H_2SO_4 on other high surface energy facets: (111), (100), and (001).[174]

The (101), (111), (100), and (001) Tetragonal Facets. For the tetragonal facets, (101), (111), (100), and (001), Huang et al. determined that chemisorbed water should be displaced by sulfate adsorption, which is more spontaneous than water adsorption on all four facets and explains the need for hydration after SZrO calcination.[174] However, the enhanced surface polarity upon sulfation should promote secondary water sorption events.[131,140,162,176] Only the (111) facet, which exhibits a negative ΔG for water dissociation (−5.6 kJ/mol) is modeled with preabsorbed water prior to H_2SO_4 deposition, though this water too should be displaced by sulfates. It is important to note this result could be influenced by Huang et al.'s decision choice to employ a 2 × 2 slab model for all tetragonal facets except the (111) facet, which uses a 2 × 1 slab model. Similar modeling was performed for the most stable facets of monoclinic zirconia. Though strongly acidic sulfated monoclinic zirconia structures are identified, the greater surface area and sulfur loading of tetragonal SZrO should still offer superior catalytic function.[174] Models of the sulfated tetragonal facets (Figure 21) indicate that, contrary to the surface energy trend of (101) < (001) < (100) < (111) determined by Piskorz et al., H_2SO_4 experiences increasing adsorption energy according to tetragonal facets most according to the following trend: (100) < (001) < (101) < (111).[174,186] One would assume that the relatively low surface energy of the (101) facet would not facilitate strong H_2SO_4 adsorption, but 3 seven-coordinate surface zirconium atoms return to eight-coordinate bulk saturation when the highly stable μ_3-SO_4^{2-} structure is deposited.[174] The hexagonal arrangement of the (101) facet's zirconium atoms form an equilateral triangle with 3.6 Å sides, ideal for μ_3-sulfation, but the other facets do not. For example, the (001) facet's zirconium atoms are arranged as squares that allow only two sulfate contact points at the 3.6 Å distance, thus favoring a μ_2-sulfate structure. Therefore, the other three facets do not allow

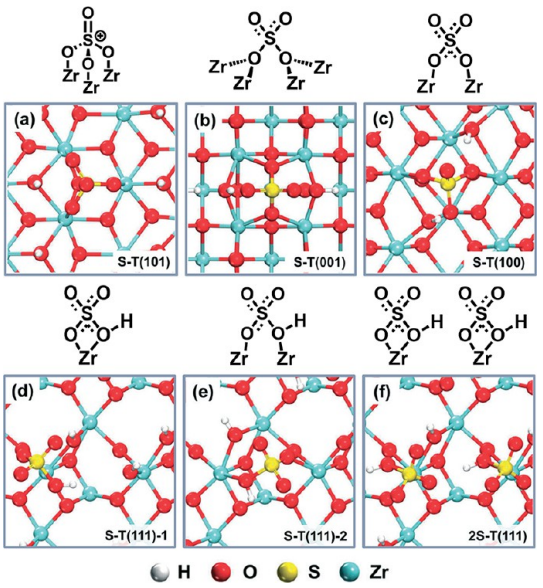

Figure 21. Optimized coordination structures for the dissociative chemisorption of H_2SO_4 on tetragonal zirconia slab models and corresponding Lewis structures for the (a) (101) facet, (b) (001) facet, (c) (100) facet, (d) (111) facet with a chelating bisulfate and water, (e) (111) facet with a μ_2-bisulfate and water, and (f) (111) facet with the water displaced by two chelating. Adapted by adding borders and corresponding Lewis structures with permission from ref 174. Copyright 2022 the Royal Society of Chemistry.

μ_3-sulfate coordination and do not restore as many degrees of saturation to surface Zr^{4+} atoms.[174,176] The highest surface energy tetragonal zirconia facet studied, (111), has the most stability to gain upon sulfation and favors a chelating bisulfate coordination to its five-coordinate zirconium atoms. Perhaps more sulfate bonds to these highly unsaturated zirconium atoms are favored but requirea a hydrogen bonding interaction to stabilize the chelating structure. Chelating sulfates were previously determined to be critical to the highest achievable Brønsted acid strength on sulfated MOF-808. The geometry optimized structure that Yaghi's group identified, in which a water's O−H bond is elongated through hydrogen bonding with a proximal chelating sulfate, closely resembles the (111) facet's chelating bisulfate.[174,180] Huang et. al considered two additional structures on the (111) facet: a μ_2-bisulfate as a similar structure was observed on higher surface energy monoclinic facets (Figure 21e), and a secondary sulfation event. This second sulfate deposition was observed to displace the preabsorbed water on the (111) facet as expected, generating a second chelating bisulfate (Figure 21f). The model of the bridging bisulfate on the (111) facet had the highest computationally determined Brønsted acidic NH_3 heat of adsorption (227 kJ/mol) in this study, greater than the next highest energies, the chelating bisulfate loaded on the (111) tetragonal facet (153 kJ/mol) (Figure 21d) and a bridging bisulfate on the monoclinic phase's highest surface energy (001) facet (179 kJ/mol).[174] Though not necessarily super-acidic, these results indicate that bisulfates are likely the source of SZrO's strongest Brønsted acid sites, having a stronger inductive effect on a closer proton source. Tetragonal zirconia's (001) and (100) facets are very similar, both having six-coordinate and seven-coordinate surface zirconium atoms, but the inequivalence of the tetragonal unit cell generates unique sulfation structures on these facets. The (100) facet forms a

https://doi.org/10.1021/acs.langmuir.3c03966
Langmuir XXXX, XXX, XXX−XXX

Pursuant to the DOE Public Access Plan, this document represents the authors' peer-reviewed, accepted manuscript. The published version of the article is available from the relevant publisher.

more typical μ_2-SO_4^{2-}, with two total contacts to oxygen atoms, but sulfates on the (001) facet bridge so its two oxygen atoms are each coordinated to 2 six-coordinate zirconium atoms. Thus, sulfation of the (001) facet is more energetically favorable.[174] Similar to the (101) facet, this unusual arrangement on the (001) facet is the result of the spatial arrangement of zirconium atoms allowing more degrees of saturation to be restored, but this coordination structure also facilitates hydrogen bonding to a proximal hydroxyl group for enhanced stability.[174] It is worth noting that Haase et al.'s study of the (101) and (001) facets found the same sulfate coordination structures but a stronger sulfate adsorption energy for the six-coordinate (001) zirconium atoms, contradicting Huang et al.'s scale.[174,176]

To summarize, the most energetically favorable sulfation event does not necessarily occur on the highest surface energy facet (i.e., the facet with the lowest coordination number surface atoms). Instead, sulfation is favored over facets with a spatial arrangement of zirconium atoms that allow a face of the tetrahedral sulfate to form the greatest number of bonds and restore the most degrees of saturation to the atoms on the surface. Huang et al.'s results provide rational for the TEM observed abundance of the (111) facet and regular faces of the (001) facet.[167] However, the abundance of the TEM observed ⟨010⟩ orientation facets, where (010) = (100), and lack of (101) facets implies that not all factors of SZrO crystal growth are accounted for by these models. Additionally, only a single sulfate deposition is considered on most of studied facets, other likely SO_x species have not been modeled on all facets, and a direct comparison with the high energy (110) facet observed in SZrO nanoparticles has yet to be reported.[167,174]

The (110) Tetragonal Facet. The (110) facet's high surface energy means it is often not considered practical as a potential tetragonal zirconia facet and few studies have attempted to model it. Hydration of the (110) facet was compared to the (101) facet on a range of slab models (i.e., 1 × 1 to 2 × 2 with increasing hydration coverage), demonstrating the substantially higher water affinity of the polar (110) facet. The dehydrated (110) facet in vacuum may undergo stabilizing surface rearrangements, potentially even reduction and elimination of surface oxygens, but the highly exothermic chemisorption of water should eliminate these reconstruction events.[212] The only reported model of the sulfated (110) facet is the seven-layer thick DFT slab model studied by Ireta et. al that provided interesting insights into the source of SZrO's acidity. Protonation of the (110) surface oxygens was observed to lower the LUMO of the surface zirconium atoms, suggesting catalytic protonation events may decrease Lewis acid strength over time. Also, hydrogen bonding between surface hydroxyl groups and proximal coordinatively unsaturated oxygens extends their O−H bond lengths and may enhance Brønsted acid strength. Although the μ_3-sulfate coordination would restore eight-fold coordination to certain zirconium atoms on the (110) surface, the μ_2-coordination proves to be more stable due to hydrogen bonding interactions with two neighboring hydroxyl groups. Though the energy difference between the μ_2- and μ_3-coordination structure is small enough that sulfates may shift to the μ_3-coordination structure at high temperatures, this suggests that stabilization from proximal hydrogen bonding species can be a more important interaction than the number of bonds restored to the coordinatively unsaturated surface atoms.[213] Synthesized SZrO samples have previously demonstrated these hypothesized thermally induced sulfate rearrangements and the potential for them to facilitate stronger acidity.[94,125] Models of methane and *n*-butane in the presence of the (110) surface show that either hydrogen bonding or electrostatic interactions with a surface bound sulfate, which are stronger with μ_3-sulfates than μ_2-sulfates, shifts the HOMO of the reactant significantly higher. The higher HOMO of *n*-butane should then be capable of facilitating a hydride abstraction interaction with SZrO, though frontier orbital overlap was not modeled.[213] The red-shift of sulfate vibrations observed upon pyridine coordination to Lewis acid sites proximal to sulfates may be relevant to paraffin coordination structures as well. Thus, the stabilization of probe molecules over Lewis acid sites by neighboring surface SO_x species may lend to the theory that sulfates play an active role in catalyzing interactions between reactants and proximal acid sites.[57,112] Dissecting the impact of the sulfate coordination structure and degree of surface oxygen atom protonation on SZrO's LUMO and the reactant's HOMO on the other facets may indicate which facet is best suited for performing hydride abstraction in the idealized depolymerization of POs.

These computational studies of the sulfated tetragonal facets have provided interesting insight into the structure−function relationships of SZrO. Effects that may not be easily distinguished by probe molecule chemisorption, such as hydrogen bonding and sulfate electrostatic interactions, were identified. The formation of pyrosulfate species across proximal acid sites with different adsorption energies was explained on the (101) facet, but the study of multi-sulfate adsorption models has not been explored for all of the tetragonal zirconia facets. Additionally, the stability of the μ_2, μ_3, and chelating coordination of sulfates differs across the high and low surface energy facets. The discrepancy in coordination preference could potentially be explained by further investigation of the spatial arrangement of surface zirconium atoms, degrees of saturation restored by sulfation, and likelihood of hydrogen bonding with proximal surface features. The strong Lewis acid sites of the faceted surfaces are likely extinguished by sulfation and hydration, but some of the weaker Lewis acid sites are retained depending on the facet, sulfate loading, steric accessibility of the zirconium atoms, and activation conditions. Despite the challenge for computational studies to model the defects and termination of facets that likely contribute to SZrO's strongest Lewis acid sites, these findings can be directly linked to laboratory observations and have revealed critical structural insights. Still, modeling sulfated and hydrated facets in the presence of Lewis acidic defects observed by TEM on tetragonal SZrO nanoparticles is a very appropriate next step. From there, controlled growth of facets has been demonstrated on other sulfated metal oxides, and design of a solvothermal or surfactant controlled growth process of high surface energy facets for SZrO is needed.[214] Although an extensive breadth of knowledge is still needed to fully comprehend the source of SZrO's acidity and optimize its synthesis, this has not delayed efforts to design more complex derivatives of SZrO.

Modified Sulfated Zirconia. A variety of dopants, supports, and specialized structures have been identified that can enhance the catalytic properties of SZrO. However, as the structure of unaltered SZrO remains ambiguous, this review prioritized identification of the critical elements of pure SZrO's acidity and synthesis. The importance of synergizing the support and metal promotor dopants is thoroughly discussed elsewhere,[50,57,96] but a few examples are highlighted here to discuss efforts to improve SZrO's thermal stability, porosity,

https://doi.org/10.1021/acs.langmuir.3c03966
Langmuir XXXX, XXX, XXX−XXX

Pursuant to the DOE Public Access Plan, this document represents the authors' peer-reviewed, accepted manuscript. The published version of the article is available from the relevant publisher.

deactivation rate, and catalytic activity. SZrO's strongest Lewis acid sites are prone to rapid coking and deactivation, but cracking activity can be retained for longer periods by doping SZrO with hydrogenation-capable and Lewis acidic metal nanoparticles.[51,210] Though metal nanoparticles capable of hydrogenolysis and hydrocracking on acidic supports (e.g., Pt, Ir) drive up cost, reduce olefin yield, and decompose sulfates, the presence of 350 psig H_2 and 0.5 wt % Pt loaded on SZrO appears to lower the onset decomposition temperature of dotriacontane PE from near 200 °C to below 170 °C. Alternatively, Lewis acidic transition metals (Mn, Fe, Ce, etc.) generate new and stronger acid sites; nevertheless, Fe and Mn nanoparticles have been reported to expose more of the lower surface energy (101) and (001) facets and block strong acid sites and pore openings.[50,53,57,58,96,210]

Modification of acidic metal oxides with surface organometallic catalysts (SOMCs), typically small alkylated or arylated transition metals, has proven to be an industrially valuable means of replicating or improving the previously discussed homogeneous organometallic catalysts' performance on a heterogeneous surface. These solid catalysts offer high selectivity and unique reaction pathways compared to their homogeneous counterparts.[215−219] SOMC loaded metal oxides also offer high-performance alternatives that consume less of the high-cost metal catalysts used in hydrogenolysis, hydrogenation, and olefin polymerization, metathesis, and functionalization reactions (e.g., Pt, Ir). These precious metals can also be replaced entirely with earth-abundant transition metals (e.g., Zr, Hf, Ni) in some cases.[126,147,216,217,219] SZrO and other sulfated oxides are of particular interest as supports, as the SOMC's activity is driven by their metal's electrophilicity which is enhanced on acidic oxide surfaces.[126,147,217,219] If an insufficient acidic strength support is used to chemisorb the complex, the primarily covalent interaction decreases the amount of catalytically active SOMC sites. For example, the number of SOMC sites that are catalytically active in ethylene polymerization increases from 12% on unsulfated alumina to >60% on sulfated alumina.[147] Highly Lewis acidic metal centers bound as an electrostatic ion pairs with the surface are produced by chemisorbing over the strongly Brønsted or Lewis acidic sites of sulfated metal oxides.[126,147,217,219] Regardless of the acid site used to anchor the organometallic complex, the acid site tends to become catalytically ineffective and is replaced by the function of the new SOMC site.[218] Side reactions performed by lingering sulfated metal oxide acid sites likely occur but are reportedly not be very significant under hydrogenation/dehydrogenation reaction conditions.[215,219] The abundance of relatively strong Brønsted and Lewis acidic sites on SZrO and sulfated alumina provide particularly abundant SOMC adsorption sites.[126,147,217,219] On these sulfated metal oxides, energy minimized chemisorption calculations have observed coordination of the cationic complexes over one or more S═O bonds, suggesting that the sulfates play an additional role in sorption of organometallics that may be relevant to interactions with reactant molecules.[126,147,217,219] The value of SOMCs on sulfated metal oxides cannot be understated. For example, deposition of $Zr(neopentyl)_4$ on sulfated alumina yields the fastest reported (i.e., <48 min) hydrogenolysis of POs to liquid products at 200 °C and 2 atm of H_2 using a noble-metal-free catalyst.[217] In the absence of the solvents and pressurized hydrogen used to catalyze these other reactions, perhaps a controlled loading of highly Lewis acidic organometallic sites on SZrO could enhance the Lewis acidity used decompose paraffins.

Though porous derivatives of SZrO are of particular interest to the superacid-mediated depolymerization of POs, porous SZrO has an abundance of exterior acid sites and other problematic drawbacks. Alternatively, various support oxides have been demonstrated to increase the surface area, porosity, and thermal stability of zirconia, even generating unsulfated tetragonal zirconia with high thermal stability (e.g., MgO, CaO, Sc_2O_3, Y_2O_3, La_2O_3, CeO_2).[167] Tetragonal zirconia crystallites above the critical nanoparticle size (>20 nm) have even been prepared by performing the synthesis in the presence of yttria or silica and subsequently digesting the support.[181,183] Coprecipitation of zirconia with supports enhances its catalytic function by either expanding its surface area and porosity (i.e., SiO_2, Y_2O_3), polarizing the exposed facets to enhance their acidity and tetragonal phase stability, or offer a mixture of both effects (i.e., TiO_2, Al_2O_3).[109,142,146,167,181,183] These materials would likely make good porous architectures for the confinement of SZrO nanoparticles, but most synthetic efforts seek to enhance the porosity of SZrO without a support.

Various authors have reported the synthesis of zirconia or SZrO with a narrow distribution of pore sizes using templating surfactants (e.g., CTAB, Pluronic P123, Brij 56) or ionic liquids to structure and stabilize the oxide surface.[134] Supercritical solvent extraction in place of air drying or heating steps can also aid pore retention.[96,220] However, unlike the lower coordination number of silicon atoms in pore-structured SiO_2 and zeolites, zirconium atoms are left more coordinatively unsaturated and have poor thermally stability upon surfactant removal above 600 °C. These structuring agents also increase the difficulty of controlling sulfate loading. Sulfation of the zirconia/surfactant composite impedes pore collapse and transition to the monoclinic phase, but the very small ∼2 nm mesopores generated are often at least partially amorphous prior to pore-collapse and have shallow pore volume.[133,221] Crystalline, even tetragonal, porous zirconia has been reported, but the precursor was not sulfated prior to calcination into zirconia which will lead to lower sulfate loadings and acid densities. Though mesoporous SZrO can improve life span for weak acid-catalyzed reactions like *n*-butane isomerization, a means of confining its active sites while retaining its strong acidity is critical to catalytic PO depolymerization. Additionally, insufficient reporting of PXRD patterns, microscopy images, adsorption isotherm data, and the structural information derived from them (e.g., crystal phase, surface area, pore size distribution, pore volumes) casts doubt on whether some SZrO samples have actually achieved an ordered mesoporous structure.[50,133,134,187] For instance, extensive characterization has previously identified speculated mesoporosity as merely interparticle condensation and impressive cracking activity as a result of its small nanoparticle size.[135]

While crystalline SZrO with uniform mesoporosity may be too challenging to generate, Al-Daou et al. successfully synthesized macroporous SZrO (validated with TEM and N_2 77 K isotherm analysis) by filling a poly(methyl methacrylate) (PMMA) template with liquid sulfuric acid and zirconyl nitrate. Although the thicker polycrystalline walls of macroporous SZrO demonstrated impressive stability, their catalytic performance suggests a large amount of $Zr(SO_4)_2$ is present that impedes uniform crystallization and acidity despite

https://doi.org/10.1021/acs.langmuir.3c03966
Langmuir XXXX, XXX, XXX−XXX

Pursuant to the DOE Public Access Plan, this document represents the authors' peer-reviewed, accepted manuscript. The published version of the article is available from the relevant publisher.

comparable sulfur wt % and surface areas that are greater than or equal to those of surface areas than conventional SZrO. Since some of the sulfur wt % was not contributing to surface stability, instead inhibiting crystal growth, the authors note that even at higher concentrations (3.2 sulfur/nm^2) some monoclinic zirconia forms. An increase in crystallite size within the wall reduced pore thickness, demonstrating that the walls are indeed largely amorphous. Thermally induced crystallite growth eventually collapsed the structure and caused rapid formation of monoclinic zirconia. When similar reaction conditions are used to synthesize SZrO without the PMMA template, the surface areas are much smaller (20.4 m^2/g) than conventional SZrO.[194] The authors also synthesized composites of this material with an exterior Y-zeolite layer, demonstrating the practicality of expanding the pore volume of a SZrO core using a more porous exterior.[109] Thus, development of mesoporous SZrO catalysts will likely find more success with strongly acidic metastable tetragonal nanoparticles confined at the bottom of porous materials that permit facile control of pore dimensions and have lower exterior acidity (e.g., SiO_2). However, despite the critical variables identified by the breadth of research discussed here, significant gaps in knowledge still impede the consistent synthesis of the structures that generate strongly acidic SZrO.

SUMMARIZING EXISTING GAPS IN KNOWLEDGE FOR SULFATED ZIRCONIA

Heterogeneous acids that can initiate alkane cracking at lower temperatures are a promising avenue to an energetically efficient circular polyolefin recycling scheme, thereby helping mitigate the global plastic waste crisis. However, the impact of confining SZrO in mesoporous architectures, thought to be necessary for enhanced product selectivity and coking resistance, cannot be clearly discerned when the origins of superacid-like behavior in solids itself remains poorly defined. As the principle superacidic solid catalyst, better comprehension of SZrO's superacid-like behavior will facilitate the intuitive synthesis, use, and design of other strong solid acid catalysts. Yet, ambiguous reporting, mishandling of synthetic and activation conditions, and inefficiencies in analytical and catalytic characterization techniques have contributed to miscomprehension of SZrO and solid superacidity as a whole.

Unlike liquid superacids, the independent strength of the Brønsted or Lewis acid sites of a solid like SZrO cannot explain their observed functional superacidity (i.e., conversion of saturated hydrocarbons below 250 °C). Additionally, confinement effects that drive the impressive activity of porous solid acids through intermediate stabilization and mass transfer should not apply to the relatively shallow and disordered pores of SZrO. Instead, SZrO seems to derive its superacid-like cracking ability from cooperativity between proximal Brønsted and Lewis acids. However, the Brønsted acid's conjugate base and a Lewis acid cannot freely associate across the solid surface. Still, as SZrO with low temperature cracking performance only facilitates H/D exchange comparable to nonsuperacidic Brønsted acids, cooperativity with a Lewis acid site appears necessary to crack C−C bonds, but not necessarily protonate alkanes. Furthermore, the abundance of Lewis acid sites on SZrO and rapid loss of C−C breaking activity upon hydration, coking, or sulfate loss demonstrates the catalytic significance of strong Lewis acids as well as surface sulfates.[51] Synthetic routes to stable, coordinatively unsaturated SZrO surfaces demand further investigation, particularly how the phase composition of tetragonal versus amorphous zirconia, sulfate and water loadings, and nanoparticle faceting may optimize Lewis acid strength, density, and stability.[116,214]

As nearly all solid acids do not meet the criteria for discretely Brønsted or Lewis "superacidity", the desirable separation and regeneration, strong acidity, and selectivity exclusive to solid acids is undervalued. The current definitions for superacidity do not consider the density of heterogeneous acid structures, intermediate stabilization, mass transfer, and other cooperative effects between surface structures that facilitate superacid-like activity in solids. Returning to the broad definition of superacidity, acid catalysts that are capable of activating saturated hydrocarbons with greater efficiency than pure sulfuric acid at low temperature and pressure, or defining one or more separate definitions for liquid superacids and solid superacids may improve perception, research, and investment in heterogeneous solid acidity. Indeed, heterogeneous acidity is influenced by the unique acid structures of different crystal facets, confinement effects, and enhancements from Lewis acidity and other surface moieties that do not impact metrics like the Hammett acidity scale, deprotonation energy, and fluoride ion affinity. A lack of consideration for these factors and the sensitivity of acidic surface structures to minor synthetic and activation variables has limited SZrO's catalytic potential and stagnated development.

To stimulate a reexamination of SZrO's potential, particularly for depolymerization of polyolefins, we have identified in this critical review the following components to SZrO's functional superacidity: (i) tetragonal phase facets bordered by defective terminations or amorphous zirconia are effective potential locations for coordination of sulfates and water near coordinatively unsaturated metal centers; (ii) acidity on the tetragonal surface is derived from sulfation-induced polarization of its naturally high surface energy facets; (iii) sulfation polarizes the surface and participates in hydrogen bonding/electrostatic interactions to improve the cationic behavior of Lewis acidic Zr^{4+} atoms and the protonation potential of Brønsted acidic hydroxyl or bisulfate groups; (iv) sulfates assume a μ_2-, μ_3-, or chelating coordination depending on the facet's arrangement of coordinatively unsaturated surface atoms and hydration/activation conditions that influence interactions between surface species; (v) Brønsted and Lewis acid sites are not superacidic on their own but the presence of both induces superacid-like activity; and (vi) the unique density of Lewis acid sites and their proximity to abundant Brønsted acid sites is critical to the generation of SZrO's superacid-like activity.

Finally, major deficiencies remain in defining the structure and mechanism by which SZrO activates saturated hydrocarbons. These gaps in knowledge can be most efficiently examined through cooperative computational and laboratory experimentation. Five topics of particular interest to comprehending these phenomena are (i) sulfate and hydroxyl coordination structures near facet terminations and other defects observed by TEM; (ii) the implications of proximity between hydroxyl groups, sulfates, and coordinatively unsaturated sites; (iii) the impact of the highly Lewis acidic amorphous phase on functional acidity; (iv) methods to synthetically promote the quantity and strength of Lewis acid sites; and (v) selective synthesis procedures for faceting sulfated tetragonal zirconia.

In conclusion, we argue that through enhanced analytical, catalytic, and computational characterization and synthetic

https://doi.org/10.1021/acs.langmuir.3c03966
Langmuir XXXX, XXX, XXX−XXX

Pursuant to the DOE Public Access Plan, this document represents the authors' peer-reviewed, accepted manuscript. The published version of the article is available from the relevant publisher.

study with a higher standard of reporting and reproducibility, sulfated zirconia may become a high-value catalyst with intuitively modulable acidity for polyolefin cracking and a variety of other acid-catalyzed reactions.

■ ASSOCIATED CONTENT

Supporting Information

The Supporting Information is available free of charge at https://pubs.acs.org/doi/10.1021/acs.langmuir.3c03966.

Sulfated Zirconia Synthesis Procedures; X-ray Fluorescence Analysis Procedure; PXRD Patterns; FT-IR Spectra; SEM-EDX spectra; TGA-IR data; Nitrogen Adsorption−Desorption Data; TEM Imagining Procedure and Image Copies (PDF)

■ AUTHOR INFORMATION

Corresponding Author

C. Michael McGuirk − *Department of Chemistry, Colorado School of Mines, Golden, Colorado 80401, United States;* orcid.org/0000-0002-7420-1169; Email: cmmcguirk@mines.edu

Authors

Scott R. Cleary − *Department of Chemistry, Colorado School of Mines, Golden, Colorado 80401, United States*

Anne K. Starace − *National Renewable Energy Laboratory, Golden, Colorado 80401, United States;* orcid.org/0000-0002-9204-2050

Caleb C. Curran-Velasco − *Department of Chemistry, Colorado School of Mines, Golden, Colorado 80401, United States*

Daniel A. Ruddy − *National Renewable Energy Laboratory, Golden, Colorado 80401, United States;* orcid.org/0000-0003-2654-3778

Complete contact information is available at: https://pubs.acs.org/10.1021/acs.langmuir.3c03966

Author Contributions

The manuscript was written through contributions of all authors. All authors have given approval to the final version of the manuscript.

Funding

We thank Colorado School of Mines for their support in the form of startup funding. This work was authored in part by the National Renewable Energy Laboratory, operated by Alliance for Sustainable Energy, LLC, for the U.S. Department of Energy (DOE) under Contract No. DE-AC36−08GO28308. This research was supported by NREL's Laboratory Directed Research & Development (LDRD) program. The views expressed in the article do not necessarily represent the views of the DOE or the U.S. Government. The U.S. Government retains and the publisher, by accepting the article for publication, acknowledges that the U.S. Government retains a nonexclusive, paid-up, irrevocable, worldwide license to publish or reproduce the published form of this work, or allow others to do so, for U.S. Government purposes.

Notes

The authors declare no competing financial interest.

■ ACKNOWLEDGMENTS

We would like to thank Luxfer MEL Technologies of Manchester, UK, particularly Chief Scientist Dave Scapens for lending us their knowledge and standard materials for analysis.

■ ABBREVIATIONS

PET, polyethylene terephthalate; PE, polyethylene; PO, polyolefin; PP, polypropylene; PS, polystyrene; PVC, polyvinyl chloride; PC, polycarbonate; PUR, polyurethane; SZrO, sulfated zirconia; FT-IR, Fourier transform infrared; TGA, thermogravimetric analysis; MS, mass spectrometry; MOF, metal−organic framework; MMT, montmorillonite; ssNMR, solid state nuclear magnetic resonance; KD, kinetic diameter; DRIFTS, diffuse reflectance infrared Fourier transform spectroscopy; TPD, temperature-programmed desorption; TMP, trimethylphosphine; TMPO, trimethylphosphine oxide; TRAPDOR, transfer of populations in double resonance; HETCOR, heteronuclear correlation; DQ, double-quantum; BET, Brunauer−Emmett−Teller; NLDFT, non localized density functional theory; H/D, hydrogen/deuterium; MBOH, methylbutynol; PXRD, powder X-ray diffraction; PTFE, polytetrafluoroethylene; PFA, perfluoroalkoxy; HOMO, highest occupied molecular orbital; LUMO, lowest unoccupied molecular orbital; SOMC, surface organometallic catalyst; CTAB, cetrimonium bromide; P123, poly(ethylene glycol)-*block*-poly(propylene glycol)-*block*-poly(ethylene glycol); Brij 56, polyoxyethylene(10) cetyl ether; PMMA, poly(methyl methacrylate)

■ REFERENCES

(1) Li, H.; Aguirre-Villegas, H. A.; Allen, R. D.; Bai, X.; Benson, C. H.; Beckham, G. T.; Bradshaw, S. L.; Brown, J. L.; Brown, R. C.; Cecon, V. S.; Curley, J. B.; Curtzwiler, G. W.; Dong, S.; Gaddameedi, S.; García, J. E.; Hermans, I.; Kim, M. S.; Ma, J.; Mark, L. O.; Mavrikakis, M.; Olafasakin, O. O.; Osswald, T. A.; Papanikolaou, K. G.; Radhakrishnan, H.; Sanchez Castillo, M. A.; Sánchez-Rivera, K. L.; Tumu, K. N.; Van Lehn, R. C.; Vorst, K. L.; Wright, M. M.; Wu, J.; Zavala, V. M.; Zhou, P.; Huber, G. W. Expanding Plastics Recycling Technologies: Chemical Aspects, Technology Status and Challenges. *Green Chem.* **2022**, *24* (23), 8899−9002.

(2) Plastics Europe. *Plastics - the Facts 2021: An Analysis of European Plastics Production Demand and Waste Data*; 2021.

(3) Geyer, R.; Jambeck, J. R.; Law, K. L. Production, Use, and Fate of All Plastics Ever Made. *Sci. Adv.* **2017**, *3* (7), 3−8.

(4) Britt, P.; Coates, G.; Winey, K. *Report of the Basic Energy Sciences Roundtable on Chemical Upcycling of Polymers*, 2019; pp 1−55.

(5) Coates, G. W.; Getzler, Y. D. Y. L. Chemical Recycling to Monomer for an Ideal, Circular Polymer Economy. *Nat. Rev. Mater.* **2020**, *5* (7), 501−516.

(6) MacArthur, D. E. Beyond Plastic Waste. *Science.* **2017**, *358* (6365), 843.

(7) Garcia, J. M.; Robertson, M. L. The Future of Plastics Recycling. *Science.* **2017**, *358* (6365), 870−872.

(8) Albertsson, A. C.; Hakkarainen, M. Designed to Degrade. *Science.* **2017**, *358* (6365), 872−873.

(9) Fitzgerald, N.; Bailey, A.; Fitzgerald, J.; Bentley, G.; Melissa, K.; Peretti, K. *Plastics for a Circular Economy Workshop: Summary Report*; U.S. Dep. Energy, Off. Energy Efficency Renew. Energy, 2019; pp 1−50.

(10) McGuirk, C. M.; Bazilian, M. D.; Kammen, D. M. Mining Plastic: Harvesting Stored Energy in a Re-Use Revolution. *One Earth* **2019**, *1* (4), 392−394.

(11) Cabernard, L.; Pfister, S.; Oberschelp, C.; Hellweg, S. Growing Environmental Footprint of Plastics Driven by Coal Combustion. *Nat. Sustain.* **2022**, *5* (2), 139−148.

(12) Wang, Y.; Peh, S. B.; Zhao, D. Alternatives to Cryogenic Distillation: Advanced Porous Materials in Adsorptive Light Olefin/Paraffin Separations. *Small* **2019**, *15* (25), 1−38.

Pursuant to the DOE Public Access Plan, this document represents the authors' peer-reviewed, accepted manuscript. The published version of the article is available from the relevant publisher.

(13) Jehanno, C.; Alty, J. W.; Roosen, M.; De Meester, S.; Dove, A. P.; Chen, E. Y.-X.; Leibfarth, F. A.; Sardon, H. Critical Advances and Future Opportunities in Upcycling Commodity Polymers. *Nature* **2022**, *603* (7903), 803−814.
(14) Milbrandt, A.; Coney, K.; Badgett, A.; Beckham, G. T. Quantification and Evaluation of Plastic Waste in the United States. *Resour. Conserv. Recycl.* **2022**, *183*, 106363.
(15) Hamilton, L. A.; Feit, S.; Muffet, C.; Kelso, M.; Rubright, S. M.; Bernhardt, C.; Schaeffer, E.; Moon, D.; Morris, J.; Labbe-Bellas, R. *Plastic & Climate: The Hidden Costs of a Plastic Planet*; CIEL, EIP, FracTracker Alliance, GAIA, 5Gyres, 2019; pp 1−108.
(16) Hahladakis, J. N.; Velis, C. A.; Weber, R.; Iacovidou, E.; Purnell, P. An Overview of Chemical Additives Present in Plastics: Migration, Release, Fate and Environmental Impact during Their Use, Disposal and Recycling. *J. Hazard. Mater.* **2018**, *344*, 179−199.
(17) Kemmlein, S.; Herzke, D.; Law, R. J. Brominated Flame Retardants in the European Chemicals Policy of REACH-Regulation and Determination in Materials. *J. Chromatogr. A* **2009**, *1216* (3), 320−333.
(18) Serrano, D. P.; Aguado, J.; Escola, J. M. Developing Advanced Catalysts for the Conversion of Polyolefinic Waste Plastics into Fuels and Chemicals. *ACS Catal.* **2012**, *2* (9), 1924−1941.
(19) Lange, J. P. Managing Plastic Waste-Sorting, Recycling, Disposal, and Product Redesign. *ACS Sustain. Chem. Eng.* **2021**, *9* (47), 15722−15738.
(20) Rahimi, A. R.; Garciá, J. M. Chemical Recycling of Waste Plastics for New Materials Production. *Nat. Rev. Chem.* **2017**, *1*, 1−11.
(21) Zhao, X.; Korey, M.; Li, K.; Copenhaver, K.; Tekinalp, H.; Celik, S.; Kalaitzidou, K.; Ruan, R.; Ragauskas, A. J.; Ozcan, S. Plastic Waste Upcycling toward a Circular Economy. *Chem. Eng. J.* **2022**, *428*, 131928.
(22) Martín, A. J.; Mondelli, C.; Jaydev, S. D.; Pérez-Ramírez, J. Catalytic Processing of Plastic Waste on the Rise. *Chem.* **2021**, *7* (6), 1487−1533.
(23) Celik, G.; Kennedy, R. M.; Hackler, R. A.; Ferrandon, M.; Tennakoon, A.; Patnaik, S.; Lapointe, A. M.; Ammal, S. C.; Heyden, A.; Perras, F. A.; Pruski, M.; Scott, S. L.; Poeppelmeier, K. R.; Sadow, A. D.; Delferro, M. Upcycling Single-Use Polyethylene into High-Quality Liquid Products. *ACS Cent. Sci.* **2019**, *5* (11), 1795−1803.
(24) Qureshi, M. S.; Oasmaa, A.; Pihkola, H.; Deviatkin, I.; Tenhunen, A.; Mannila, J.; Minkkinen, H.; Pohjakallio, M.; Laine-Ylijoki, J. Pyrolysis of Plastic Waste: Opportunities and Challenges. *J. Anal. Appl. Pyrolysis* **2020**, *152* (2020), 104804.
(25) Burange, A. S.; Gawande, M. B.; Lam, F. L. Y.; Jayaram, R. V.; Luque, R. Heterogeneously Catalyzed Strategies for the Deconstruction of High Density Polyethylene: Plastic Waste Valorisation to Fuels. *Green Chem.* **2015**, *17* (1), 146−156.
(26) Rorrer, J. E.; Beckham, G. T.; Román-Leshkov, Y. Conversion of Polyolefin Waste to Liquid Alkanes with Ru-Based Catalysts under Mild Conditions. *JACS Au* **2021**, *1* (1), 8−12.
(27) Aguado, J.; Serrano, D. P.; Escola, J. M. Fuels from Waste Plastics by Thermal and Catalytic Processes: A Review. *Ind. Eng. Chem. Res.* **2008**, *47* (21), 7982−7992.
(28) Hogue, C. Chemical recycling of plastic gets a boost in 18 US states—but environmentalists question whether it really is recycling. *C&EN* **2022**, *100* (17), 1−32.
(29) Huffman, J. *Break Free From Plastic Pollution Act of 2021, S.984*; 117th Congr, 2021.
(30) Shabtai, J.; Xiao, X.; Zmierczak, W. Depolymerization-Liquefaction of Plastics and Rubbers. 1. Polyethylene, Polypropylene, and Polybutadiene. *Energy Fuels* **1997**, *11* (1), 76−87.
(31) Miandad, R.; Barakat, M. A.; Aburiazaiza, A. S.; Rehan, M.; Nizami, A. S. Catalytic Pyrolysis of Plastic Waste: A Review. *Process Saf. Environ. Prot.* **2016**, *102*, 822−838.
(32) Liu, S.; Kots, P. A.; Vance, B. C.; Danielson, A.; Vlachos, D. G. Plastic Waste to Fuels by Hydrocracking at Mild Conditions. *Sci. Adv.* **2021**, *7* (17), 1−10.
(33) Ellis, L. D.; Rorrer, N. A.; Sullivan, K. P.; Otto, M.; McGeehan, J. E.; Román-Leshkov, Y.; Wierckx, N.; Beckham, G. T. Chemical and Biological Catalysis for Plastics Deconstruction, Recycling, and Upcycling. *Nat. Catal.* **2021**, *4*, 539−556.
(34) Cao, F.; Wang, L.; Zheng, R.; Guo, L.; Chen, Y.; Qian, X. Research and Progress of Chemical Depolymerization of Waste PET and High-Value Application of Its Depolymerization Products. *RSC Adv.* **2022**, *12* (49), 31564−31576.
(35) Lin, R.; White, R. L. Effects of Catalyst Acidity and HZSM-5 Channel Volume on the Catalytic Cracking of Poly(ethylene). *J. Appl. Polym. Sci.* **1995**, *58* (7), 1151−1159.
(36) Serrano, D. P.; Aguado, J.; Escola, J. M.; Rodríguez, J. M. Influence of Nanocrystalline HZSM-5 External Surface on the Catalytic Cracking of Polyolefins. *J. Anal. Appl. Pyrolysis* **2005**, *74* (1−2), 353−360.
(37) Negelein, D. L.; Lin, R.; White, R. L. Effects of Catalyst Acidity and HZSM-5 Channel Volume on Polypropylene Cracking. *J. Appl. Polym. Sci.* **1998**, *67* (2), 341−348.
(38) Zheng, J.; Lin, Y.; Liu, F.; Tan, H.; Wang, Y.; Tang, T. Controlled Chain-Scission of Polybutadiene by the Schwartz Hydrozirconation. *Chem. - A Eur. J.* **2013**, *19* (2), 541−548.
(39) Gu, Y.; Lin, Y.; Zheng, J.; Ye, L.; Wang, S.; Li, S.; Ma, L.; Cui, D.; Tang, T. Cp_2ZrHCl Induced Catalytic Chain Scission of Diene-Based Polymers under Mild Conditions: Influence of Chemical Environment around C = C Bonds. *Polymer* **2019**, *161*, 181−189.
(40) Kanbur, U.; Zang, G.; Paterson, A. L.; Chatterjee, P.; Hackler, R. A.; Delferro, M.; Slowing, I. I.; Perras, F. A.; Sun, P.; Sadow, A. D. Catalytic Carbon-Carbon Bond Cleavage and Carbon-Element Bond Formation Give New Life for Polyolefins as Biodegradable Surfactants. *Chem.* **2021**, *7* (5), 1347−1362.
(41) Tennakoon, A.; Wu, X.; Paterson, A. L.; Patnaik, S.; Pei, Y.; LaPointe, A. M.; Ammal, S. C.; Hackler, R. A.; Heyden, A.; Slowing, I. I.; Coates, G. W.; Delferro, M.; Peters, B.; Huang, W.; Sadow, A. D.; Perras, F. A. Catalytic Upcycling of High-Density Polyethylene via a Processive Mechanism. *Nat. Catal.* **2020**, *3* (11), 893−901.
(42) Conk, R. J.; Hanna, S.; Shi, J. X.; Yang, J.; Ciccia, N. R.; Qi, L.; Bloomer, B. J.; Heuvel, S.; Wills, T.; Su, J.; Bell, A. T.; Hartwig, J. F. Catalytic Deconstruction of Waste Polyethylene with Ethylene to Form Propylene. *Science.* **2022**, *377* (6614), 1561−1566.
(43) Dorn, R. W.; Mark, L. O.; Hung, I.; Cendejas, M. C.; Xu, Y.; Gor'Kov, P. L.; Mao, W.; Ibrahim, F.; Gan, Z.; Hermans, I.; Rossini, A. J. An Atomistic Picture of Boron Oxide Catalysts for Oxidative Dehydrogenation Revealed by Ultrahigh Field ^{11}B-^{17}O Solid-State NMR Spectroscopy. *J. Am. Chem. Soc.* **2022**, *144* (41), 18766−18771.
(44) Arroyave, A.; Cui, S.; Lopez, J. C.; Kocen, A. L.; Lapointe, A. M.; Delferro, M.; Coates, G. W. Catalytic Chemical Recycling of Post-Consumer Polyethylene. *J. Am. Chem. Soc.* **2022**, *144* (51), 23280−23285.
(45) Zhao, T. Y.; Meirow, M.; Tennakoon, A.; Wu, X.; Paterson, A. L.; Qi, L.; LaPointe, A. M.; Lamb, J. V.; Kobayashi, T.; Delferro, M.; Sadow, A. D.; Huang, W.; Luijten, E.; Perras, F. A. Mechanistic Insights into Processive Polyethylene Hydrogenolysis through In Situ NMR. *Macromolecules* **2023**, *56* (11), 4287−4295.
(46) Tennakoon, A.; Wu, X.; Meirow, M.; Howell, D.; Willmon, J.; Yu, J.; Lamb, J. V.; Delferro, M.; Luijten, E.; Huang, W.; Sadow, A. D. Two Mesoporous Domains Are Better Than One for Catalytic Deconstruction of Polyolefins. *J. Am. Chem. Soc.* **2023**, *145*, 17936−17944.
(47) Wu, X.; Tennakoon, A.; Yappert, R.; Esveld, M.; Ferrandon, M. S.; Hackler, R. A.; LaPointe, A. M.; Heyden, A.; Delferro, M.; Peters, B.; Sadow, A. D.; Huang, W. Size-Controlled Nanoparticles Embedded in a Mesoporous Architecture Leading to Efficient and Selective Hydrogenolysis of Polyolefins. *J. Am. Chem. Soc.* **2022**, *144* (12), 5323−5334.
(48) Sun, J.; Lee, Y.-H.; Yappert, R. D.; LaPointe, A. M.; Coates, G. W.; Peters, B.; Abu-Omar, M. M.; Scott, S. L. Bifunctional Tandem Catalytic Upcycling of Polyethylene to Surfactant-Range Alkylaromatics. *Chem.* **2023**, *9* (8), 2318−2336.
(49) Zhang, F.; Zeng, M.; Yappert, R. D.; Sun, J.; Lee, Y. H.; LaPointe, A. M.; Peters, B.; Abu-Omar, M. M.; Scott, S. L.

Pursuant to the DOE Public Access Plan, this document represents the authors' peer-reviewed, accepted manuscript. The published version of the article is available from the relevant publisher.

Polyethylene Upcycling to Long-Chain Alkylaromatics by Tandem Hydrogenolysis/Aromatization. *Science.* **2020**, *370* (6515), 437−441.
(50) Potter, M. E.; Le Brocq, J. J. M.; Oakley, A. E.; McShane, E. B.; Vandegehuchte, B. D.; Raja, R. Butane Isomerization as a Diagnostic Tool in the Rational Design of Solid Acid Catalysts. *Catalysts* **2020**, *10* (9), 1099.
(51) Signoretto, M.; Pinna, F.; Strukul, G.; Chies, P.; Cerrato, G.; Di Ciero, S.; Morterra, C. Platinum-Promoted and Unpromoted Sulfated Zirconia Catalysts Prepared by a One-Step Aerogel Procedure. *J. Catal.* **1997**, *167* (2), 522−532.
(52) Gruene, P.; Belova, A. G.; Yegulalp, T. M.; Farrauto, R. J.; Castaldi, M. J. Dispersed Calcium Oxide as a Reversible and Efficient CO_2-Sorbent at Intermediate Temperatures. *Ind. Eng. Chem. Res.* **2011**, *50* (7), 4042−4049.
(53) Venkatesh, K. R.; Hu, J.; Wang, W.; Holder, G. D.; Tierney, J. W.; Wender, I. Hydrocracking and Hydroisomerization of Long-Chain Alkanes and Polyolefins over Metal-Promoted Anion-Modified Zirconium Oxides. *Energy Fuels* **1996**, *10* (6), 1163−1170.
(54) Busca, G.; Gervasini, A. Solid Acids, Surface Acidity and Heterogeneous Acid Catalysis. *Adv. Catal.* **2020**, *67*, 1−90.
(55) Olah, G. A.; Surya Prakash, G. K.; Molnr, A.; Sommer, J. *Superacid Chemistry*, 2nd ed.; John Wiley & Sons, Inc., 2009.
(56) Corma, A.; Martinez, A.; Martinez, C. The Effect of Sulfation Conditions and Activation Temperature of Sulfate Doped ZrO_2, TiO_2, and SnO_2 Catalysts during Isobutane/2-Butene Alkylation. *Appl. Catal. A Gen.* **1996**, *144*, 249−268.
(57) Yadav, G. D.; Nair, J. J. Sulfated Zirconia and Its Modified Versions as Promising Catalysts for Industrial Processes. *Microporous Mesoporous Mater.* **1999**, *33* (1−3), 1−48.
(58) Sekewael, S. J.; Pratika, R. A.; Hauli, L.; Amin, A. K.; Utami, M.; Wijaya, K. Recent Progress on Sulfated Nanozirconia as a Solid Acid Catalyst in the Hydrocracking Reaction. *Catalysts* **2022**, *12* (2), 191.
(59) Katada, N.; Endo, J. I.; Notsu, K. I.; Yasunobu, N.; Naito, N.; Niwa, M. Superacidity and Catalytic Activity of Sulfated Zirconia. *J. Phys. Chem. B* **2000**, *104* (44), 10321−10328.
(60) Morterra, C.; Cerrato, G.; Bolis, V.; Di Ciero, S.; Signoretto, M. On the Strength of Lewis- and Brønsted-Acid Sites at the Surface of Sulfated Zirconia Catalysts. *J. Chem. Soc. - Faraday Trans.* **1997**, *93* (6), 1179−1184.
(61) Parera, J. M. Promotion of Zirconia Acidity by Addition of Sulfate Ion. *Catal. Today* **1992**, *15*, 481−490.
(62) Almustapha, M. N.; Farooq, M.; Andresen, J. M. Sulphated Zirconia Catalysed Conversion of High Density Polyethylene to Value-Added Products Using a Fixed-Bed Reactor. *J. Anal. Appl. Pyrolysis* **2017**, *125*, 296−303.
(63) Bornes, C.; Fischer, M.; Amelse, J. A.; Geraldes, C. F. G. C.; Rocha, J.; Mafra, L. What Is Being Measured with P-Bearing NMR Probe Molecules Adsorbed on Zeolites? *J. Am. Chem. Soc.* **2021**, *143* (34), 13616−13623.
(64) Chen, W.-H.; Ko, H.-H.; Sakthivel, A.; Huang, S.-J.; Liu, S.-H.; Lo, A.-Y.; Tsai, T.-C.; Liu, S.-B. A Solid-State NMR, FT-IR and TPD Study on Acid Properties of Sulfated and Metal-Promoted Zirconia: Influence of Promoter and Sulfation Treatment. *Catal. Today* **2006**, *116*, 111−120.
(65) Wang, Y.; Xin, S.; Chu, Y.; Xu, J.; Qi, G.; Wang, Q.; Xia, Q.; Deng, F. Influence of Trimethylphosphine Oxide Loading on the Measurement of Zeolite Acidity by Solid-State NMR Spectroscopy. *J. Phys. Chem. C* **2021**, *125* (17), 9497−9506.
(66) Zholobenko, V.; Freitas, C.; Jendrlin, M.; Bazin, P.; Travert, A.; Thibault-Starzyk, F. Probing the Acid Sites of Zeolites with Pyridine: Quantitative AGIR Measurements of the Molar Absorption Coefficients. *J. Catal.* **2020**, *385*, 52−60.
(67) Zheng, A.; Liu, S.-B.; Deng, F. Bin; Deng, F. ^{31}P NMR Chemical Shifts of Phosphorus Probes as Reliable and Practical Acidity Scales for Solid and Liquid Catalysts. *Chem. Rev.* **2017**, *117* (19), 12475−12531.
(68) Parrillo, D. J.; Gorte, R. J. Characterization of Stoichiometric Adsorption Complexes in H-ZSM-5 Using Microcalorimetry. *Catal. Lett.* **1992**, *16*, 17−25.
(69) Wang, Y.; Wang, C.; Wang, L.; Wang, L.; Xiao, F. S. Zeolite Fixed Metal Nanoparticles: New Perspective in Catalysis. *Acc. Chem. Res.* **2021**, *54* (11), 2579−2590.
(70) Niwa, M.; Habuta, Y.; Okumura, K.; Katada, N. Solid Acidity of Metal Oxide Monolayer and Its Role in Catalytic Reactions. *Catal. Today* **2003**, *87*, 213−218.
(71) Védrine, J. C. Recent Developments and Prospectives of Acid-Base and Redox Catalytic Processes by Metal Oxides. *Appl. Catal. A Gen.* **2019**, *575*, 170−179.
(72) Jiang, J.; Gándara, F.; Zhang, Y. B.; Na, K.; Yaghi, O. M.; Klemperer, W. G. Superacidity in Sulfated Metal-Organic Framework-808. *J. Am. Chem. Soc.* **2014**, *136* (37), 12844−12847.
(73) Li, H.; Chu, H.; Ma, X.; Wang, G.; Liu, F.; Guo, M.; Lu, W.; Zhou, S.; Yu, M. Efficient Heterogeneous Acid Synthesis and Stability Enhancement of UiO-66 Impregnated with Ammonium Sulfate for Biodiesel Production. *Chem. Eng. J.* **2021**, *408*, 127277.
(74) Yi, X.; Peng, Y. K.; Chen, W.; Liu, Z.; Zheng, A. Surface Fingerprinting of Faceted Metal Oxides and Porous Zeolite Catalysts by Probe-Assisted Solid-State NMR Approaches. *Acc. Chem. Res.* **2021**, *54* (10), 2421−2433.
(75) Wisniak, J. The History of Catalysis. From the Beginning to Nobel Prizes. *Educ. Quim.* **2010**, *21* (1), 60−69.
(76) Sommer, J.; Jost, R. Carbenium and Carbonium Ions in Liquid- and Solid-Superacid-Catalyzed Activation of Small Alkanes. *Pure Appl. Chem.* **2000**, *72* (12), 2309−2318.
(77) Verdoliva, V.; Saviano, M.; De Luca, S. Zeolites as Acid/Basic Solid Catalysts: Recent Synthetic Developments. *Catalysts* **2019**, *9* (3), 248.
(78) Busca, G. Acid Catalysts in Industrial Hydrocarbon Chemistry. *Chem. Rev.* **2007**, *107* (11), 5366−5410.
(79) Arata, K.; Matsuhashi, H.; Hino, M.; Nakamura, H. Synthesis of Solid Superacids and Their Activities for Reactions of Alkanes. *Catal. Today* **2003**, *81* (1), 17−30.
(80) Vedrine, J. C. Heterogeneous Catalysis on Metal Oxides. *Catalysts* **2017**, *7*, 341.
(81) Johnson, C. D.; Stratton, B. Concerning the Hammett Acidity Function Method for Determination of pK_a Values. *J. Org. Chem.* **1986**, *51* (22), 4100−4106.
(82) Yamaguchi, T. Recent Progress in Solid Superacid. *Appl. Catal.* **1990**, *61* (1), 1−25.
(83) Chu, Y.; Yu, Z.; Zheng, A.; Fang, H.; Zhang, H.; Huang, S.-J.; Liu, S.-B.; Deng, F. Acidic Strengths of Brønsted and Lewis Acid Sites in Solid Acids Scaled by ^{31}P NMR Chemical Shifts of Adsorbed Trimethylphosphine. *J. Phys. Chem. C* **2011**, *115* (15), 7660−7667.
(84) Ansari, Y.; Ueno, K.; Angell, C. A. Protic Ionic Liquids Can Be Both Free Proton Conductors and Benign Superacids. *J. Phys. Chem. B* **2021**, *125*, 7855−7862.
(85) Greb, L. Lewis Superacids: Classifications, Candidates, and Applications. *Chem. - A Eur. J.* **2018**, *24* (68), 17881−17896.
(86) Amarasekara, A. S. Acidic Ionic Liquids. *Chem. Rev.* **2016**, *116*, 6133−6183.
(87) Jentoft, F. C.; Gates, B. C. Solid-Acid-Catalyzed Alkane Cracking Mechanisms: Evidence from Reactions of Small Probe Molecules. *Top. Catal.* **1997**, *4*, 1−13.
(88) Chen, F. R.; Coudurier, G.; Joly, J. F.; Vedrine, J. C. Superacid and Catalytic Properties of Sulfated Zirconia. *J. Catal.* **1993**, *143*, 616−626.
(89) Yu, H.; Fang, H.; Zhang, H.; Li, B.; Deng, F. Acidity of Sulfated Tin Oxide and Sulfated Zirconia: A View from Solid-State NMR Spectroscopy. *Catal. Commun.* **2009**, *10* (6), 920−924.
(90) Liu, F.; Yi, X.; Chen, W.; Liu, Z.; Chen, W.; Qi, C.-Z.; Song, Y.-F.; Zheng, A. Developing Two-Dimensional Solid Superacids with Enhanced Mass Transport, Extremely High Acid Strength and Superior Catalytic Performance. *Chem. Sci.* **2019**, *10* (23), 5875−5883.
(91) Xu, L.; Liang, H. W.; Yang, Y.; Yu, S. H. Stability and Reactivity: Positive and Negative Aspects for Nanoparticle Processing. *Chem. Rev.* **2018**, *118* (7), 3209−3250.

https://doi.org/10.1021/acs.langmuir.3c03966
Langmuir XXXX, XXX, XXX−XXX

Pursuant to the DOE Public Access Plan, this document represents the authors' peer-reviewed, accepted manuscript. The published version of the article is available from the relevant publisher.

(92) Yaluris, G.; Larson, R. B.; Kobe, J. M.; González, M. R.; Fogash, K. B.; Dumesic, J. A. Selective Poisoning and Deactivation of Acid Sites on Sulfated Zirconia Catalysts for n-Butane Isomerization. *J. Catal.* **1996**, *158* (1), 336−342.
(93) Li, T.; Chung, S. H.; Nastase, S.; Galilea, A.; Wang, Y.; Mukhambetov, I.; Zaarour, M.; Navarro de Miguel, J. C.; Cazemier, J.; Dokania, A.; Panarone, L.; Gascon, J.; Cavallo, L.; Ruiz-Martínez, J. Influence of Active-Site Proximity in Zeolites on Brønsted Acid-Catalyzed Reactions at the Microscopic and Mesoscopic Levels. *Chem. Catal.* **2023**, *3* (6), 100540.
(94) Li, X.; Nagaoka, K.; Simon, L. J.; Lercher, J. A.; Wrabetz, S.; Jentoft, F. C.; Breitkopf, C.; Matysik, S.; Papp, H. Interaction between Sulfated Zirconia and Alkanes: Prerequisites for Active Sites-Formation and Stability of Reaction Intermediates. *J. Catal.* **2005**, *230* (1), 214−225.
(95) Ilias, S.; Bhan, A. Mechanism of the Catalytic Conversion of Methanol to Hydrocarbons. *ACS Catal.* **2013**, *3* (1), 18−31.
(96) Song, X.; Sayari, A. Sulfated Zirconia-Based Strong Solid-Acid Catalysts: Recent Progress. *Catal. Rev. Sci. Eng.* **1996**, *38* (3), 329−412.
(97) Li, Y.; Kanbur, U.; Cui, J.; Wang, G.; Kobayashi, T.; Sadow, A. D.; Qi, L. Supported Lanthanum Borohydride Catalyzes CH Borylation Inside Zeolite Micropores. *Angew. Chemie - Int. Ed. Ed.* **2022**, *61*, 1−5.
(98) Singh, A. S.; Leyva-Perez, A. Cyclododecene Isomeric Separation by (Supported) Rhodium(I)-Catalysed Selective Dehydrogenative Borylation Reaction. *Org. Chem. Front.* **2024**, *11*, 1124−1131.
(99) Miller, J. H.; Starace, A. K.; Ruddy, D. A. Catalytic Activation of Polyethylene Model Compounds Over Metal-Exchanged Beta Zeolites. *ChemSusChem* **2022**, *15* (1), 1−10.
(100) Duan, J.; Chen, W.; Wang, C.; Wang, L.; Liu, Z.; Yi, X.; Fang, W.; Wang, H.; Wei, H.; Xu, S.; Yang, Y.; Yang, Q.; Bao, Z.; Zhang, Z.; Ren, Q.; Zhou, H.; Qin, X.; Zheng, A.; Xiao, F.-S. Coking-Resistant Polyethylene Upcycling Modulated by Zeolite Micropore Diffusion. *J. Am. Chem. Soc.* **2022**, *144* (31), 14269−14277.
(101) Narbeshuber, T. F.; Vinek, H.; Lercher, J. A. Monomolecular Conversion of Light Alkanes over H-ZSM-5. *J. Catal.* **1995**, *157* (2), 388−395.
(102) Fu, J.; Feng, X.; Liu, Y.; Shan, H.; Yang, C. Mechanistic Insights into the Pore Confinement Effect on Bimolecular and Monomolecular Cracking Mechanisms of n-Octane over HY and HZSM-5 Zeolites: A DFT Study. *J. Phys. Chem. C* **2018**, *122* (23), 12222−12230.
(103) Kumar, S.; Panda, A. K.; Singh, R. K. A Review on Tertiary Recycling of High-Density Polyethylene to Fuel. *Resour. Conserv. Recycl.* **2011**, *55* (11), 893−910.
(104) Grifoni, E.; Piccini, G. M.; Lercher, J. A.; Glezakou, V. A.; Rousseau, R.; Parrinello, M. Confinement Effects and Acid Strength in Zeolites. *Nat. Commun.* **2021**, *12* (1), 1−9.
(105) Parrillo, D. J.; Gorte, R. J. Characterization of Acidity in H-ZSM-5, H-ZSM-12, H-Mordenite, and H-Y Using Microcalorimetry. *J. Phys. Chem. B* **1993**, *97*, 8786−8792.
(106) Liu, Y.; Vjunov, A.; Shi, H.; Eckstein, S.; Camaioni, D. M.; Mei, D.; Baráth, E.; Lercher, J. A. Enhancing the Catalytic Activity of Hydronium Ions through Constrained Environments. *Nat. Commun.* **2017**, *8*, 2−9.
(107) Moliner, M. State of the Art of Lewis Acid-Containing Zeolites: Lessons from Fine Chemistry to New Biomass Transformation Processes. *Dalt. Trans.* **2014**, *43* (11), 4197−4208.
(108) Yappert, R.; Peters, B. Processive Depolymerization Catalysts: A Population Balance Model for Chemistry's "While" Loop. *ACS Catal.* **2022**, *12* (16), 10353−10360.
(109) Wang, Z.; Al-Daous, M. A.; Kiesel, E. R.; Li, F.; Stein, A. Design and Synthesis of 3D Ordered Macroporous ZrO_2/Zeolite Nanocomposites. *Microporous Mesoporous Mater.* **2009**, *120* (3), 351−358.
(110) Larsen, S. C. Nanocrystalline Zeolites and Zeolite Structures: Synthesis, Characterization, and Applications. *J. Phys. Chem. C* **2007**, *111*, 18464−18474.
(111) Dacquin, J. P.; Cross, H. E.; Brown, D. R.; Düren, T.; Williams, J. J.; Lee, A. F.; Wilson, K. Interdependent Lateral Interactions, Hydrophobicity and Acid Strength and Their Influence on the Catalytic Activity of Nanoporous Sulfonic Acid Silicas. *Green Chem.* **2010**, *12* (8), 1383−1391.
(112) Smirnova, M. Y.; Toktarev, A. V.; Ayupov, A. B.; Echevsky, G. V. Sulfated Alumina and Zirconia in Isobutane/Butene Alkylation and n-Pentane Isomerization: Catalysis, Acidity, and Surface Sulfate Species. *Catal. Today* **2010**, *152* (1−4), 17−23.
(113) Chen, W.; Yi, X.; Huang, L.; Liu, W.; Li, G.; Acharya, D.; Sun, X.; Zheng, A. Can Hammett Indicators Accurately Measure the Acidity of Zeolite Catalysts with Confined Space? Insights into the Mechanism of Coloration. *Catal. Sci. Technol.* **2019**, *9* (18), 5045−5057.
(114) Busca, G. Spectroscopic Characterization of the Acid Properties of Metal Oxide Catalysts. *Catal. Today* **1998**, *41* (1−3), 191−206.
(115) Morterra, C.; Cerrato, G. Titrating Surface Acidity of Sulfated Zirconia Catalysts: Is the Adsorption of Pyridine a Suitable Probe? *Phys. Chem. Chem. Phys.* **1999**, *1* (11), 2825−2831.
(116) Ma, Z. Y.; Yang, C.; Wei, W.; Li, W. H.; Sun, Y. H. Surface Properties and CO Adsorption on Zirconia Polymorphs. *J. Mol. Catal. A Chem.* **2005**, *227*, 119−124.
(117) Velthoen, M. E. Z.; Nab, S.; Weckhuysen, B. M. Probing Acid Sites in Solid Catalysts with Pyridine UV-Vis Spectroscopy. *Phys. Chem. Chem. Phys.* **2018**, *20* (33), 21647−21659.
(118) Kumar, S.; Srivastava, R.; Koh, J. Utilization of Zeolites as CO_2 Capturing Agents: Advances and Future Perspectives. *J. CO_2 Util.* **2020**, *41*, 101251.
(119) Sharma, S. B.; Meyers, B. L.; Chen, D. T.; Miller, J.; Dumesic, J. A. Characterization of Catalyst Acidity by Microcalorimetry and Temperature-Programmed Desorption. *Appl. Catal. A, Gen.* **1993**, *102* (2), 253−265.
(120) Fesenko, E. A.; Barnes, P. A.; Parkes, G. M. B.; Brown, D. R.; Naderi, M. A New Approach to the Study of the Reactivity of Solid-Acid Catalysts: The Application of Constant Rate Thermal Analysis to the Desorption and Surface Reaction of Isopropylamine from NaY and HY Zeolites. *J. Phys. Chem. B* **2001**, *105* (26), 6178−6185.
(121) Bolis, V.; Cerrato, G.; Magnacca, G.; Morterra, C. Surface Acidity of Metal Oxides. Combined Microcalorimetric and IR-Spectroscopic Studies of Variously Dehydrated Systems. *Thermochim. Acta* **1998**, *312* (1−2), 63−77.
(122) Takeuchi, M.; Tsukamoto, T.; Kondo, A.; Matsuoka, M. Investigation of NH_3 and NH_4^+ Adsorbed on ZSM-5 Zeolites by near and Middle Infrared Spectroscopy. *Catal. Sci. Technol.* **2015**, *5* (9), 4587−4593.
(123) Delarmelina, M.; Deshmukh, G.; Goguet, A.; Catlow, C. R. A.; Manyar, H. Role of Sulfation of Zirconia Catalysts in Vapor Phase Ketonization of Acetic Acid. *J. Phys. Chem. C* **2021**, *125* (50), 27578−27595.
(124) Tittensor, J. G.; Gorte, R. J.; Chapman, D. M. Isopropylamine Adsorption for the Characterization of Acid Sites in Silica-Alumina Catalysts. *J. Catal.* **1992**, *138* (2), 714−720.
(125) Babou, F.; Coudurier, G.; Vedrine, J. C. Acidic Properties of Sulfated Zirconia: An Infrared Spectroscopic Study. *J. Catal.* **1995**, *152* (2), 341−349.
(126) Rodriguez, J.; Culver, D. B.; Conley, M. P. Generation of Phosphonium Sites on Sulfated Zirconium Oxide: Relationship to Brønsted Acid Strength of Surface -OH Sites. *J. Am. Chem. Soc.* **2019**, *141*, 1484−1488.
(127) Osterrieth, J. W. M.; James Rampersad, D. G. M.; Rampal, N.; Skoric, L.; Connolly, B.; Allendorf, M.; Stavila, V.; Snider, J.; Ameloot, R.; Marreiros, J.; Ania, C. O.; Azevedo, D. C. S.; Vilarrasa-García, E.; Santos, B. F.; Bu, X.-H.; Zang, X.; Bunzen, H.; Champness, N. R.; Griffin, S. L.; Chen, B.; Lin, R.-B.; Coasne, B.; Cohen, S. M.; Moreton, J. C.; Colon, Y. J.; Chen, L.; Clowes, R.; Coudert, F.-X.;

Pursuant to the DOE Public Access Plan, this document represents the authors' peer-reviewed, accepted manuscript. The published version of the article is available from the relevant publisher.

Cui, Y.; Hou, B.; D'alessandro, D.; Doheny, P. W.; Dinca, M.; Sun, C.; Doonan, C.; Huxley, M.; Evans, J. D.; Falcaro, P.; Ricco, R.; Farha, O. K.; Idrees, K. B.; Islamoglu, T.; Feng, P.; Yang, H.; Forgan, R.; Bara, D.; Furukawa, S.; Sanchez, E.; Gascon, J.; Telalovic, S.; Ghosha, S. K.; Mukherjee, S.; Hill, M. R.; Sadiq, M. M.; Horcajada, P.; Salcedo-Abraira, P.; Kaneko, K.; Kukobat, R.; Kenvin, J.; Keskin, S.; Kitagawa, S.; Otake, K.; Lively, R. P.; Dewitt, S. J. A.; Llewellyn, P. L.; Lotsch, B.; Emmerling, S. T.; Pütz, A.; Martí-Gastaldo, C.; Muñoz, N.; Garcia-Martinez, J.; Linares, N.; Maspoch, D.; Suarez, J. A.; Moghadam, P.; Oktavian, R.; Morris, R.; Wheatley, P.; Navarro, J.; Petit, C.; Danaci, D.; Rosseinsky, M.; Katsoulidis, A.; Schroder, M.; Han, X.; Yang, S.; Serre, C.; Mouchaham, G.; Sholl, D.; Thyagarajan, R.; Siderius, D.; Snurr, R. Q.; Goncalves, R. B.; Ting, V.; Rowlandson, J.; Uemura, T.; Iiyuka, T.; Van Der Veen, M.; Rega, D.; Vanspeybroeck, V.; Lamaire, A.; Rogge, S.; Walton, K.; Bingel, L. W.; Wuttke, S.; Andreo, J.; Yaghi, O.; Zhang, B.; Yavuz, C.; Nguyen, T.; Zamora, F.; Montoro, C.; Zhou, H.-C.; Angelo, K.; Fairen-Jimenez, D. How Reproducible Are Surface Areas Calculated from the BET Equation? *Adv. Mater.* **2021**, *34*, 1−12.

(128) Walspurger, S.; Sun, Y.; Sido, A. S. S.; Sommer, J. Neopentane and Solid Acids: Direct Hydron Exchange before Cracking. *J. Phys. Chem. B* **2006**, *110* (37), 18368−18373.

(129) Matsuhashi, H.; Miyazaki, H.; Arata, K. The Preparation of Solid Superacid of Sulfated Tin Oxide with Acidity Higher than Sulfated Zirconia. *Chem. Mater.* **2001**, *13* (9), 3038−3042.

(130) Wang, G.; Cai, G. Cooperative Catalytic Effects between Brønsted and Lewis Acid Sites and Kinetics for Production of Methyl Methacrylate on SO_4^{2-}/TiO_2-SiO_2. *Chem. Eng. Sci.* **2021**, *229*, 116165.

(131) Rabee, A. I. M.; Mekhemer, G. A. H.; Osatiashtiani, A.; Isaacs, M. A.; Lee, A. F.; Wilson, K.; Zaki, M. I. Acidity-Reactivity Relationships in Catalytic Esterification over Ammonium Sulfate-Derived Sulfated Zirconia. *Catalysts* **2017**, *7* (7), 204.

(132) Mekhemer, G. A. H.; Zaki, M. I. In Situ FTIR Spectroscopic Assessment of Methylbutynol Catalytic Conversion Products in Relation to the Surface Acid-Base Properties of Systematically Modified Aluminas. *Surf. Sci.* **2016**, *652* (2), 269−277.

(133) Guo, G. Y.; Chen, Y. L.; Xu, S. A Luminescent Mesoporous Zirconium Complex and It as a Precursor of Environmentally Benign Catalysts. *Microporous Mesoporous Mater.* **2015**, *213*, 100−107.

(134) Banerjee, B.; Bhunia, S.; Bhaumik, A. Self-Assembled Sulfated Zirconia Nanocrystals with Mesoscopic Void Space Synthesized via Ionic Liquid as a Porogen and Its Catalytic Activity for the Synthesis of Biodiesels. *Appl. Catal. A Gen.* **2015**, *502*, 380−387.

(135) Sun, Y.; Ma, S.; Du, Y.; Yuan, L.; Wang, S.; Yang, J.; Deng, F.; Xiao, F. S. Solvent-Free Preparation of Nanosized Sulfated Zirconia with Brønsted Acidic Sites from a Simple Calcination. *J. Phys. Chem. B* **2005**, *109* (7), 2567−2572.

(136) Vera, C. R.; Pieck, C. L.; Shimizu, K.; Parera, J. M. Tetragonal Structure, Anionic Vacancies and Catalytic Activity of SO_4^{2-}-ZrO_2 Catalysts for n-Butane Isomerization. *Appl. Catal. A Gen.* **2002**, *230* (1−2), 137−151.

(137) Chambon, F.; Rataboul, F.; Pinel, C.; Cabiac, A.; Guillon, E.; Essayem, N. Cellulose Hydrothermal Conversion Promoted by Heterogeneous Brønsted and Lewis Acids: Remarkable Efficiency of Solid Lewis Acids to Produce Lactic Acid. *Appl. Catal. B Environ.* **2011**, *105* (1−2), 171−181.

(138) Gorunova, O. N.; Novitskiy, I. M.; Grishin, Y. K.; Gloriozov, I. P.; Roznyatovsky, V. A.; Khrustalev, V. N.; Kochetkov, K. A.; Dunina, V. V. When Applying the Mercury Poisoning Test to Palladacycle-Catalyzed Reactions, One Should Not Consider the Common Misconception of Mercury(0) Selectivity. *Organometallics* **2018**, *37* (17), 2842−2858.

(139) Hemmann, F.; Jaeger, C.; Kemnitz, E. Comparison of Acidic Site Quantification Methods for a Series of Nanoscopic Aluminum Hydroxide Fluorides. *RSC Adv.* **2014**, *4* (100), 56900−56909.

(140) Breitkopf, C.; Papp, H.; Li, X.; Olindo, R.; Lercher, J. A.; Lloyd, R.; Wrabetz, S.; Jentoft, F. C.; Meinel, K.; Förster, S.; Schindler, K. M.; Neddermeyer, H.; Widdra, W.; Hofmann, A.; Sauer, J. Activation and Isomerization of n-Butane on Sulfated Zirconia Model Systems - An Integrated Study across the Materials and Pressure Gaps. *Phys. Chem. Chem. Phys.* **2007**, *9* (27), 3600−3618.

(141) Massimi, S. E.; Metzger, K. E.; McGuirk, C. M.; Trewyn, B. G. Best Practices in the Characterization of MOF@MSN Composites. *Inorg. Chem.* **2022**, *61* (10), 4219−4234.

(142) Lónyi, F.; Valyon, J.; Engelhardt, J.; Mizukami, F. Characterization and Catalytic Properties of Sulfated ZrO_2-TiO_2 Mixed Oxides. *J. Catal.* **1996**, *160* (2), 279−289.

(143) Matsuhashi, H. Synthesis of Solid Acid Catalysts of MgO-Al_2O_3 Mixed Oxide Containing Oxyanions by Thermal Decomposition of Anion-Exchanged Hydrotalcites. *Catal. Surv. from Asia* **2023**, *27* (2), 132−138.

(144) Wang, J.; Liu, L.; Dong, X.; Alfilfil, L.; Hsiung, C. E.; Liu, Z.; Han, Y. Converting Hierarchical to Bulk Structure: A Strategy for Encapsulating Metal Oxides and Noble Metals in Zeolites. *Chem. Mater.* **2018**, *30* (18), 6361−6369.

(145) Gupta, P.; Paul, S. Solid Acids: Green Alternatives for Acid Catalysis. *Catal. Today* **2014**, *236*, 153−170.

(146) Lei, T.; Xu, J. S.; Tang, Y.; Hua, W. M.; Gao, Z. New Solid Superacid Catalysts for n-Butane Isomerization: γ-Al_2O_3 or SiO_2 Supported Sulfated Zirconia. *Appl. Catal. A Gen.* **2000**, *192* (2), 181−188.

(147) Stalzer, M. M.; Delferro, M.; Marks, T. J. Supported Single-Site Organometallic Catalysts for the Synthesis of High-Performance Polyolefins. *Catal. Lett.* **2015**, *145*, 3−14.

(148) Brzeski, J.; Skurski, P.; Simons, J. Caralumane Superacids of Lewis and Brønsted Character. *J. Phys. Chem. A* **2021**, *125* (4), 999−1011.

(149) Reed, C. A. Carborane Acids. New "Strong Yet Gentle" Acids for Organic and Inorganic Chemistry. *Chem. Commun.* **2005**, 1669−1677.

(150) Duffy, J. A. Ionic-Covalent Character of Metal and Nonmetal Oxides. *J. Phys. Chem. A* **2006**, *110* (49), 13245−13248.

(151) Munyentwali, A.; Li, H.; Yang, Q. Review of Advances in Bifunctional Solid Acid/Base Catalysts for Sustainable Biodiesel Production. *Appl. Catal. A Gen.* **2022**, *633*, 118525.

(152) Afanasiev, P.; Geantet, C.; Breysse, M. Role of Oxoanions in the Stabilization of Tetragonal Zirconia. *J. Mater. Chem.* **1994**, *4* (10), 1653−1657.

(153) Marlowe, J.; Acharya, S.; Zuber, A.; Tsilomelekis, G. Characterization of Sulfated SnO_2-ZrO_2 Catalysts and Their Catalytic Performance on the Tert-Butylation of Phenol. *Catalysts* **2020**, *10* (7), 726.

(154) Hofmann, A.; Sauer, J. Surface Structure of Hydroxylated and Sulfated Zirconia. A Periodic Density-Functional Study. *J. Phys. Chem. B* **2004**, *108* (38), 14652−14662.

(155) Hino, M.; Kobayashi, S.; Arata, K. Reactions of Butane and Isobutane Catalyzed by Zirconium Oxide Treated with Sulfate Ion. *ACS* **1979**, *101* (21), 6439−6441.

(156) Sigwadi, R.; Mokrani, T.; Msomi, P.; Nemavhola, F. The Effect of Sulfated Zirconia and Zirconium Phosphate Nanocomposite Membranes on Fuel-Cell Efficiency. *Polymers* **2022**, *14* (2), 263.

(157) Iskandarova, I. M.; Knizhnik, A. A.; Rykova, E. A.; Bagatur'yants, A. A.; Potapkin, B. V.; Korkin, A. A. First-Principle Investigation of the Hydroxylation of Zirconia and Hafnia Surfaces. *Microelectron. Eng.* **2003**, *69*, 587−593.

(158) Yan, G. X.; Wang, A.; Wachs, I. E.; Baltrusaitis, J. Critical Review on the Active Site Structure of Sulfated Zirconia Catalysts and Prospects in Fuel Production. *Appl. Catal. A Gen.* **2019**, *572*, 210−225.

(159) Diaz-Silvarrey, L. S.; McMahon, A.; Phan, A. N. Benzoic Acid Recovery via Waste Poly(Ethylene Terephthalate) (PET) Catalytic Pyrolysis Using Sulphated Zirconia Catalyst. *J. Anal. Appl. Pyrolysis* **2018**, *134*, 621−631.

(160) Liu, J.; Liu, N.; Ren, K.; Shi, L.; Meng, X. Sulfated Zirconia Synthesized in a One Step Solvent-Free Method for Removal of Olefins from Aromatics. *Ind. Eng. Chem. Res.* **2017**, *56* (27), 7693−7699.

Pursuant to the DOE Public Access Plan, this document represents the authors' peer-reviewed, accepted manuscript. The published version of the article is available from the relevant publisher.

(161) Shimizu, K.; Kounami, N.; Wada, H.; Shishido, T.; Hattori, H. Isomerization of n-Butane by Sulfated Zirconia: The Effect of Calcination Temperature and Characterization of Its Surface Acidity. *Catal. Lett.* **1998**, *54* (3), 153−158.
(162) Song, S. X.; Kydd, R. A. Activation of Sulfated Zirconia Catalysts Effect of Water Content on Their Activity in n-Butane Isomerization. *J. Chem. Soc. - Faraday Trans.* **1998**, *94* (9), 1333−1338.
(163) Ivanov, V. K.; Baranchikov, A. Y.; Kopitsa, G. P.; Lermontov, S. A.; Yurkova, L. L.; Gubanova, N. N.; Ivanova, O. S.; Lermontov, A. S.; Rumyantseva, M. N.; Vasilyeva, L. P.; Sharp, M.; Pranzas, P. K.; Tretyakov, Y. D. pH Control of the Structure, Composition, and Catalytic Activity of Sulfated Zirconia. *J. Solid State Chem.* **2013**, *198*, 496−505.
(164) Lee, J. H.; Shin, C. H.; Suh, Y. W. Higher Brønsted Acidity of WO_x/ZrO_2 Catalysts Prepared Using a High-Surface-Area Zirconium Oxyhydroxide. *Mol. Catal.* **2017**, *438*, 272−279.
(165) Patel; Goyena, R. Structural and Active Site Characterization of Sulfated Zirconia Catalysts for Light Alkane Isomerization. In *Proceedings of the DGMK-Conference "Chances for Innovative Processes at the Interface between Refining and Petrochemistry*; 2002; pp 23−30.
(166) Fraenkel, D. Structure of Sulfated Metal Oxides and Its Correlation with Catalytic Activity. *Ind. Eng. Chem. Res.* **1997**, *36* (1), 52−59.
(167) Benaïssa, M.; Santiesteban, J. G.; Díaz, G.; Chang, C. D.; José-Yacamán, M. Interaction of Sulfate Groups with the Surface of Zirconia: An HRTEM Characterization Study. *J. Catal.* **1996**, *161* (2), 694−703.
(168) Guo, C.; Liao, S.; Qian, Z.; Tanabe, K. Alkylation of Isobutane with Butenes over Solid Acid Catalysts. *Appl. Catal. A, Gen.* **1994**, *107* (2), 239−248.
(169) Bolis, V.; Magnacca, G.; Cerrato, G.; Morterra, C. Effect of Sulfation on the Acid-Base Properties of Tetragonal Zirconia. A Calorimetric and IR Spectroscopic Study. *Top. Catal.* **2002**, *19* (3−4), 259−269.
(170) Ellis, L. D.; Orski, S. V.; Kenlaw, G. A.; Norman, A. G.; Beers, K. L.; Román-Leshkov, Y.; Beckham, G. T. Tandem Heterogeneous Catalysis for Polyethylene Depolymerization via an Olefin-Intermediate Process. *ACS Sustain. Chem. Eng.* **2021**, *9*, 623−628.
(171) Kar, S.; Goeppert, A.; Prakash, G. K. S. Combined CO_2 Capture and Hydrogenation to Methanol: Amine Immobilization Enables Easy Recycling of Active Elements. *ChemSusChem* **2019**, *12* (13), 3172−3177.
(172) Baddour, F. G.; Nash, C. P.; Schaidle, J. A.; Ruddy, D. A. Synthesis of α-MoC_{1-x} Nanoparticles with a Surface-Modified SBA-15 Hard Template: Determination of Structure-Function Relationships in Acetic Acid Deoxygenation. *Angew. Chemie - Int. Ed.* **2016**, *55* (31), 9026−9029.
(173) Kim, K. D.; Wang, Z.; Jiang, Y.; Hunger, M.; Huang, J. The Cooperative Effect of Lewis and Brønsted Acid Sites on Sn-MCM-41 Catalysts for the Conversion of 1,3-Dihydroxyacetone to Ethyl Lactate. *Green Chem.* **2019**, *21* (12), 3383−3393.
(174) Huang, D.; Chen, S.; Ma, S.; Chen, X.; Ren, Y.; Wang, M.; Ye, L.; Zhang, L.; Chen, X.; Liu, Z. P.; Yue, B.; He, H. Determination of Acid Structures on the Surface of Sulfated Monoclinic and Tetragonal Zirconia through Experimental and Theoretical Approaches. *Catal. Sci. Technol.* **2022**, *12* (2), 596−605.
(175) Kobe, J. M.; Gonzalez, M. R.; Fogash, K. B.; Dumesic, J. A. Effects of Water on the Performance of Sulfated Zirconia Catalysts for Butane Isomerization. *J. Catal.* **1996**, *164*, 459−466.
(176) Haase, F.; Sauer, J. The Surface Structure of Sulfated Zirconia: Periodic Ab Initio Study of Sulfuric Acid Adsorbed on ZrO_2(101) and ZrO_2(001). *J. Am. Chem. Soc.* **1998**, *120* (51), 13503−13512.
(177) Escalona Platero, E.; Penarroya Mentruit, M.; Otero Arean, C.; Zecchina, A. FTIR Studies on the Acidity of Sulfated Zirconia Prepared by Thermolysis of Zirconium Sulfate. *J. Catal.* **1996**, *162* (2), 268−276.
(178) Morterra, C.; Cerrato, G.; Pinna, F.; Signoretto, M. Brønsted Acidity of Superacid Sulfate-Doped ZrO_2 System. *J. Phys. Chem.* **1994**, *98*, 12373−12381.
(179) Bensitel, M.; Saur, O.; Lavalley, J.-C.; Morrow, B. A. An Infrared Study of Sulfated Zirconia. *Mater. Chem. Phys.* **1988**, *19*, 147−156.
(180) Trickett, C. A.; Osborn Popp, T. M.; Su, J.; Yan, C.; Weisberg, J.; Huq, A.; Urban, P.; Jiang, J.; Kalmutzki, M. J.; Liu, Q.; Baek, J.; Head-Gordon, M. P.; Somorjai, G. A.; Reimer, J. A.; Yaghi, O. M. Identification of the Strong Brønsted Acid Site in a Metal-Organic Framework Solid Acid Catalyst. *Nat. Chem.* **2019**, *11* (2), 170−176.
(181) Shimoda, N.; Nakayama, K.; Kiyota, K.; Satokawa, S. Synthesis of Tetragonal Zirconia in Mesoporous Silica and Its Catalytic Properties for Methanol Oxidative Decomposition. *RSC Adv.* **2017**, *7* (88), 55819−55829.
(182) Garvie, R. C. The Occurrence of Metastable Tetragonal Zirconia as a Crystallite Size Effect. *J. Phys. Chem.* **1965**, *69* (4), 1238−1243.
(183) Chevalier, J.; Gremillard, L.; Virkar, A. V.; Clarke, D. R. The Tetragonal-Monoclinic Transformation in Zirconia: Lessons Learned and Future Trends. *J. Am. Ceram. Soc.* **2009**, *92* (9), 1901−1920.
(184) Bachiller-Baeza, B.; Rodriguez-Ramos, I.; Guerrero-Ruiz, A. Interaction of Carbon Dioxide with the Surface of Zirconia Polymorphs. *Langmuir* **1998**, *14* (13), 3556−3564.
(185) Piskorz, W.; Gryboś, J.; Zasada, F.; Cristol, S.; Paul, J. F.; Adamski, A.; Sojka, Z. Periodic DFT and Atomistic Thermodynamic Modeling of the Surface Hydration Equilibria and Morphology of Monoclinic ZrO_2 Nanocrystals. *J. Phys. Chem. C* **2011**, *115* (49), 24274−24286.
(186) Piskorz, W.; Gryboś, J.; Zasada, F.; Zapała, P.; Cristol, S.; Paul, J. F.; Sojka, Z. Periodic DFT Study of the Tetragonal ZrO_2 Nanocrystals: Equilibrium Morphology Modeling and Atomistic Surface Hydration Thermodynamics. *J. Phys. Chem. C* **2012**, *116* (36), 19307−19320.
(187) Shao, Y.; Li, Y.; Sun, K.; Zhang, Z.; Tian, H.; Gao, G.; Li, Q.; Liu, Q.; Liu, Q.; Hu, X. Sulfated Zirconia with Different Crystal Phases for the Production of Ethyl Levulinate and 5-Hydroxymethylfurfural. *Energy Technol.* **2020**, *8* (3), 1−10.
(188) Arata, K.; Hino, M.; Yamagata, N. Acidity and Catalytic Activity of Zirconium and Titanium Sulfates Heat-Treated at High Temperature. *Chem. Soc. Japan* **1990**, *63* (1), 244−246.
(189) Clearfield, A.; Serrette, G. P. D.; Khazi-Syed, A. H. Nature of Hydrous Zirconia and Sulfated Hydrous Zirconia. *Catal. Today* **1994**, *20* (2), 295−312.
(190) Osatiashtiani, A.; Lee, A. F.; Granollers, M.; Brown, D. R.; Olivi, L.; Morales, G.; Melero, J. A.; Wilson, K. Hydrothermally Stable, Conformal, Sulfated Zirconia Monolayer Catalysts for Glucose Conversion to 5-HMF. *ACS Catal.* **2015**, *5* (7), 4345−4352.
(191) Wu, Y.; Chen, X.; Huang, D.; Zhang, L.; Ren, Y.; Tang, G.; Chen, X.; Yue, B.; He, H. A Study on the Acidity of Sulfated CuO Layers Grown by Surface Reconstruction of Cu_2O with Specific Exposed Facets. *Catal. Sci. Technol.* **2020**, *10* (12), 3985−3993.
(192) Sohn, J. R.; Kim, H. W. Catalytic and Surface Properties of ZrO_2 Modified with Sulfur Compounds. *J. Mol. Catal.* **1989**, *52* (3), 361−374.
(193) Stichert, W.; Schüth, F.; Kuba, S.; Knözinger, H. Monoclinic and Tetragonal High Surface Area Sulfated Zirconias in Butane Isomerization: CO Adsorption and Catalytic Results. *J. Catal.* **2001**, *198* (2), 277−285.
(194) Al-Daous, M. A.; Stein, A. Preparation and Catalytic Evaluation of Macroporous Crystalline Sulfated Zirconium Dioxide Templated with Colloidal Crystals. *Chem. Mater.* **2003**, *15* (13), 2638−2645.
(195) Scholz, J.; Scholz, K.; McQuillan, A. J. In Situ Infrared Spectroscopic Analysis of the Water Modes of $[Zr_4(OH)_8(H_2O)_{16}]^{8+}$ during the Thermal Dehydration of $ZrOCl_2{\cdot}8H_2O$. *J. Phys. Chem. A* **2010**, *114* (29), 7733−7741.
(196) Clearfield, A. The Mechanism of Hydrolytic Polymerization of Zirconyl Solutions. *J. Mater. Res.* **1990**, *5* (1), 161−162.

https://doi.org/10.1021/acs.langmuir.3c03966
Langmuir XXXX, XXX, XXX−XXX

Pursuant to the DOE Public Access Plan, this document represents the authors' peer-reviewed, accepted manuscript. The published version of the article is available from the relevant publisher.

(197) Yamaguchi, T.; Tanabe, K.; Yao Chin Kung. Preparation and Characterization of ZrO_2 and SO_4^{2-}-Promoted ZrO_2. *Mater. Chem. Phys.* **1987**, *16* (1), 67−77.
(198) Srinivasan, R.; Davis, B. H.; Harris, M. B.; Simpson, S. F.; De Angelis, R. J. Zirconium Oxide Crystal Phase: The Role of the pH and Time to Attain the Final pH for Precipitation of the Hydrous Oxide. *J. Mater. Res.* **1988**, *3* (4), 787−797.
(199) Li, Y. N.; He, L. N.; Diao, Z. F.; Yang, Z. Z. Carbon Capture with Simultaneous Activation and Its Subsequent Transformation. *Adv. Inorg. Chem.* **2014**, *66*, 289−345.
(200) Kuznetsova, T. G.; Sadykov, V. A. Specific Features of the Defect Structure of Metastable Nanodisperse Ceria, Zirconia, and Related Materials. *Kinet. Catal.* **2008**, *49* (6), 840−858.
(201) Haw, J. F.; Zhang, J.; Shimizu, K.; Venkatraman, T. N.; Luigi, D. P.; Song, W.; Barich, D. H.; Nicholas, J. B. NMR and Theoretical Study of Acidity Probes on Sulfated Zirconia Catalysts. *J. Am. Chem. Soc.* **2000**, *122* (50), 12561−12570.
(202) Nascimento, P.; Akratopoulou, C.; Oszagyan, M.; Coudurier, G.; Travers, C.; Joly, J. F.; Vedrine, J. C. ZrO_2-SO_4^{2-} Catalyts. Nature and Stability of Acid Sites Responsible for n-Butane Isomerization. In *Proceedings of the 10th International Congress on Catalysis*, 19-24 July, 1992, Budapest, Hungary; 1993; pp 1185−1197.
(203) Tran, M. T.; Gnep, N. S.; Szabo, G.; Guisnet, M. Isomerization of n-Butane over H-Mordenites under Nitrogen and Hydrogen: Influence of the Acid Site Density. *J. Catal.* **1998**, *174* (2), 185−190.
(204) Fărcaşiu, D.; Li, J. Q. Preparation of Sulfated Zirconia Catalysts with Improved Control of Sulfur Content. *Appl. Catal. A, Gen.* **1995**, *128* (1), 97−105.
(205) Ren, K.; Kong, D.; Meng, X.; Wang, X.; Shi, L.; Liu, N. The Effects of Ammonium Sulfate and Sulfamic Acid on the Surface Acidity of Sulfated Zirconia. *J. Saudi Chem. Soc.* **2019**, *23* (2), 198−204.
(206) Li, X.; Nagaoka, K.; Olindo, R.; Lercher, J. A. Synthesis of Highly Active Sulfated Zirconia by Sulfation with SO_3. *J. Catal.* **2006**, *238* (1), 39−45.
(207) Likith, S. R. J.; Farberow, C. A.; Manna, S.; Abdulslam, A.; Stevanović, V.; Ruddy, D. A.; Schaidle, J. A.; Robichaud, D. J.; Ciobanu, C. V. Thermodynamic Stability of Molybdenum Oxycarbides Formed from Orthorhombic Mo_2C in Oxygen-Rich Environments. *J. Phys. Chem. C* **2018**, *122* (2), 1223−1233.
(208) Balderas, R. I.; Ciobanu, C. V.; Richards, R. M. (111) Faceted Metal Oxides: A Review of Synthetic Methods. *Cryst. Growth Des.* **2022**, *22* (10), 6296−6322.
(209) Bentley, A. K.; Skrabalak, S. E. A Primer on Lattice Planes, Crystal Facets, and Nanoparticle Shape Control. *J. Chem. Educ.* **2023**, *100*, 3425−3433.
(210) Benaïssa, M.; Santiesteban, J. G.; Diaz, G.; José-Yacamán, M. Surface Atomic Resolution Microscopy of Sulfated-Zirconia and Fe/Mn Promoted Sulfated Zirconia. *Mater. Res. Soc. Symp. Proc.* **1996**, *466*, 267−272.
(211) Añez, R.; Sierraalta, A.; Martorell, G. Theoretical Study of CO and H_2O Interaction on (110) and (101) Zirconia Surfaces. *J. Mol. Struct. THEOCHEM* **2009**, *900* (1−3), 59−63.
(212) Añez, R.; Sierraalta, A.; Martorell, G.; Sautet, P. Stabilization of the (1 1 0) Tetragonal Zirconia Surface by Hydroxyl Chemical Transformation. *Surf. Sci.* **2009**, *603* (16), 2526−2531.
(213) Ireta, J.; Aparicio, F.; Viniegra, M.; Galván, M. The Role of the Protons and the Electrostatic Potential in the Reactivity of the (110) Sulfated Zirconia Surface. *J. Phys. Chem. B* **2003**, *107* (3), 811−818.
(214) Hu, Y.; Guo, B.; Fu, Y.; Ren, Y.; Tang, G.; Chen, X.; Yue, B.; He, H. Facet-Dependent Acidic and Catalytic Properties of Sulfated Titania Solid Superacids. *Chem. Commun.* **2015**, *51* (75), 14219−14222.
(215) Syed, Z. H.; Kaphan, D. M.; Perras, F. A.; Pruski, M.; Ferrandon, M. S.; Wegener, E. C.; Celik, G.; Wen, J.; Liu, C.; Dogan, F.; Goldberg, K. I.; Delferro, M. Electrophilic Organoiridium(III) Pincer Complexes on Sulfated Zirconia for Hydrocarbon Activation and Functionalization. *J. Am. Chem. Soc.* **2019**, *141*, 6325−6337.
(216) Kanbur, U.; Witzke, R. J.; Xu, J.; Ferrandon, M. S.; Goetjen, T. A.; Kropf, A. J.; Perras, A.; Liu, C.; Tilley, T. D.; Kaphan, D. M.; Delferro, M. Supported Electrophilic Organoruthenium Catalyst for the Hydrosilylation of Olefins. *ACS Catal.* **2023**, *13*, 13383−13394.
(217) Mason, A. H.; Motta, A.; Das, A.; Ma, Q.; Bedzyk, M. J.; Kratish, Y.; Marks, T. J. Rapid Atom-Efficient Polyolefin Plastics Hydrogenolysis Mediated by a Well-Defined Single-Site Electrophilic/Cationic Organo-Zirconium Catalyst. *Nat. Commun.* **2022**, *13*, 1−12.
(218) Tafazolian, H.; Culver, D. B.; Conley, M. P. A Well-Defined Ni(II) α-Diimine Catalyst Supported on Sulfated Zirconia for Polymerization Catalysis. *Organometallics* **2017**, *36*, 2385−2388.
(219) Zhang, J.; Mason, A. H.; Wang, Y.; Motta, A.; Kobayashi, T.; Pruski, M.; Gao, Y.; Marks, T. J. Beyond the Active Site. Cp*$ZrMe_3$/Sulfated Alumina-Catalyzed Olefin Polymerization Tacticity via Catalyst···Surface Ion-Pairing. *ChemCatChem.* **2021**, *13*, 2564−2569.
(220) Miao, C. X.; Gao, Z. Preparation and Properties of Ultrafine SO_4^{2-} /ZrO_2 Superacid Catalysts. *Mater. Chem. Phys.* **1997**, *50* (1), 15−19.
(221) Huang, Y.; Mccarthy, T. J.; Sachtler, W. M. H. Preparation and Catalytic Testing of Mesoporous Sulfated Zirconium Dioxide with Partially Tetragonal Wall Structure. *Appl. Catal. A, Gen.* **1996**, *148* (1), 135−154.

https://doi.org/10.1021/acs.langmuir.3c03966
Langmuir XXXX, XXX, XXX−XXX